Head-up Display Combiner Unit stress and deformation analysis

Rui Pedro Beleza de Almeida

Dissertação de Mestrado

Orientador na FEUP: Prof. José Manuel Ferreira Duarte

Supervisor na empresa: Sezgin Goekcen

Orientador na empresa: Rui Barros

Mestrado Integrado em Engenharia Mecânica

Janeiro de 2019

“The great fights with your strongest rivals are always the biggest motivation.”

Valentino Rossi

Resumo

Este trabalho centrou-se no estudo de um subsistema pertencente ao "Head-up display" (HUD), desenvolvido na Bosch Car Multimédia em Braga, que integra a quarta geração do Ford Focus (modelo de 2018). O elemento em questão é o "Combiner Unit" que é composto por dois componentes: um elemento ótico transparente, em policarbonato, que projeta a imagem virtual do HUD, designada "Combiner" e o seu suporte, designado "Combiner Support". Estes componentes encontram-se simplesmente colados um ao outro. Devido à sua menor rigidez, o "Combiner" adapta a sua forma à do "Combiner Support" que contem pequenas diferenças dimensionais (inseridas no fabrico deste) em relação ao seu desenho. Este fenómeno, para além de induzir deformações no "Combiner", cria tensões internas no mesmo. Fazendo parte do sistema de projeção ótico do HUD, trata-se de uma peça sensível a deformações pois estas podem causar distorções na imagem visualizada pelo condutor. Ao mesmo tempo as tensões internas podem causar instabilidade na adesão entre o "Combiner" e o "Combiner Support", quando submetidos a temperaturas e humidades mais elevadas. Tendo este problema em vista, o objetivo deste trabalho foi analisar as tensões internas, a deformação no "Combiner" quando colado ao "Combiner Support" e procurar entender o seu impacto na adesão entre as duas peças.

Desta forma, numa primeira análise verificou-se a estabilidade geométrica do suporte. Recorrendo a um instrumento de medição de coordenadas (CMM), mediu-se qual a variação dimensional do suporte quando submetido a elevadas temperaturas e a humidade.

Numa segunda análise utilizou-se um Scanner 3D para fazer um levantamento da geometria do "Combiner" antes e após o processo de colagem, para entender quais os desvios na superfície, induzidos pelo "Combiner Support". No âmbito do estudo das tensões internas do "Combiner", empregou-se o método da fotoelasticidade, através do uso de um polariscópio.

Dada a complexidade da simulação e validação de um modelo composto por dois elementos colados entre eles, como no caso do "Combiner Unit, foi tomada a decisão de criar um modelo simplificado onde se tem em conta apenas o "Combiner". Este modelo simplificado tem como objetivo validar primeiro o modelo do "Combiner" induzindo um deslocamento/força conhecida num determinado ponto, comparando os resultados obtidos de tensão e deformação por simulação com os resultados experimentais. Após a boa validação do modelo do "Combiner" fica como trabalho futuro a introdução do "Combiner Support" e do elemento de fixação entre os dois. Experimentalmente, desenvolveu-se e fabricou-se um equipamento de suporte (Jig) para poder aplicar uma força/deslocamento conhecido. Solicitou-se um "Combiner" com uma força conhecida e fez-se uma análise de tensões e um levantamento geométrico da sua superfície.

Para a simulação do modelo, recorreu-se ao método de elementos finitos, tendo sido posteriormente validada a simulação com os resultados obtidos pelo método.

Os resultados da simulação demonstraram que as deformações causadas no "Combiner", quando comparadas com os resultados obtidos no Scanner 3D do "Combiner" solicitado no Jig experimental, são comparáveis. Já para as tensões verificou-se uma diferença da simulação para o que foi verificado experimentalmente no polariscópio. De forma a aprimorar os resultados desta simulação, pode como trabalho futuro fazer-se a simulação das tensões residuais (devidas à injeção) no "Combiner", remover algumas aproximações que foram feitas na simulação (como a espessura da peça) e ainda fazer uma validação do modulo de Young do material.

Head-up Display Combiner Display Stress and Deformation Analysis

Abstract

This work centered on the study of a subsystem of the Head-up Display (HUD), developed by Bosch Car Multimedia in Braga, to integrate the fourth generation of the Ford Focus (2018 model). The element in question is the Combiner Unit, which is composed by two components: a transparent optical element made with polycarbonate designated Combiner, which projects the virtual image of the HUD and its support designated Combiner Support. These components are simply glued to each other. Due its inferior rigidity, the Combiner adapts its shape to the Combiner Support, that contains small dimensional deviations (that occur during the fabrication process), when compared with the nominal design. This phenomenon, beside transmit deformations into the Combiner, creates internal stress in it. As this part, composes the HUD optical projection system, is very sensitive to deformations, because they can cause image distortions that can be visualized by the driver. At the same time the internal stress, can cause instability in the bonding between both parts, when submitted to higher temperature and humidity conditions. Knowing this problem, the goal of this work was to analyze the internal stress and the deformation in the Combiner, when this part is glued to the Combiner Support.

This way, the first analysis was to check the geometric stability of the Combiner Support. Using a coordinate measuring machine (CMM), the dimensional variation of the Combiner was studied, when submitted to higher temperature and humidity conditions.

In a second analysis, using a 3D scanner, the Combiner geometry was studied, before and after the gluing process, in order to understand what were the deviations that the Combiner Support transmitted to the Combiner. In the scope of the study of the Combiner internal stress, the photoelasticity method was used, with the resort of a polariscope.

Due the complexity of this simulation and validation of a model composed by two elements glued between them, like the combiner unit it was taken the decision to create a simplified model where only the combiner was considered. This simplified model had as first purpose the validation of the model by inducing a known force/displacement, in a certain point, so later compare these results with a simulation. After a good validation of the model, stayed as a future work the introduction of the combiner support and the fixation element. Experimentally, it was developed and fabricated a support jig to be able to apply a known displacement / force. A known force was applied into the combiner, and a stress and surface geometry analysis was made.

A simulation of this model was made finite element method, and the results were validated with the simplified model ones.

The results of the simulation showed that the deformations in the Combiner were comparable with the 3D scanner ones. As for the internal stress, there was a slight difference between the simulation and what was visualized in the polariscope. In the path of getting more refined results, as a future work, the residual stress (due to the injection process) in the Combiner could be simulated, some approximations could be removed (like the Combiner thickness), and validate the Young modulus of the material.

Acknowledgements

I would like to express my sincere thanks to everyone involved in the development of this thesis.

To my tutor at FEUP, Prof. José Manuel Ferreira Duarte, for all the support, guidance and companionship throughout this project. I would like also to thank the other teachers that helped me with my work, with a special mention to Prof. Mário Vaz.

To my tutor at Bosch Car Multimedia Rui Barros to the intense support and dedication supporting this thesis, to my manager Sezgin Goekcen and to my team mates, Bruno Vilaça to his tireless support, Pedro Monteiro, Daniela Santos, Pedro Moreira, Vasco Pinto, Hernani Abreu, Manuel Sarmento, Carlos Oliveira, João Marques, Anibal Portinha, Filipe Valente and Marcelo Domingues. I would also like to thank all the people in Bosch Car Multimedia that at a certain moment helped me.

To my integration team at Bosch Car Multimedia Carlos Pires, Catarina Almeida, Rui Costa, Beatriz Mucambe and João Martins.

To my family that gave me a constant support, especially to my parents, my brother, and my girlfriend.

To my friends, that helped this work by giving constant support especially to Roque, Gonçalo Carvalho, Bruno Tulha, Tiago Costa, Maria Pina and Diogo Sousa that followed closely this work.

Content Index

Acronyms

C_b- Brewster constant
CAD – computer aided design
CAE - complete Abaqus environment
CHUD – combiner Head-up Display
CMM - coordinate measuring machine
CVD – chemical vapor deposition
FDM – fused deposition modelling
HUD – Head-up Display
n – Index of refraction
PC – polycarbonate
PGU – picture generation unit
PVD – physical vapor deposition
RPM – rotations per minute
STL – stereolithography
UV – ultra violet

δ – Light retardation
σ - Stress

Figure Index

Table Index

1 Introduction

This first chapter presents the framework and motivation for this project, as well as the Bosch Group and Bosch Car Multimedia, S.A., where the internship took place.

Also described in this chapter are the project goals, methodology and the thesis structure.

1.1 Project Framework and Motivation

The internship was performed at Bosch Car Multimedia in Braga at CM/CI2-ECM8 team, which belongs to the development department. This team is responsible for the development and support of the production of the combiner Head-up Display (CHUD) (section 2.2) for the new Ford Focus (2018 model), BMW 2 series active tourer and all Mini models.

In the case of the Ford Focus CHUD (Figure 1), the development team is facing validation issues of the product when submitted to ageing tests (power humidity and thermal cycles). One of the failures was glue adhesion between the combiner and the combiner support. A possible root cause can be related to shape deviations and thermal behavior of the combiner support that can transmit stress through the bonding area to the combiner, affecting the stability of the adhesion between both parts. With the problem known, it was proposed to evaluate the correlation between combiner support shape deviations and the internal stress installed in the glued combiner, plus the possible correlations between the internal stress and the glued adhesion problems.

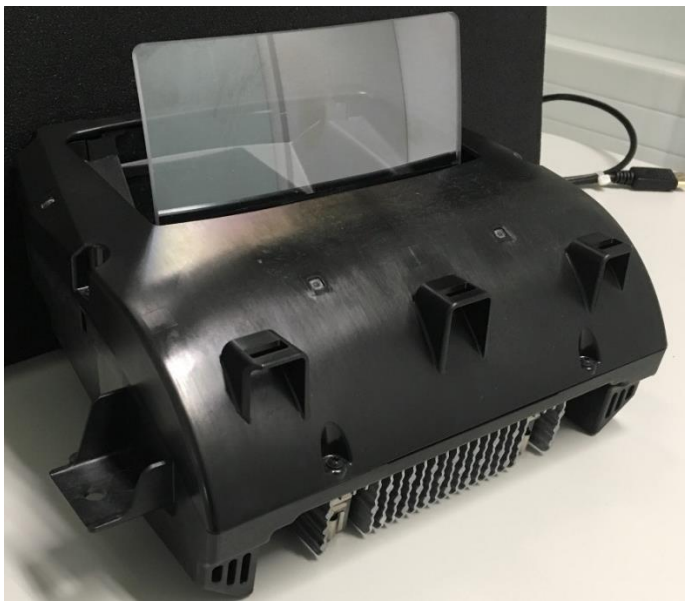

Figure 1 – Ford Focus CHUD

1.2 Bosch Group

The Bosch Group (Figure 2) was founded in 1886, when Robert Bosch opened the "Workshop for Precision Mechanics and Electrical Engineering" in Stuttgart, Germany. (Bosch, Bosch History 2018)

BOSCH
Technik fürs Leben

Figure 2 – Bosch Group logo

Since 1964, as Figure 3 shows, Bosch's majority shareholder has been Robert Bosch Stiftung GmbH. The others Shareholders are the Bosch Family and Robert Bosch GmbH. (Bosch, Bosch Figures 2018)

Figure 3 – Bosch Shareholders (Bosch, Bosch Figures 2018)

The Bosch Group, is a global company and employs approximately 402000 associates worldwide (value for December 31, 2017). This company has its operations divided into four business sectors:

1. Mobility Solutions;
2. Industrial Technology;
3. Consumer Goods;
4. Energy and Building Technology;

In 2017, the company invoiced 78.1 billion euros. Figure 4 shows how this invoice is divided through the four sectors.

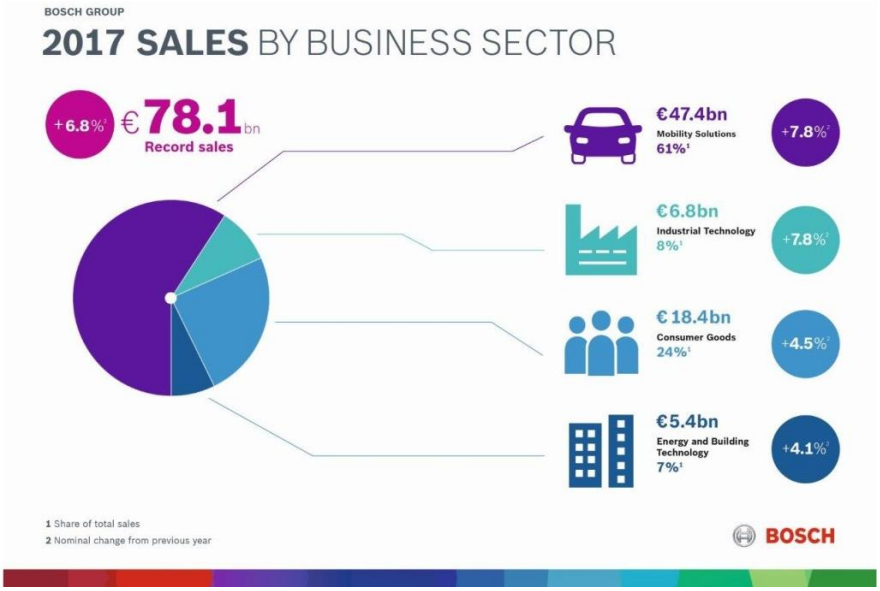

Figure 4 – 2017 Bosch Group sales by Business sector (Bosch, Bosch Figures 2018)

The Bosch Group's strategic objective is to deliver innovations for a connected life. With the slogan "technik fürs leben" which in English means "Technology for life", the Bosch Group tries to spark enthusiasm, improve people's life quality and help to preserve natural resources. (Bosch, Bosch Brand 2018)

1.3 Bosch Car Multimedia Portugal, S.A.

The Bosch Group has five locations in Portugal, divided by three different business areas:

- Bosch Car Multimedia;
- Bosch Termotecnologia;
- Bosch Security Systems;

Bosch Car Multimedia (Figure 5) is located in Braga and started in 1990. Braga has the largest plant of the Car Multimedia section in Bosch. Being a reference company in Car Multimedia, recent investments were made and now Bosch Car Multimedia in Braga has an important development center. (Bosch, Bosch Portugal 2018)

Figure 5 – Bosch Car Multimedia S.A. development department in Braga

1.4 Project goals

The goal of this project is to understand how a Ford Focus CHUD combiner internal stress distribution and shape, change when the combiner is glued to its support. Also the combiner unit suffers from adhesive failure when submitted to higher temperatures and humidity conditions. Therefore, the second goal was to create a correlation between the internal stress installed in the combiner unit and the adhesive failure.

To do this study, the following tasks were performed:

- Analyze the geometric stability of the combiner support in different conditions;
- Analyze the shape and the internal stress of the combiner before and after gluing;
- Model simulation using finite element analysis method to have a better comprehension of the part behavior;
- Experimental model to input a displacement/force in the combiner with known conditions;
- Validate the simulation with the model created;
- Correlate combiner support shape deviations with induced stress into the combiner;

- Analyze (and correlate if possible) the effects of the combiner internal stress in the adhesive failure;

1.5 Methodology

To develop this work, it was necessary to understand how the Ford Focus CHUD works, and to verify the problems that lead to this study. Therefore, the first few days in this internship were in the production line, to understand the gluing and the unit assembling process.

The second task was to understand the 3D scanner data and study about photoelasticity, in order to perform the stress analysis.

The third task was to learn and analyze the stress and deformation in the studied part under the different conditions, and create a correlation with the adhesive failure.

The final task was the creation of a simplified model of the part to study the stress and deformation, and consequent validation of that model.

Figure 6 shows a flowchart of the developed project.

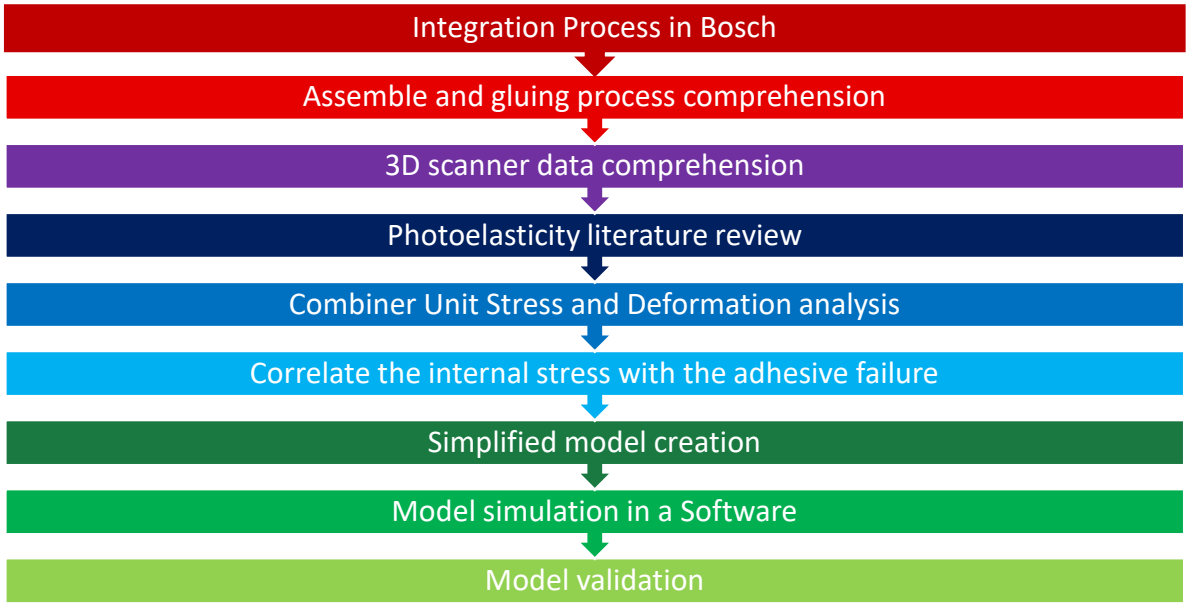

Figure 6 – Flowchart of the developed project

1.6 Structure

In addition to this chapter, this thesis is organized with six more chapters;

- Chapter 2: Literature Review. This chapter makes an introduction on the HUD and the CHUD. Describes the type of parts in study and in the end introduces the concept of photoelasticity.
- Chapter 3: Ford Focus Head-up Display Combiner unit. Here, is described the parts from our Unit that are going to be studied.
- Chapter 4: Combiner Unit stress and geometry analysis. This chapter makes an analysis of the geometric stability of the combiner support, the deformation and stress induced in the combiner during the gluing process and finally the problems adhesive failure is studied.
- Chapter 5: Creation of a controlled conditions model. In this chapter, is a description of the design of a jig used to study the combiner stress and deformation.
- Chapter 6: Simulation and validation of the controlled model. In this chapter, is made a simulation of the model created in chapter 5. The results of the model and the simulation are compared.
- Chapter 7: Conclusions and Future work. This chapter presents the conclusions of this thesis, and perspectives of future work.
- Appendix: Description of other work developed during the internship.

2 Literature review

2.1 An introduction to the information interface between car and driver

Since the creation of the automobile, there has been a necessity to read the car information. With the evolution of the automobile and with the increase in the complexity of the machine, the number of parameters to read also increased. As an example, the Ford T (Figure 7), known as the first production car (1908-1927), only had an ammeter as standard (Daddario 2017). With the increase of information, the dashboard as is known today started to appear.

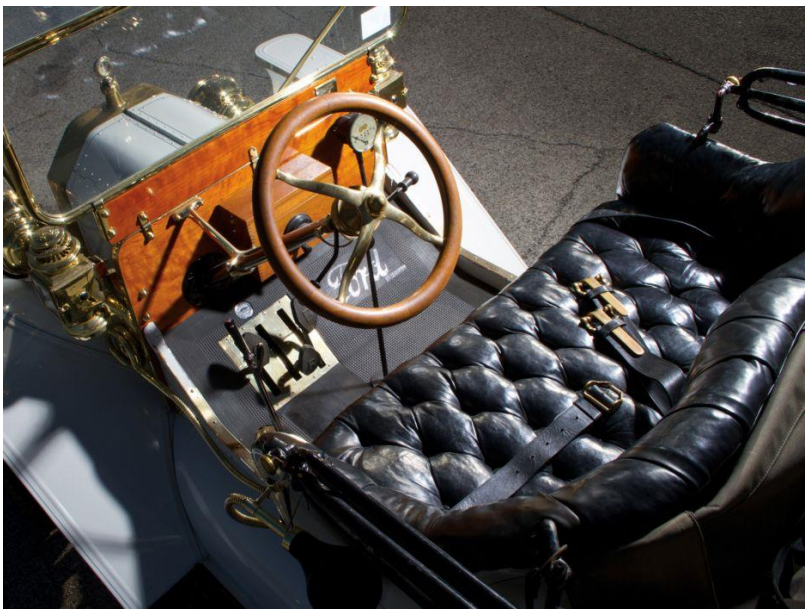

Figure 7 – Ford Model T interior (Harder 2012)

Nowadays, cars have all kinds of information in the dashboard (Figure 8), such as speed, RPM, oil temperature, water temperature, fuel level, indicator lights, warning lights, music and radio information, gear indicators and shifting indicators, power and torque information and many other types of information. With so many information to be displayed to the driver, the dashboard starts being a distraction to the driving itself. So with this problem in mind the introduction of the HUD in the car was made.

Figure 8 – Porsche Panamera Turbo S E-Hybrid Dashboard (Porsche 2018)

2.2 HUD (Head up Display)

A Head-Up-Display (hereafter HUD) is an informative display system that is defined in the oxford dictionary as "a display of instrument readings in an aircraft or vehicle that can be seen without lowering the eyes, typically through being projected on to the windscreen or visor". (dictionaries 2018) (Lee, et al. 2016)

A Head up Display is a device that displays information above the dashboard, by projecting an image into the car windshield (Figure 11) or into a transparent combiner (Figure 9 and 10) (the CHUD). The main advantage of this system compared to the traditional dashboard, is that the driver doesn't need to look down to the dashboard to see the speed, RPM or even GPS indications and with that the driver doesn't need to take the eyes of the road to get trip information, improving reaction times and with that improving safety. Another advantage of the HUD is due to his position further away than the dashboard, reduces also the focal accommodation time (Annie 2015) which can improve reaction times and eye comfort.

The HUD was invented to use in military aircraft, so fighter pilots had the information always in front of their eyes, and avoid that the pilots had to look away from their usual view (Annie 2015). Later General Motors imported that technology to the automotive industry in 1988.

Figure 9- Mini CHuD (Flora 2014)

There are two types of Head up Displays: the ones that project the image in the windshield (HUD) (that requires the windshield to be treated in a way that can reflect the image onto the driver), or the ones that use a small combiner (CHUD).

Figure 10 – 2019 Ford Focus CHUD (Panait 2018)

Figure 11- BMW 5 Series windshield HUD (Howard 2012)

This thesis focus on the CHUD (Figure 12), especially on the combiner itself. This type of HUD has essentially three major components: A PGU (picture generation unit), an imaging system and the housing with the kinematics system.

The PGU is composed by a light source and a display, and combined this unit creates the image that will be seen by the driver. That image will be projected through the fold mirror that redirects the original image into the combiner. Finally, the combiner creates a virtual image to be seen by the driver.

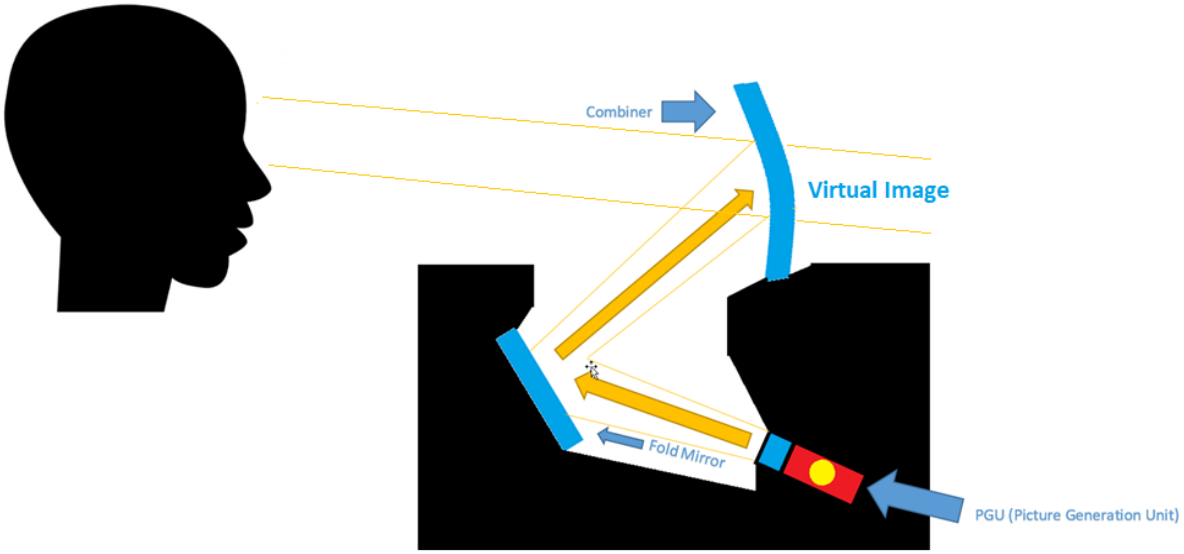

Figure 12 – Combiner HUD diagram

To hide the combiner unit when the car is turned off, the CHUD has a Kinematics system that is connected to the combiner support, which allows this part to rotate or slide inside the CHUD unit when the car is off and make this part appear when the car is on, or if activated by the driver.

2.3 Combiner Unit

The combiner unit (Figure 13) is a subsystem from the CHUD. This subsystem will project the virtual image that the driver visualizes and is composed by two parts:

- The combiner
- The combiner Support

This part is connected to the system kinematics, in order to control the rotational position of this part. To fix both parts, a screw system can be used or the use of an adhesive is also a common solution. It is important to maintain both parts tightly fixed, without transmitting any kind of deformation from one to the other.

Figure 13 – BMW CHUD combiner unit

2.3.1 Combiner

The combiner (Figure 14) is the part that projects the virtual image that the driver visualizes. This part has a free form surface, meaning that requires a careful shape planning, in order to avoid image distortion or double image. Both surfaces of the part must have a certain shape and angle between each other, so the driver does not see a second image refracted by the back surface (the double image effect).

This part has to be transparent, to let the driver see through it but at the same time must reflect the projected image to the driver's eyes.

The combiner can be made out of different types of materials, as long as they are transparent. The most common used material is polycarbonate.

Figure 14 – Mini cooper combiner (Nica 2013)

2.3.2 Combiner Support

The combiner Support (Figure 15) is the part that makes the interface between the Combiner and the CHUD, more specifically with the CHUD kinematics system. To fulfill its purpose, this part requires a certain rigidity, to maintain the combiner always in the same shape. The precision and quality in this part must be high, because if there is some problem (for example a dimensional deviation), is very probable that might be transmitted to the combiner, and that can cause optical problems or even compromise the bond between both parts. Therefore, to accomplish this, the material must be rigid, and be geometrically stable in every conditions. The most common material are plastics, because they can fulfill the rigidity and precision required and at the same time is a cheap material.

This part must have a connection with the kinematic system that will depend on the type of kinematics system the CHUD has. Another important aspect are the guiding features, which are responsible for putting the combiner on its correct position. This design feature must be tight because, once again, the shape and positioning of the combiner is very important, and it cannot transmit deformations to the combiner.

Figure 15 – Combiner Support of the 2018 Ford focus

2.4 Photoelasticity

Photoelasticity is a method to measure and visualize internal stress in parts. This method is used to study the combiner internal stress in this work. This method is resorted in transparent parts like the combiner, although, if adapted it can be used to visualize internal stress in non-transparent parts.

2.4.1 Main Concepts

To understand the concept of photoelasticity, first is very important to understand the definition of polarized light, refractive index or index of refraction and birefringence.

Light propagates in every direction, and is a wave that vibrates in perpendicular planes from the direction of the propagation of the light beam. (Feingold 2002) When a beam of light passes through a polarizing lens or filter, all of the components of the light except the components with the same vibration as the polarizing filter, are filtered. Therefore, after the filter, the beam of light stays with a unidirectional vector of light so it is said that the light has been linearly polarized. That is shown in Figure 16. (B. Murphy, R. Spring e W. Davidson 2018)

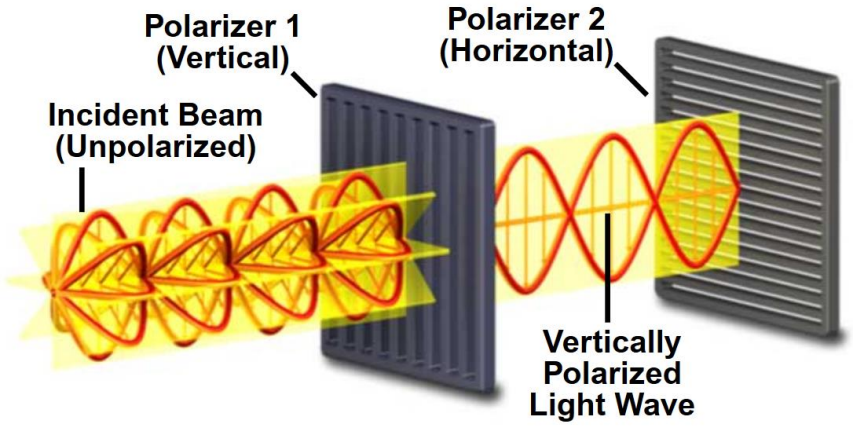

Figure 16 – Beam of light passing in a polarizing filter (B. Murphy, R. Spring e W. Davidson 2018)

Index of refraction is a dimensionless number that indicates how many times faster the speed of light in vacuum is comparing to the material in study. This value corresponds to the velocity of light in vacuum divided by the light velocity in the studied material.

Birefringence is an optical property in some materials whose index of refraction depends on the polarization and light direction. This means that a certain part has two index of refraction, that can be associated to the part or it can be induced by applying stress. In this case the directions of the indexes of refraction will be parallel to the orientation of the principal stress directions. The technic that analyzes the stress of materials by his birefringence properties is called photoelasticity. (Post 1989)

When light passes through a birefringent material, due to the two indexes of refraction, light will suffer a retardation which is associated to a light rotation. Figure 17 demonstrates the retardation in the light.

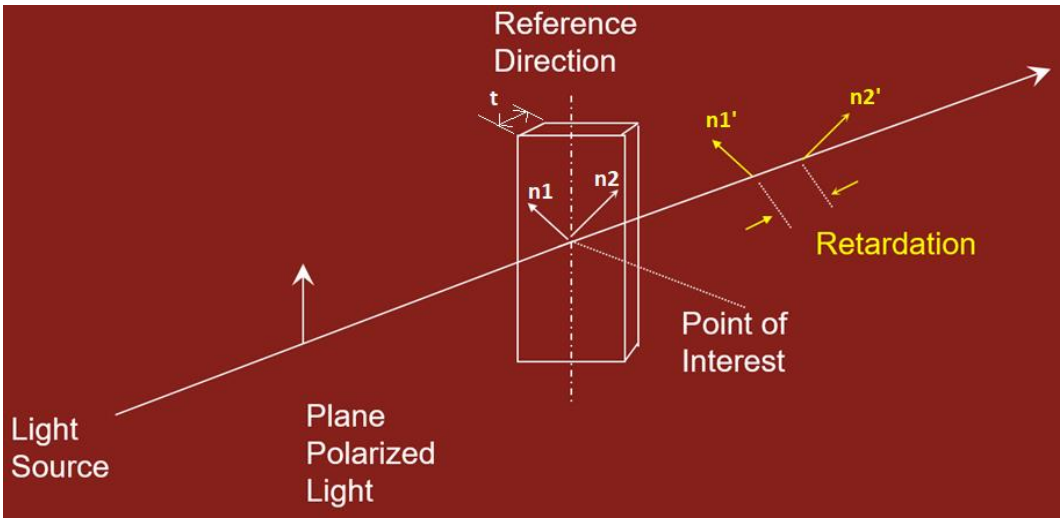

Figure 17 – Light retardation when passing through a birefringent material adapted from (Feingold 2002)

2.4.2 Stress measurement with photo elasticity

As the two different index of refraction have the same directions as the principal stress directions, there is a law called Brewster's Law, which correlates the index of refraction with the stress. (Feingold 2002)

$$(n_1 - n_2) = C_b * (\sigma_1 - \sigma_2) \quad 2.1$$

Where:

$(n_1 - n_2)$ = Indexes of refraction

C_b = Stress-optical constant in Brewster (is associated to the material)

$(\sigma_1 - \sigma_2)$ = Principal stress (MPa)

To measure $(n_1 - n_2)$, the following expression is used: (Feingold 2002)

$$(n_1 - n_2) = \frac{\delta}{t} \quad 2.2$$

Where:

$(n_1 - n_2)$ = Indexes of refraction

δ= retardation value (nm)

t= part thickness (mm)

Adding both expressions, the following expression is obtained: (Yeager 2010)

$$\sigma = \frac{\delta}{t * C_B} \quad 2.3$$

Where:

σ = stress (MPa)

δ= retardation value (nm)

t= part thickness (mm)

C_B = Brewster's constant (for Polycarbonate is approximately 84)

To be able to know the retardation value, a polariscope is used. A polariscope, is a device where a light source emits a beam of light through a first linear polarizing filter. Then the polarized light passes through the stressed part. This will create the retardations between vibrations. After passing the stressed part, the light passes through a second perpendicular polarizing filter, called analyzer. After passing the second filter, is visible in the stressed areas a color, which belongs to an interference chart or spectrum. That chart demonstrates the correspondence between the color and the associated light retardation. Figure 18 shows how the polariscope works. Figure 19 shows the polariscope setup used in this work.

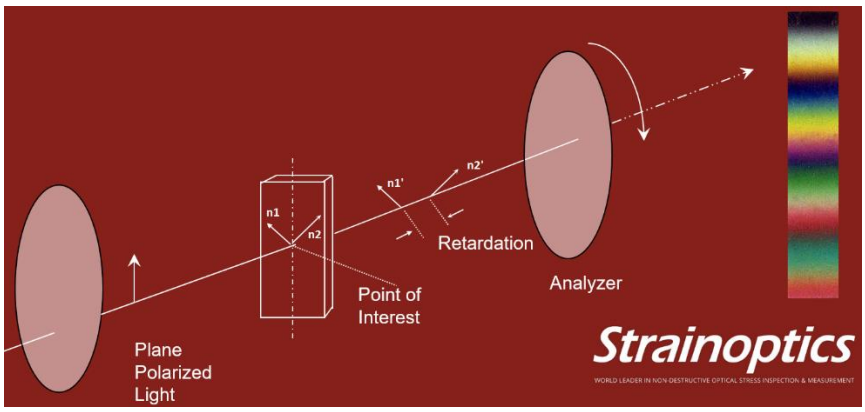

Figure 18 – Polariscope diagram adapted from (Feingold 2002)

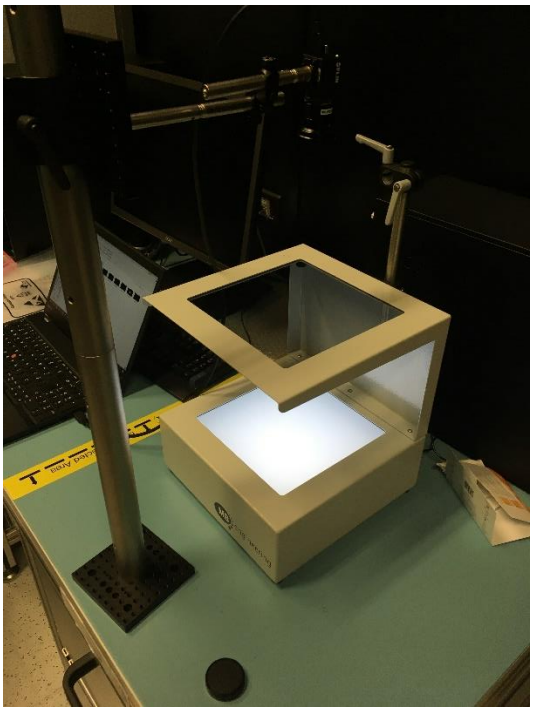

Figure 19 – Polariscope setup used in this study

3 Ford Focus Head-up Display Combiner Unit

In the Ford Focus CHUD, the combiner unit has only two components that are bonded together by an adhesive with no further kind of support. An epoxy resin glues both components. Figure 20 shows both components before the assembly, and Figure 21 shows the Combiner Unit assembled.

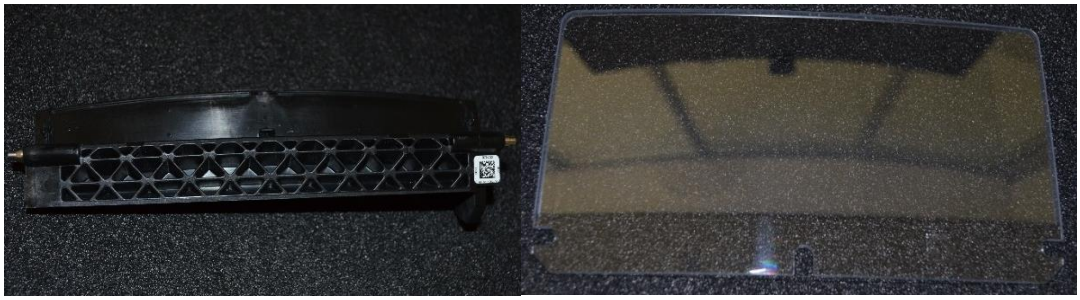

Figure 20 – Combiner Support (left) and Combiner (right) separated

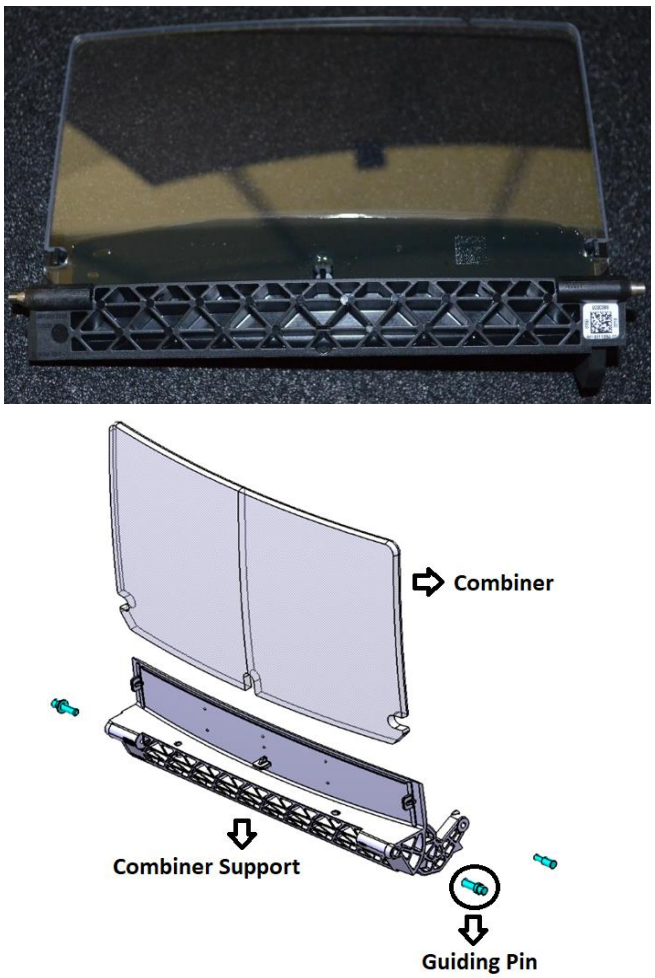

Figure 21- Combiner unit (on top) and an exploded view (below)

This part is assembled in the CHUD kinematics, as visible in Figure 22 and is located on the top of the unit. When retracted, a cover can hide this sub-system.

Figure 22 – Combiner Unit visible (left) and retracted (right) in the CHUD

3.1 Combiner

This part is made with Polycarbonate, since is an engineering thermoplastic which is a strong and tough material and is optically transparent. This part is made by injection and later is milled to the final shape. In Figure 23, the part can be seen before milling.

Figure 23 – Combiner before milling

In order to avoid scratches and to reflect some of the light, the part has two coatings. A hard coating that prevents scratches in the part and an optical coating that allows the part to reflect the image to the driver's eyes.

Polycarbonate (PC), offers very high impact strength and a high modulus of elasticity. This material absorbs very little moisture and has a very good thermal and dimensional stability. Also maintains rigidity up to 140 ˚C. Some problems with PC are the chemical and scratch resistance and its tendency to turn yellow upon long-term exposure to UV light. (federation 2018)

3.2 Combiner Support

Figure 24 – Combiner Support

The combiner support (Figure 24) is the part where the combiner will be glued. This injected part is made out of a glass fiber reinforced plastic.

In the CHUD, this part has to rotate in order to hide the combiner unit inside the CHUD. To be able to fulfill this, the part has three metallic pins that make the connection with the CHUD Kinematic system. Two of them are responsible for the support rotation axle and the third pin is responsible to make the rotation of the combiner unit. Figure 25 shows the combiner support pins.

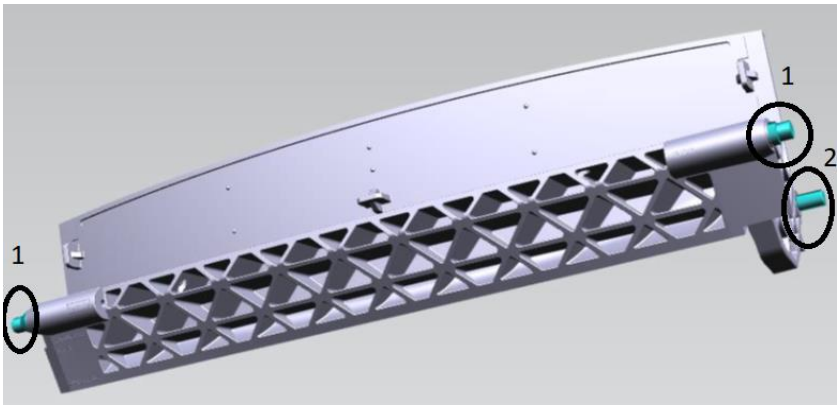

Figure 25 – The combiner support pins 1- Rotation pins 2- Guiding pin

This part requires a high rigidity and precision. At the moment this part faces some difficulties in the injection process, which creates dimensional problems.

Figure 26 – Combiner Support injection mold

The surface where the combiner is glued has some design features in order to maintain the combiner in a correct position. Those features are the lateral pads, the spheres, a grove to retain the excess of glue and the combiner position control elements.

3.2.1 Glass fiber reinforced plastic

Glass fiber reinforced plastic was the chosen material for this part because this type of material is lightweight, and it has a very good stiffness and strength (S. Rudzinski, et al. 2010). Also with this material, it is possible to achieve a good dimensional precision, which will be required to mount the combiner with low stress and without deforming its shape in order to accomplish very precise optical parameters.

The composition of the part material is chosen knowing that it must exist a compromise between the percentage of polyamide and the percentage of glass fiber. The addition of glass fiber increases the stiffness, the tensile strength and lowers the values of failure strain. Noticing that the percentage of glass fiber does not change the failure strain, except if it is zero percent. In this case, the polyamide has a ductile behavior. This means that after the addition of glass fiber in this material, will make it behave just in an elastic way. A study performed by B. Mouhmid, (B. Mouhmid, et al. 2006) shows the result of adding glass fiber in the polyamide, in terms of strength, strain, and failure strain. In his study it is compared Polyamide 66 with 0% of Glass fiber, 15%, 30% and 50% (Figure 27).

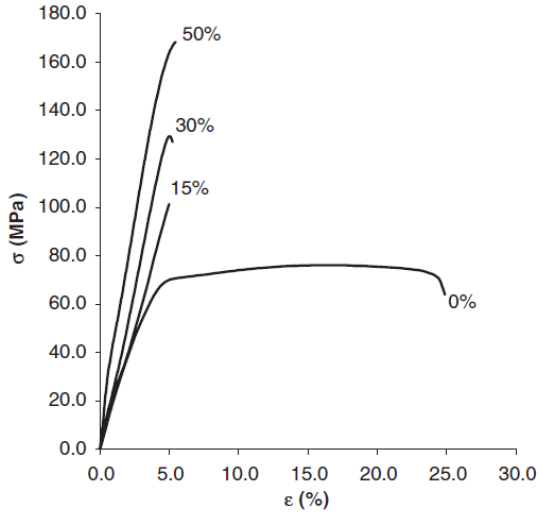

Figure 27 – Stress –strain curves with different glass fiber ratios at 20˚C (B. Mouhmid, et al. 2006)

As Figure 27 shows, with the addition of glass fiber, there is a sudden loss of ductility, but with 50% glass fiber, the gain in maximum stress is more than the double.

Analyzing the material behavior with the temperature, and examining the curves in Figure 28, it is visible that the addition of glass fiber to the polyamide 66, increases the normalized tensile strength and that is valid with the increase of temperature. In addition, Figure 28 shows that with the temperature increase, the normalized tensile strength decreases. This is valid for the four samples in study.

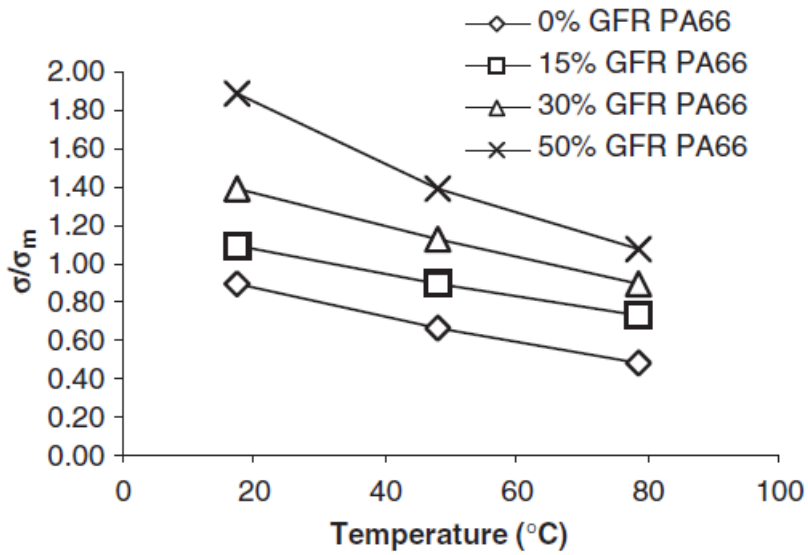

Figure 28 – Normalized tensile strength versus temperature with 0%, 15%, 30% and 50% Glass fiber reinforced Polyamide 66 (B. Mouhmid, et al. 2006)

Figure 29, shows that the addition of glass fiber to polyamide reduces the material ductility, and makes the failure strain constant through the temperature increase. This ductility reduction is also visible in Figure 27.

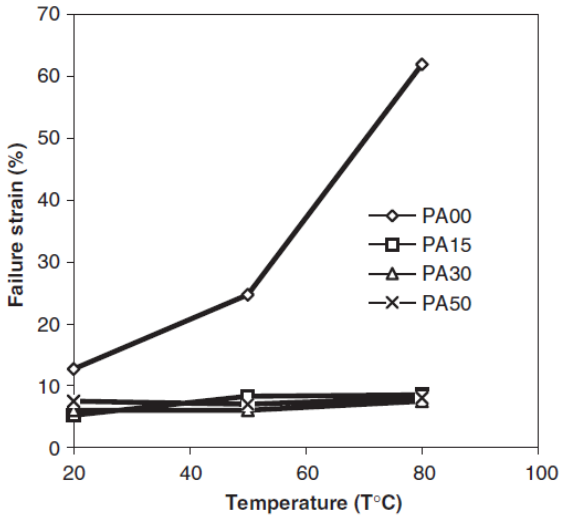

Figure 29 – Effect of temperature on failure strain (B. Mouhmid, et al. 2006)

Figure 29 demonstrates, that the addition of glass fiber keeps the failure strain approximately constant and lower, when the temperature raises when compared with no addition of glass fiber. At the same time, the failure strain between 15%, 30% and 50% is similar.

To conclude, the addition of glass fiber reduces ductility and increases the stiffness and the tensile strength. The percentage of glass fiber will not make difference in the ductility but it will

influence the stiffness and the strength. The addition of glass fiber, allows to make a part with the same stiffness using less material, comparing with a part with less glass fiber.

The main problem with the introduction of glass fiber is that it increases the wear in the tool. (F. J. G. Silva, et al. 2011) As this material is going to be used in a production part, the tool wear must be controlled. If the tool starts to degrade the part quality also degrades, therefore there are some treatments that are required in the mold. The most common treatments are nitriding the mold and add coatings like PVD or CVD. In Figure 30 is visible the mold used in the production of the combiner support.

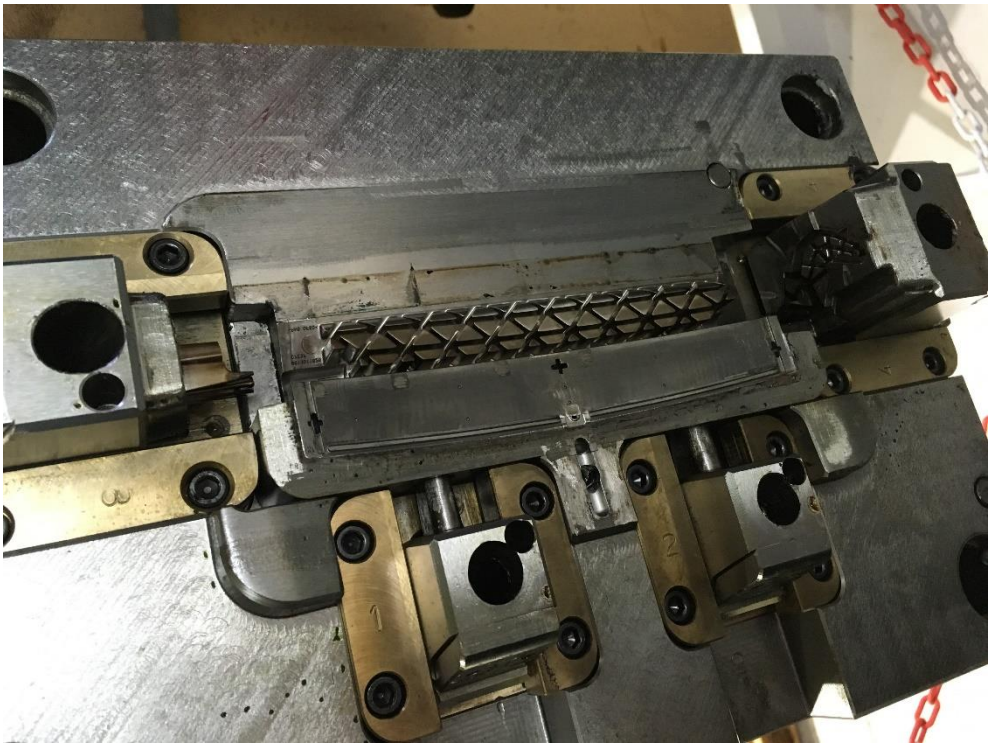

Figure 30- Combiner support injection mold

3.3 Adhesive

To bond the combiner to the support, it is used only an adhesive. A common type of adhesive used in the automotive industry is the epoxy resin. This type of adhesive is very common in this industry because of his versatility (it can be used in many types of substrates). Another advantage of this type of adhesive is the excellent resistance to tensile and shear stress. Since this part will be exposed to the air, it is also important that the adhesive is resistant to humidity and solvents. There are two types of epoxy resins: the single part epoxy adhesives, which is composed by an epoxy resin that is cured by an exterior agent (like and UV light) or it can be separated into two part epoxy adhesive, that is composed by the epoxy resin and an hardener. We will use a single part, so below in table 1 there are some characteristics of this kind of epoxy. (Silva, Magalhães e Moura 2007)

Table 1- Single part epoxy resin characteristics (Silva, Magalhães e Moura 2007)

Service temperature	-40 to 100 ˚C
Advantages	Resistance and durability
Disadvantages	Product storage
Resistance to the environment :Oil, Water, Solvents	Good; Good; Good
Health and safety	Can cause skin and breathing problems
Applications	Airplanes, helicopters, cars, trains…

In terms of the gluing process, this type of adhesive is chosen because it is very good in gap filling, which creates a smoother gluing surface. Despite the versatility of this adhesive, it is not very effective when applied to polymers due to the low surface energy. So in order to use this kind of adhesive on a polymer, is required to do a surface treatment which in this case is a plasma treatment. This increases the surface energy, and the adhesion.

The main problem with the epoxy resin, is that despite the good resistance to shear and tensile stress, this adhesive is not very adequate to endure peeling. In order to solve that problem is normally applied what is called a modified epoxy resin which is the type of adhesive used in this part.

This kind of adhesive has a polymer mixed with the epoxy resin in order to improve certain some characteristics of the epoxy resin. (Silva, Magalhães e Moura 2007)

Table 2- Comparison of an epoxy with and without rubber modifications (Silva, Magalhães e Moura 2007)

Properties	**Non modified epoxy**	**Modified epoxy**
Young modulus (GPa)	3,2	2,8
Rupture stress (MPa)	63	58
Maximum strain (%)	5	9
Shock toughness (J/m)	0,7	3-5

4 Combiner Unit stress and geometry analysis

This chapter is dedicated to study the geometric stability of the Combiner Support, and the stress and deformation that is caused by the gluing process in the Combiner.

As at it is described is chapter 3, the combiner and the combiner support are glued together and due to deviations in both parts, in comparison to their nominal dimensions, these parts have different shapes in their surfaces. This will make the less rigid part (in this case the combiner) to deform and adapt his shape to the combiner support shape, which will create not only deformations in the combiner, but also install internal stress in it. This shape alteration in the combiner will cause deformations and insert stress in the combiner. The deformation can cause optical problems (Figure 31) and the stress might cause adhesive failure (Figure 32) which will be studied in this chapter.

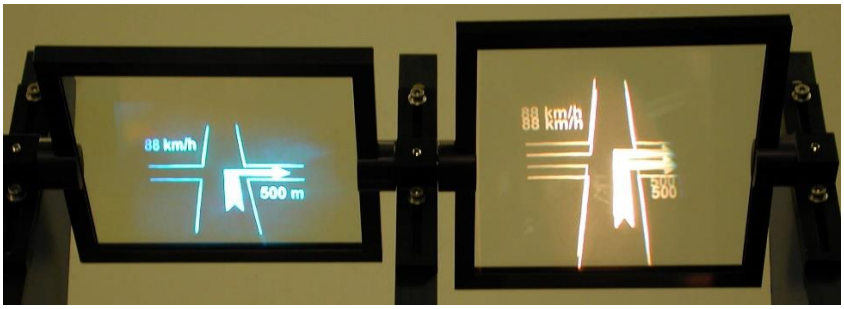

Figure 31- HUD double image effect (BLANCHE 2018)

A study was made where parts were submitted into different temperature and humidity conditions to understand how the internal stress could be related to the adhesive failure. Also in this chapter, it was demonstrated the internal stress and deformation, induced by the gluing process.

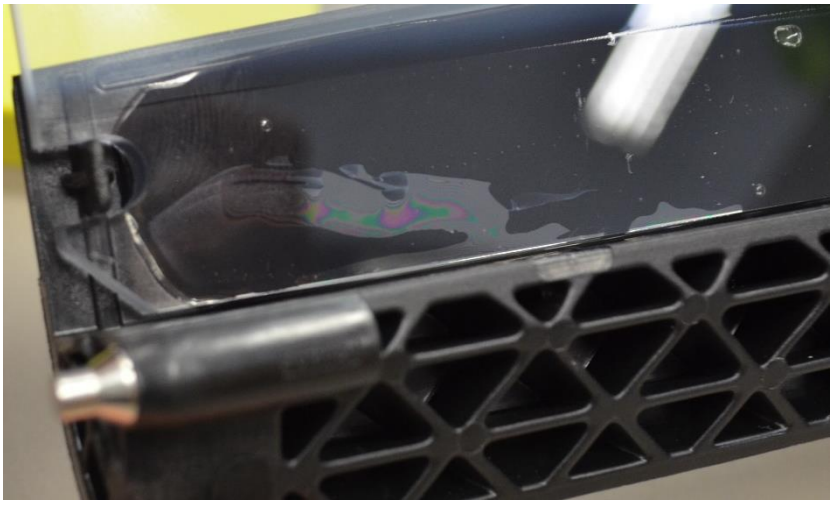

Figure 32 – Adhesive failure

In this work, the studied causes were the geometric stability of the combiner support when submitted to different conditions of temperature and humidity. For the combiner, the studies made had the purpose of creating a correlation between the internal stress and the areas where the adhesive failed.

4.1 Combiner Support measurement and geometric stability analysis

To analyze the combiner support dimensions, a batch of parts was taken to the Bosch Car Multimedia measurement Lab, where those parts were measured using a CMM machine.

To study the geometric stability of the part, two studies were made to understand how the combiner support behaves when submitted to humidity and heat, like it can happen in a car. The humidity test, had the goal of verifying if the Combiner Support when submitted to humidity would create a dimensional variation. As for the heat test, the purpose was to comprehend if the residual stress release, could make the part change his shape.

For the first analysis, a set of five parts was taken to the lab to be measured.

The points measured by the CMM machine belong to the surface displayed in Figure 33. For confidentiality reasons the exact points cannot be marked.

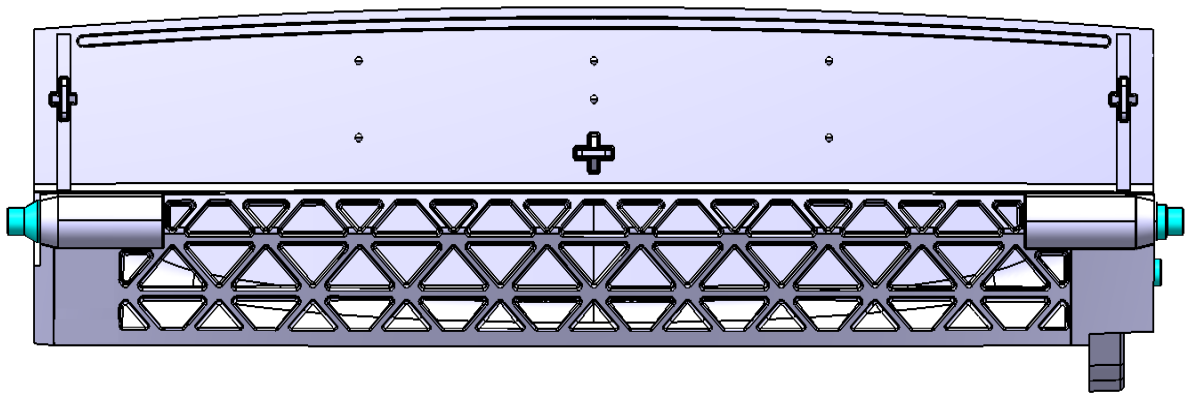

Figure 33- Front view of the Combiner Support

The points are divided into two groups: the points M, that are points in the glued surface and the P points that are more critical and have tighter tolerances. The six graphs (Figures 34 to 39), are in mm and they measure the difference to the nominal dimensions of the combiner support. For confidentiality, reasons the side scale was hidden.

The P and M points have different tolerances due to their shapes. Those tolerances were calculated based in the norm “DIN16742:2013-10 for plastic molded parts tolerances as symmetrical limit for dimension sizes”.

In the first test, the set of parts was measured, then it was taken to an oven to do a thermal cycle at 85˚C during 48 hours, and then they were measured again.

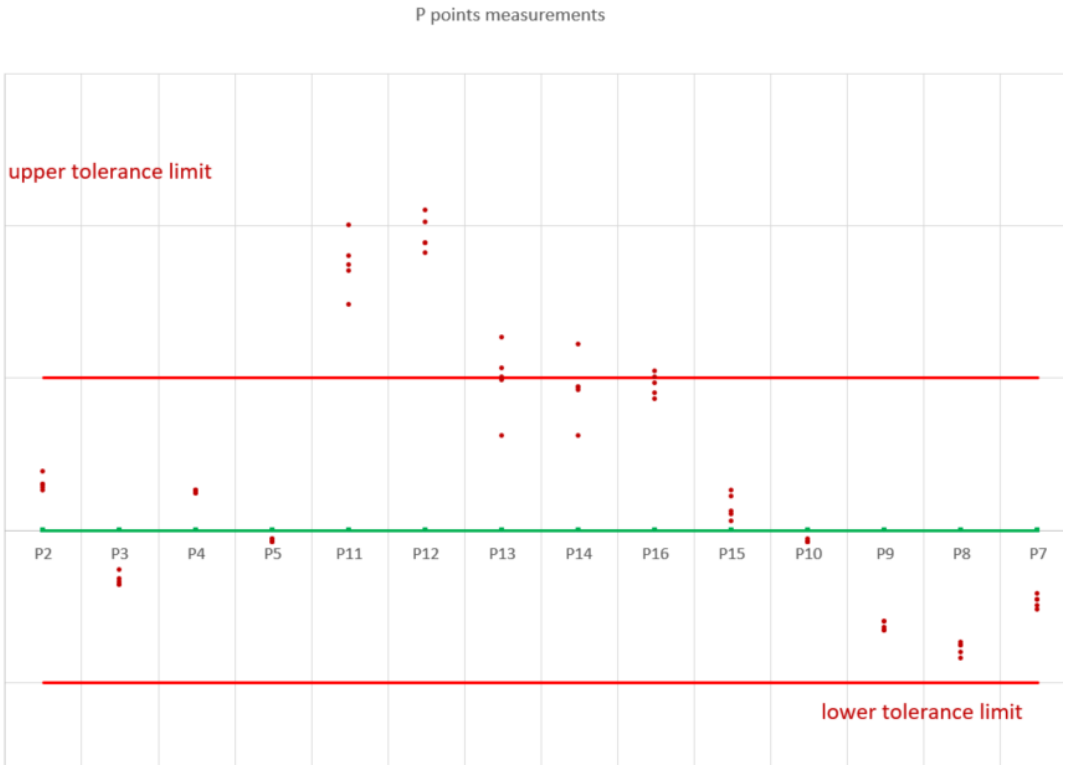

Figure 34- P points (in mm) of the set of five parts before going to the oven

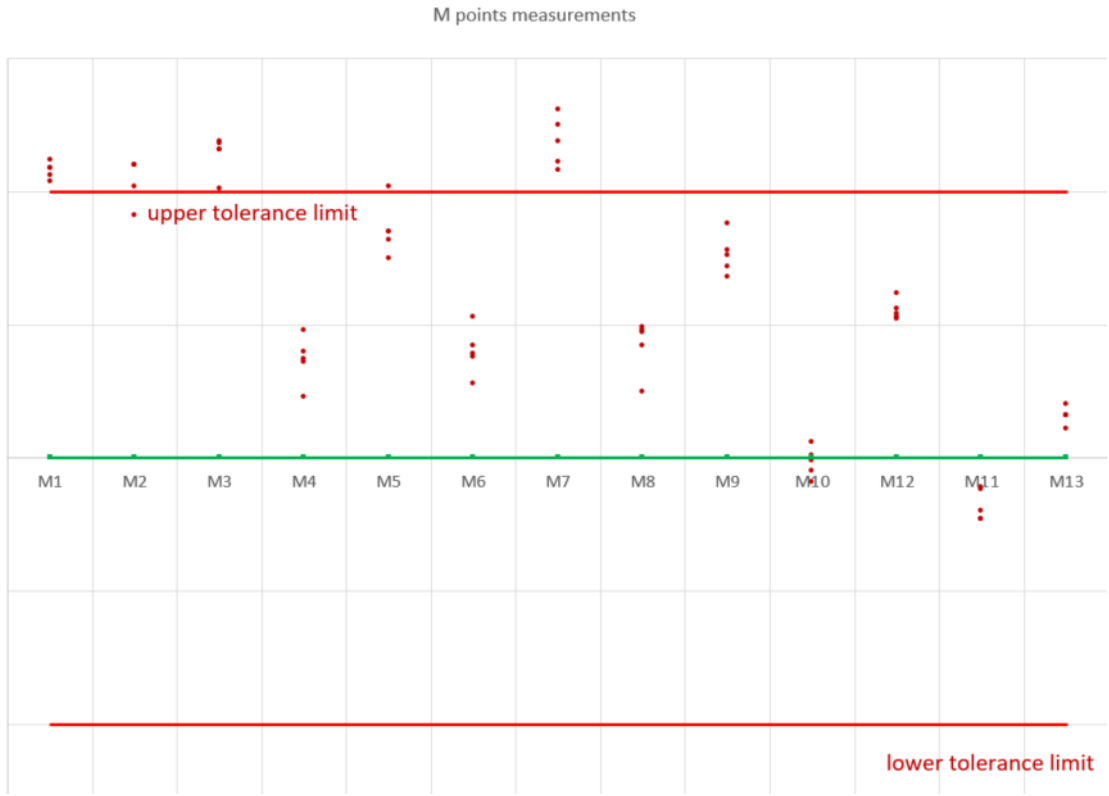

Figure 35 – M points (in mm) of the set of five parts before going to the oven

As Figure 34 and 35 shows, points P11 and P12 dimensions are out of specification in our sample, as for points P13, P14 and P16 dimensions are very close to the tolerance limits and in some parts are even out of specification. In the M points, the problem is the same for points M1, M2, M3, M5 and M7 (especially M7) the dimensions are very close to the defined tolerance (and in some parts is even out of specification).

After these measurements, the parts went to an oven at 85˚C for 48 hours. The second measurements were made 24 hours after the parts were taken from the oven. The results are in Figure 36 and 37.

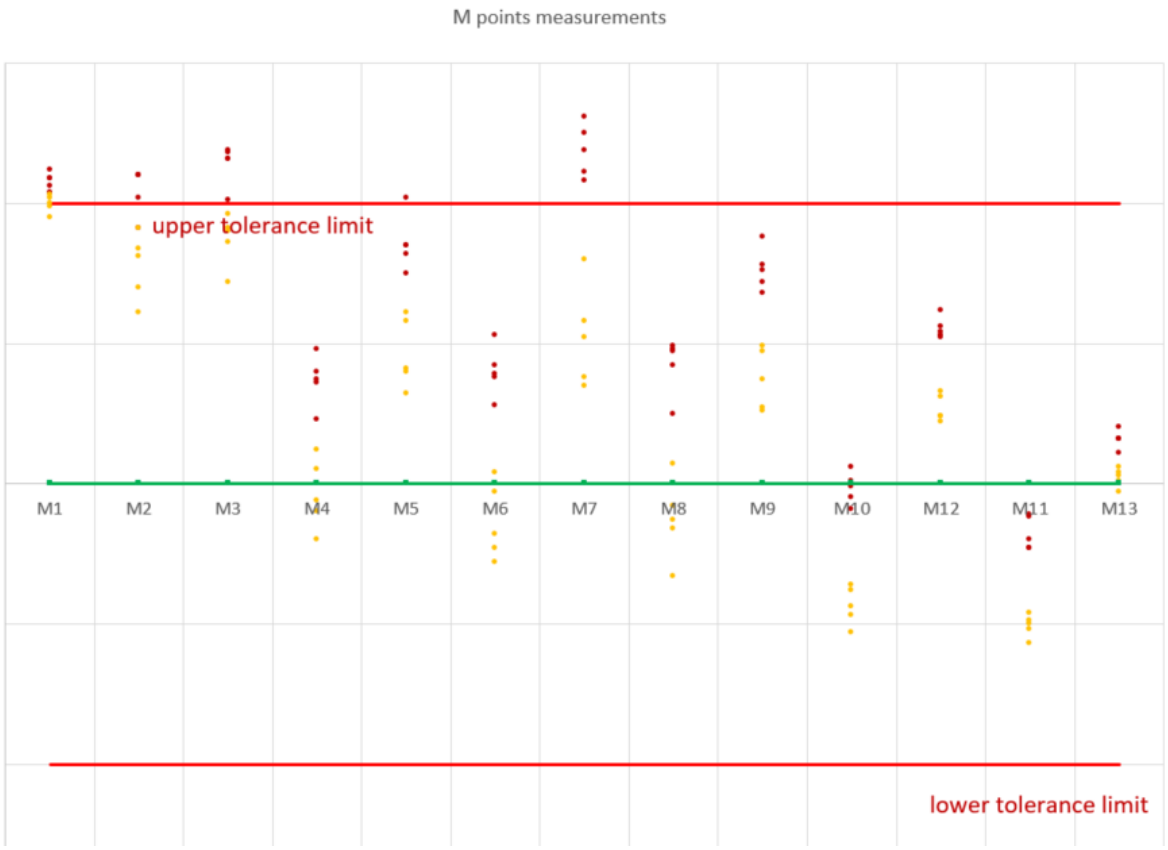

Figure 36 - M points (in mm) measurements after the oven 24 hours later in Yellow and in Red the measurements before the oven

The results in Figure 36 and 37 show, the measurements of the parts after the oven test. The analysis of these results show that the measurements approximate towards the nominal values. Despite some points still being out of tolerance, the dimensions approached the nominal ones. At the same time this test shows that the part can change his dimensions when submitted to high temperatures (a scenario that is possible for example when you leave a car exposed to the sun in a hot day), which can create stress in the glue and in the combiner, and later lead to adhesive failure.

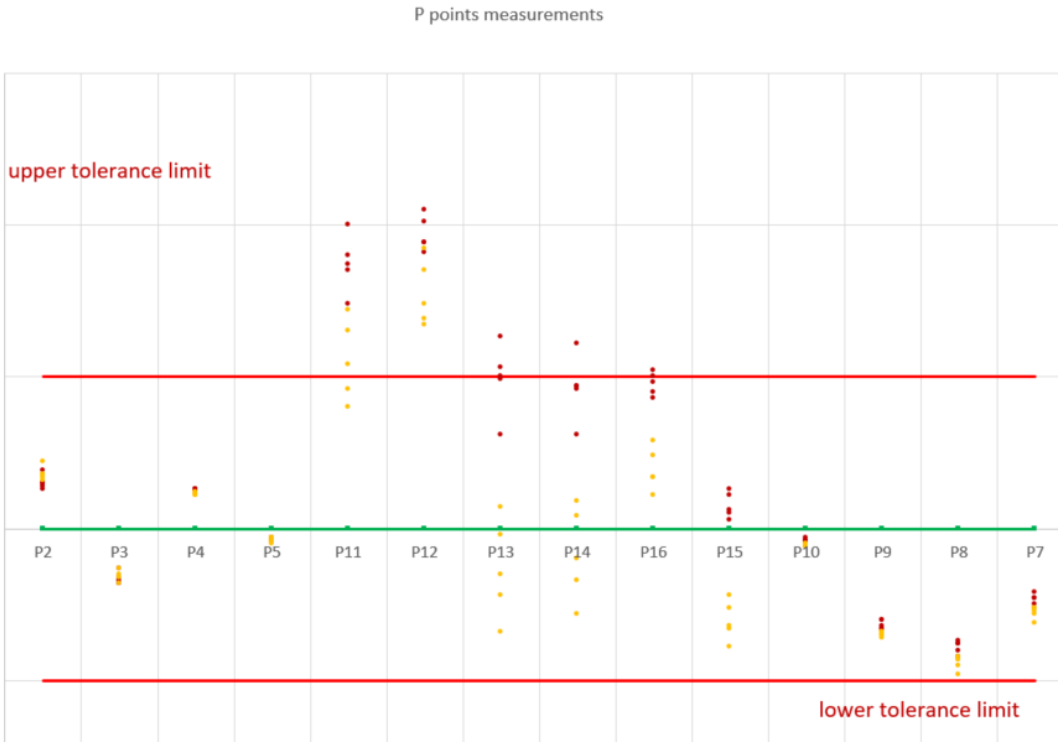

Figure 37 – P points (in mm) measurements after the oven 24 hours later in Yellow and in Red the measurements before the oven

After the temperature test, the next test had the purpose of knowing the effects of humidity in the part. So, 18 parts from the same injection batch were used. Nine of those parts were immersed in water for 24 hours and then dried with a cloth and measured, and the other nine parts were measured in the same conditions they were taken from the production line to be the reference units. Results are in Figure 38 and 39.

As the results show, no significant differences between the reference parts and the water immersed ones. Therefore, we can conclude that the exposure to the humidity (in these conditions) did not create a difference in part geometry.

After these two studies, it is now possible to have a better comprehension of the geometric stability of the combiner support, and know the conditions where the part can induce deviations in the combiner, and weaken the bond. Analyzing the peak-to-peak deviations of all the parts in this study, the range of values is between 150 μm and 344 μm.

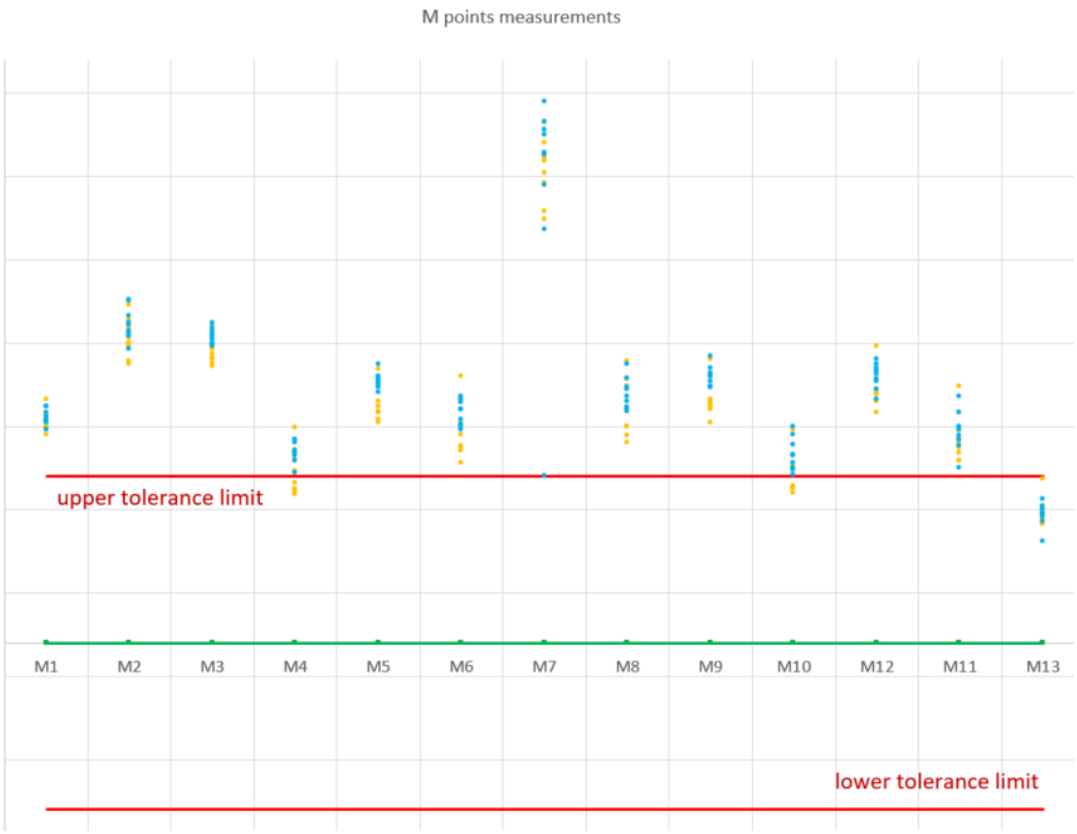

Figure 38 – M points (in mm) measurements of the humidity test (in Blue the parts in water and in Yellow the reference parts)

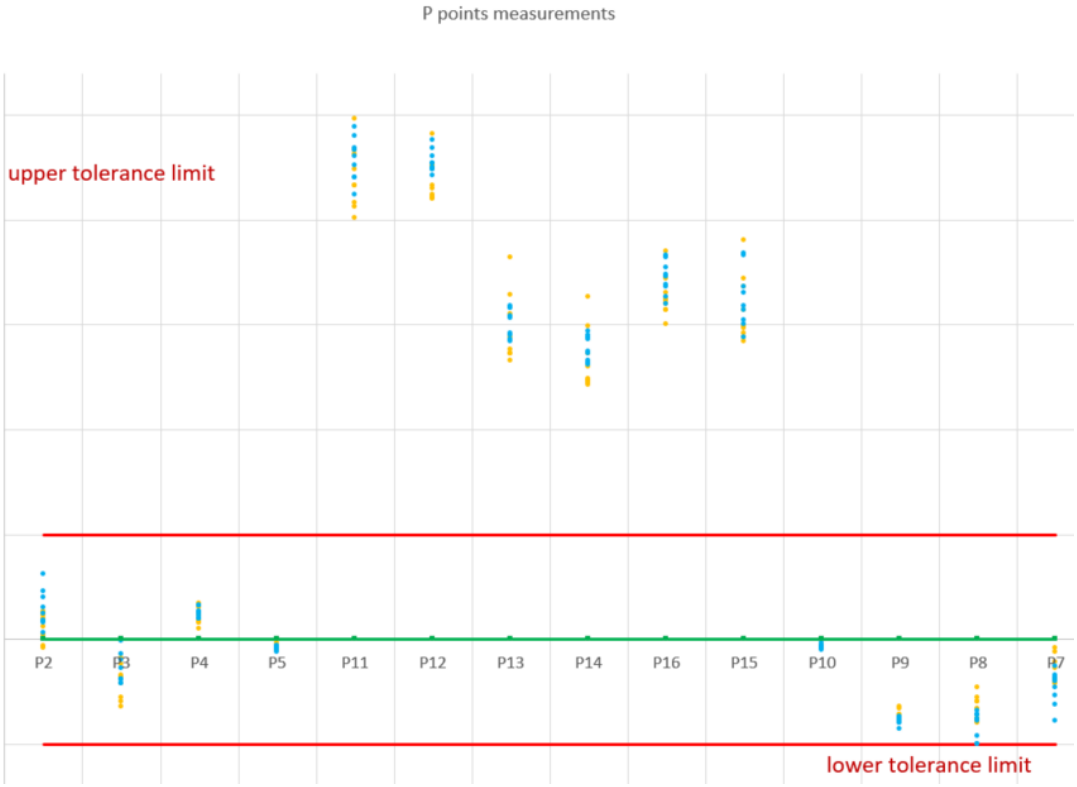

Figure 39 – P points (in mm) measurements of the humidity test (in Blue the parts in water and in Yellow the reference parts)

4.2 Combiner stress and geometry analysis

In this section, it is made an analysis of the deformations and the internal stress induces after the gluing process. To make this study, the combiner shape and internal stress will be analyzed before and after the gluing process. Knowing the impact of the gluing process, in the deformation and especially in the stress, later on it will be able, to study the correlation between the internal stress and the adhesive failure.

4.2.1 Combiner geometry analysis

To analyze the deformation induced, in the combiner, during the gluing process, it was used a 3D scanner machine (Figure 40). A Matlab code (made by Bosch) treats the information, provided by the 3D scanner, and shows several graphics with the height deviation profile, slopes and torsions, comparing the measurements with the nominal CAD. To this study, only the deviation profiles were considered. The deviation profile is in comparison with the nominal CAD from the combiner as Figure 41 shows.

Figure 40 – 3D shape measuring setup

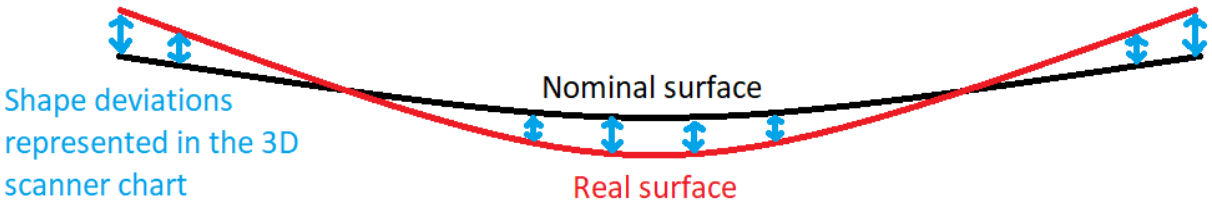

Figure 41 – Representation of the data displayed by the 3D shape

To study the influence of the gluing process in the combiner geometry, three combiners (fulfilling the specifications) were selected to be glued into combiner supports from the production line. In Figures 42, 43 and 44, are the 3D scanner data, for the deviation profile, of the combiners before assembling. In Figures 42 to 47 the color scale bar on the right is in mm and the text results are in µm. The peak-to-peak valleys are in µm.

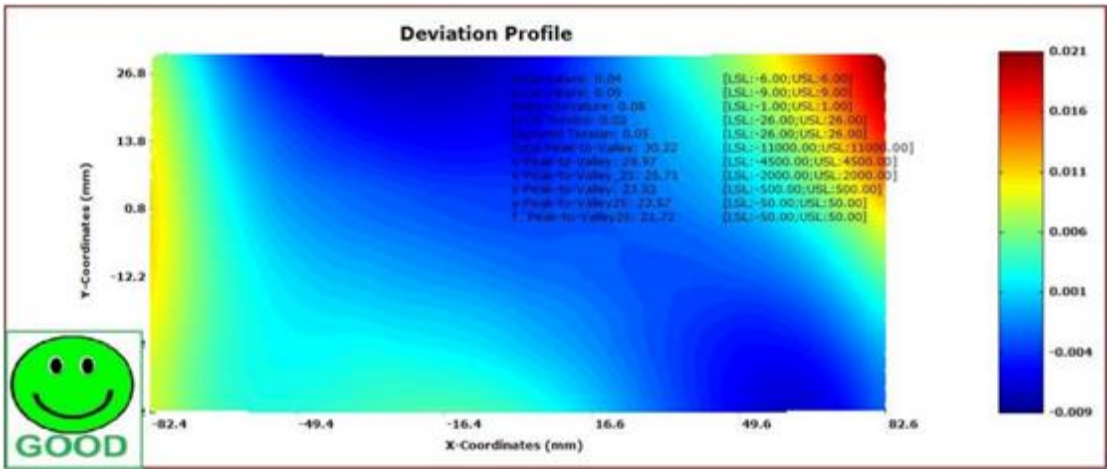

Figure 42 – 3D shape of the combiner 1 before gluing

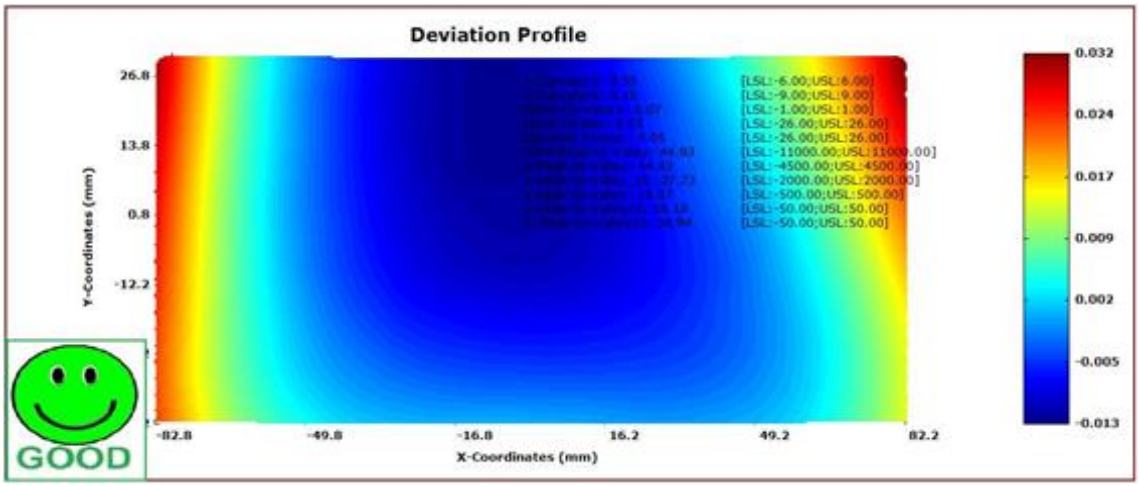

Figure 43 - 3D shape of the combiner 2 before gluing

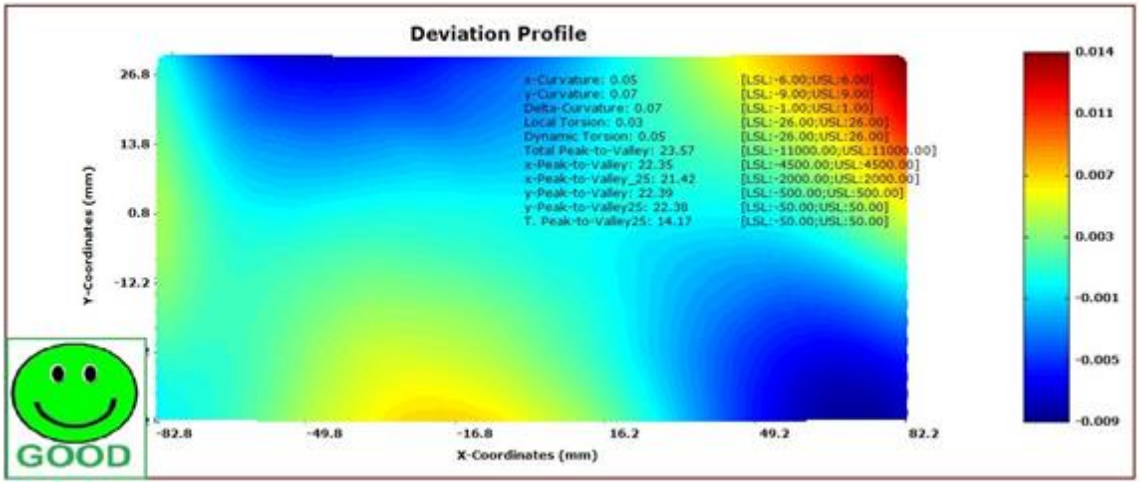

Figure 44 - 3D shape of the combiner 3 before gluing

The three combiner's, before the assembling process, showed a peak-to-peak valley (the delta of maximum and minimum deviations), between, 23.57 and 44.93 μm, which fulfills the specifications. Although it is visible in the three parts that they have small deviations to the nominal shape, they show different deformation patterns in the chart. After the measurements before the gluing process, the combiners were taken to the production line, and were glued. After this procedure, the combiner units had their shapes again measured, and the results are in Figure 45, 46 and 47.

Figures 45, 46 and 47 shows that after glued the deviation profile patterns become much more similar, which can indicate that the combiner support is in fact inducing geometric changes in the combiner.

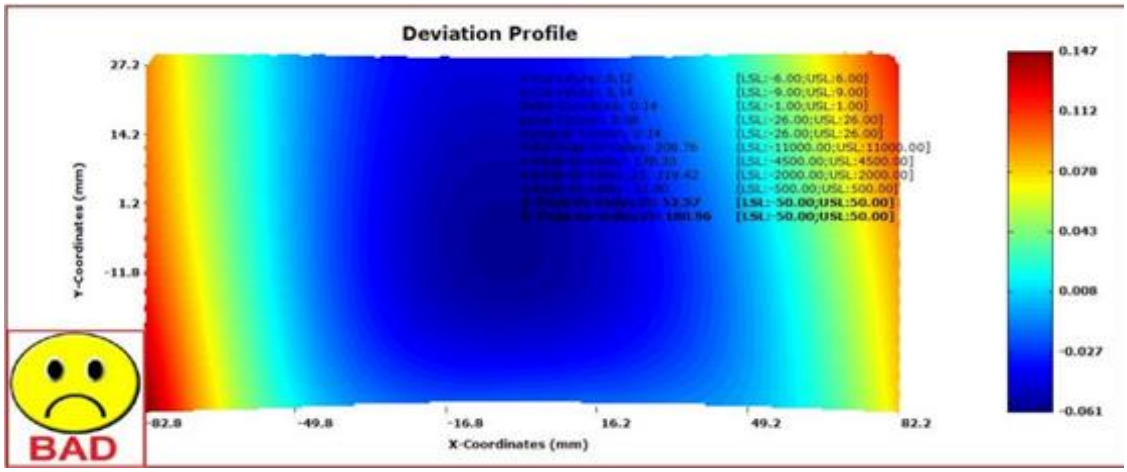

Figure 45 - 3D shape of the combiner 1 after gluing

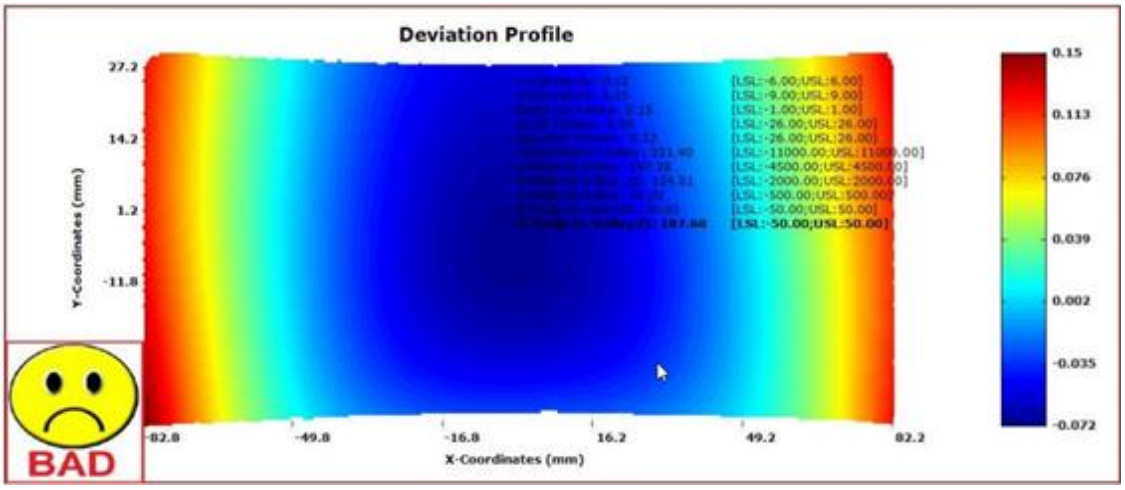

Figure 46 - 3D shape of the combiner 2 after gluing

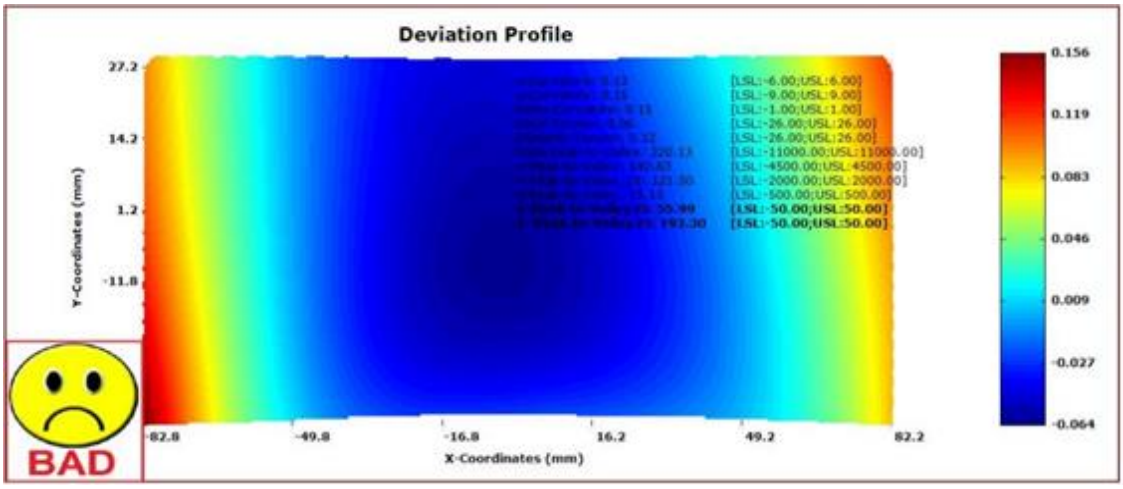

Figure 47 - 3D shape of the combiner 3 after gluing

Analyzing Figures 45, 46 and 47, the peak-to-peak valley has raised from a range between 23.57 and 44.93 micrometers to a much more significate range between 208.76 and 221.40 μm. This means that the peak-to-peak is now 6 times higher then the combiner before being assembled to the support. Also the peak-to-peak deviations are inside the range of deviations from the combiner support (section 4.1) which can indicate that the combiner support might be the responsible part that induces the deviations in this sub-system. This change of shape in the combiner, can cause optical problems and make the combiner unit be rejected in the production line.

4.2.2 Combiner stress analysis

To analyze the stress in the combiner, it was used photoelasticity. This method gives fast results and show the stress distribution in the part. However, without a complex setup it will not be possible to measure stress very precisely.

The used setup was a simple plane polariscope with two linear polarizers.

Before measuring the stress in the glued combiner, the single combiner was analyzed to see the stress in the part before the gluing process. As this part is made by injection, it has residual stress. In Figure 48 and 49, there is a single combiner in the polariscope, where stress is visible. Pictures were taken with a 32 bit RGB camera. The polariscope was configured to be in black field (it filters all the light, so the stress is detected in the white spots). The black-field setup was used because is more sensible to stress changes.

To determine the internal stress, before gluing, two single combiners (Figures 48 and 49) were taken from the production line (fulfilling the specifications).

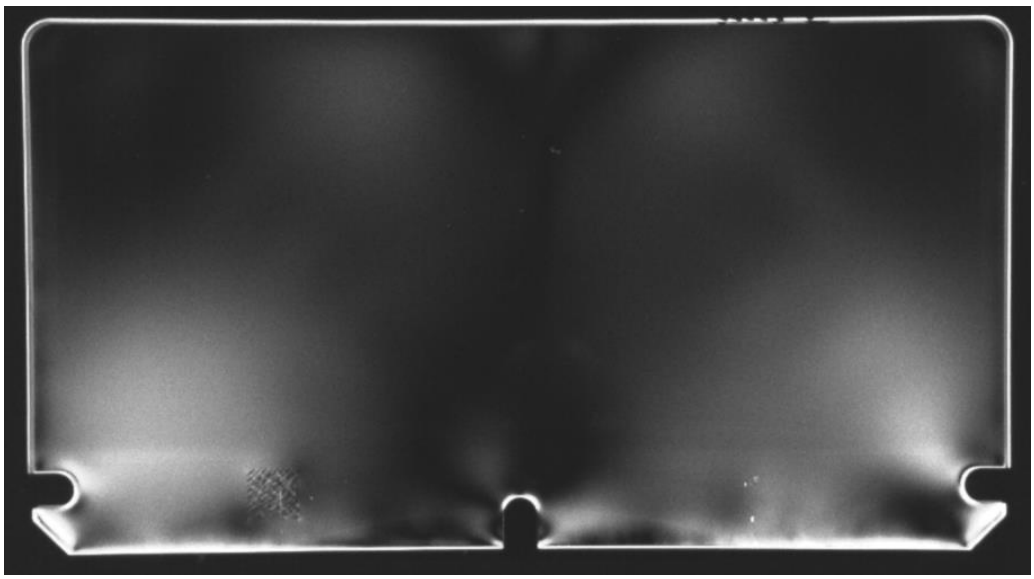

Figure 48 – Single combiner number 1 in the polariscope

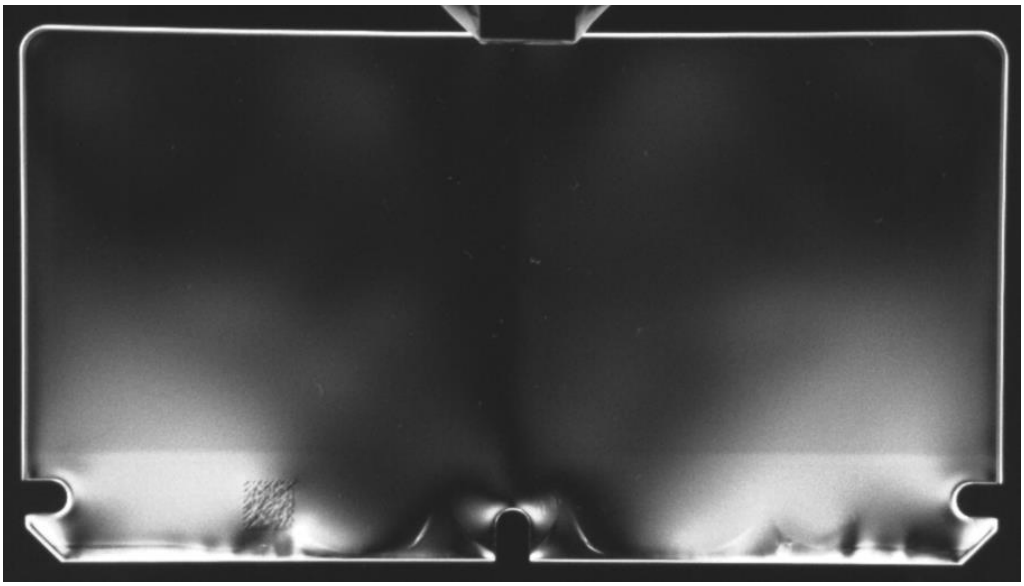

Figure 49 – Single combiner number 2 in the polariscope

Figure 48 and 49 show the stress of both combiners which have different intensities and distributions of residual stress. Another aspect that can be visualized is the induced stress due to the milling process. The combiner number 1 has an inferior stress intensity, despite having more stress distributed to all the part. In both parts, the stress in very low as shown later in this section.

To study the influence of the gluing process, a batch of 14 combiners were taken to the production line where they were glued into combiner supports. As it happened in the deformation analysis (Figure 42 to 47), after being glued, all the combiners stayed with a similar stress pattern. At the same time is visible that now there are stressed areas that were unstressed before the gluing process, which proves that the combiner support in fact, inducing stress into the combiner. In Figure 50, 51 and 52 are three examples from the 14 parts batch, in the polariscope. These three examples were chosen because they have different stress intensities, and make a good comparison.

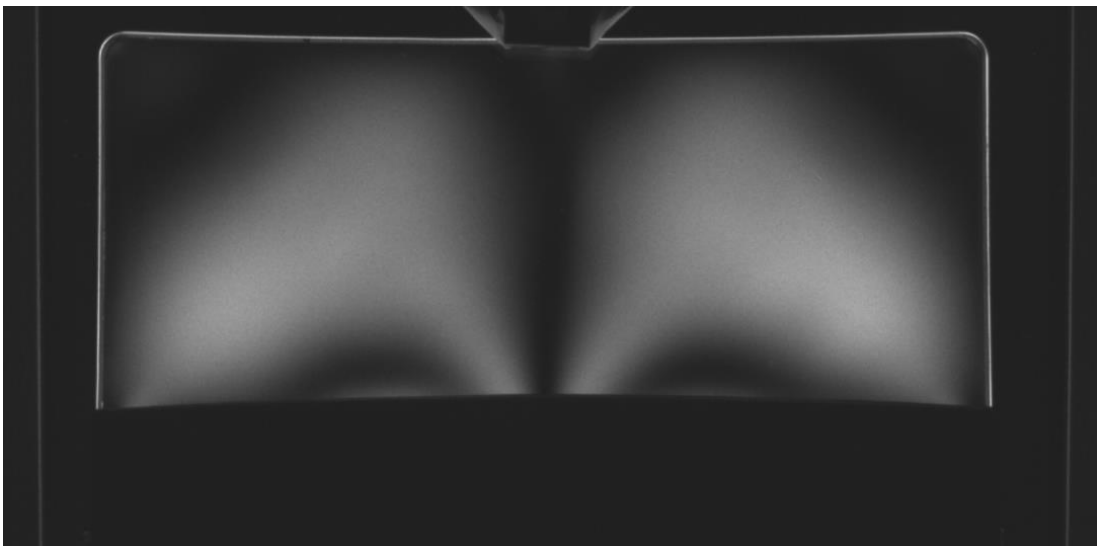

Figure 50 – Combiner unit number 1 (less stressed)

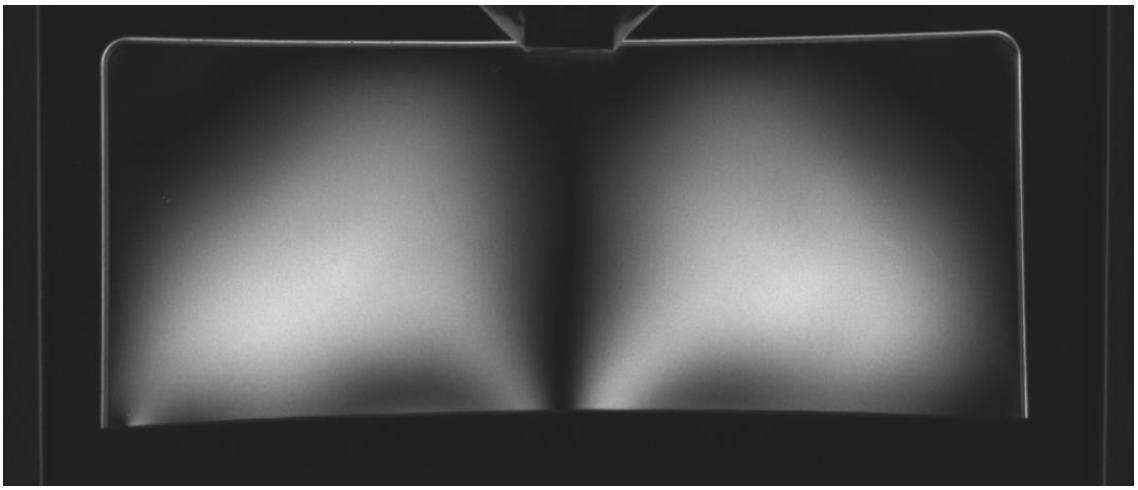

Figure 51 – Combiner unit number 14 (médium stress)

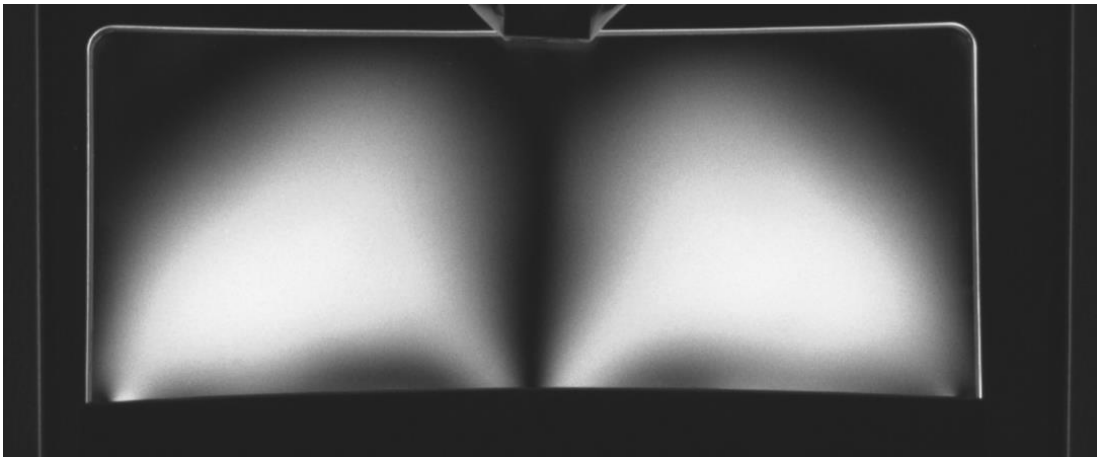

Figure 52 – Combiner unit number 17 (very stressed)

As the stress distribution and intensity are a subjective analysis, the combiner stress has been measured. As it was said in section 4.2.2 the used setup was not very precise (especially in low values of stress). However, it was enough to give values that could be used for comparison between different combiners.

To measure the stress, the studied parts were inserted in the polariscope, and then to calculate the stress with the polariscope picture, the following formula (Yeager 2010) was applied:

$$\sigma = \frac{\delta}{t * C_B} \quad 4.1$$

Where:

σ = stress (MPa)

δ= retardation value (nm)

t= part thickness (mm)

C_B = Brewster's constant (for Polycarbonate is approximately 84) (Yeager 2010)

The combiner has an approximate constant thickness of 3.3mm. To know the retardation value, the color in the picture must be analyzed. To measure the light retardation, was used an Interference color chart . The Figure 53 shows the Michel Lévy interference color chart (Magnus 2011), that correlates the color in the part with the light retardation. If the part has zero stress, it will be completely black (0 light retardation). The stress in the part, is visualized by a color alteration that it can be seen in the polariscope.

In the stressed glued combiners can be seen that the range of colors that is between black (0 nm of retardation) and a very intense white that corresponds to an approximate 250 nm of light retardation.

With this analysis made, now is possible to estimate the stress in some points. In Figure 54, is represented the combiner 14 from the polariscope pictures, with 3 points indicated. The stress will be calculated in those three points to give and idea of the magnitude of the stress in the part.

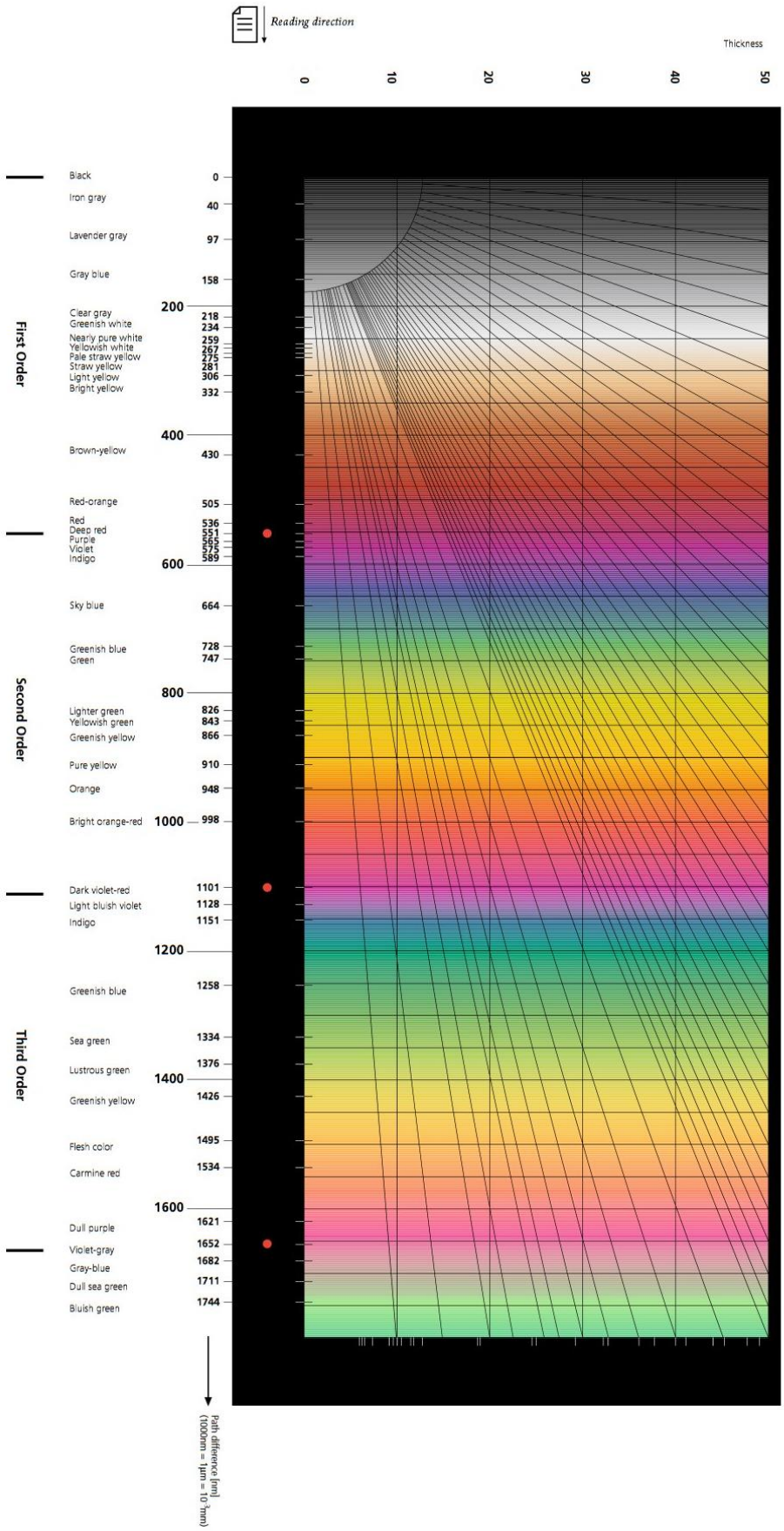

Figure 53 – Adapted from Michel-Lévy interference Color Chart (Magnus 2011)

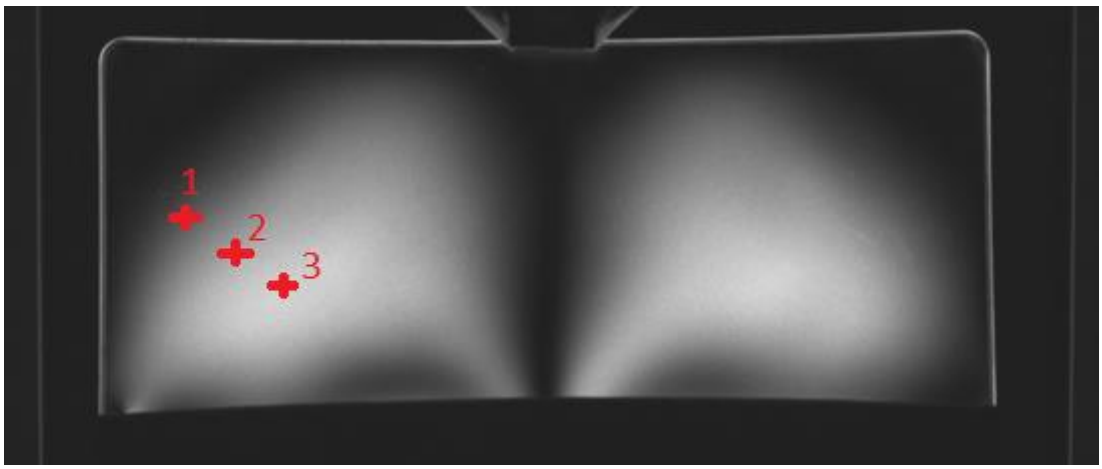

Figure 54 – Combiner unit 14 with 3 points indicated for analizys

Stress calculation for point 1:

δ ≈ 80 nm (dark gray)

t = 3.3 mm

$C_B \approx 84$

$$\sigma = \frac{80}{3.3 * 84} = 0.29\ MPa \quad (4.2)$$

Stress calculation for point 2:

δ ≈ 150 nm (light gray)

t = 3.3 mm

$C_B \approx 84$

$$\sigma = \frac{150}{3.3 * 84} = 0.54\ MPa \quad (4.3)$$

Stress calculation for point 3:

δ ≈250 nm (white)

t = 3.3 mm

$C_B \approx 84$

$$\sigma = \frac{250}{3.3 * 84} = 0.90\ MPa \quad (4.4)$$

These values show that, despite the combiner support increases the stress intensity and distribution in the combiner, the stress value remain low especially when compared with the glue capacities.

4.3 Combiner unit problem analysis

The deformation and the stress studied in section 4.2 can cause two types of problems in the combiner unit: Optical problems and mechanical problems.

The optical problems are related to the combiner deformation: image distortion (visible in Figure 55 (Scollar 2011)) and lack of homogeneity in the image. The optical problems are detected in the production line.

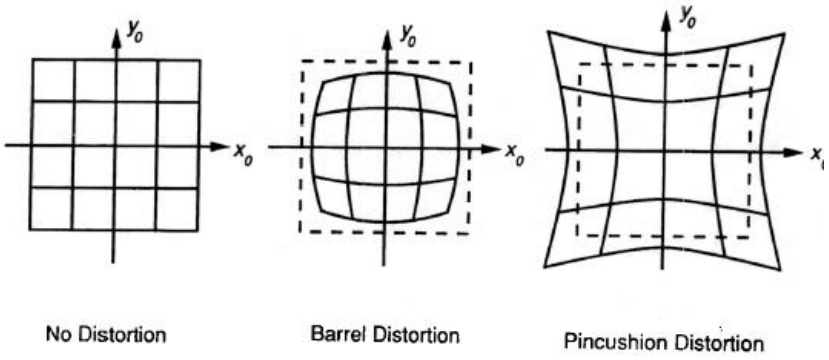

Figure 55 – Image distortion (Scollar 2011)

The most significant mechanical problem caused by stress and deformation in the combiner is adhesive failure. To understand the correlation between the combiner internal stress and the adhesive failure, the fourteen combiner units glued in section 4.2.2 were taken to an oven to make a thermal cycle for 48h at 85˚C (Figure 56). These conditions caused delamination, as the Figures 58, 61, 64 and 67 show. This way it was possible to compare the adhesive failure with the internal stress before the thermal cycle. After the thermal cycle, the batch of parts was analyzed again in the polariscope, to verify if the adhesive failure caused alterations stress intensity and distribution.

Figure 56 – The batch of fourteen parts in the oven

To make this analysis, it was measured the glued area that failed after the thermal cycle. The results from the adhesive failure are in table 3.

Table 3 – Adhesive failure results

Part number	**Percentage of area where the adhesive failed**
1	60%
2	20%
3	50%
4	30%
5	10%
6	30%
7	20%
8	15%
9	20%
10	10%
11	50%
12	15%
13	15%
14	10%

To discuss the internal stress and the adhesive failure after the thermal cycle, four parts were selected. Figure 57 shows the combiner unit number 1 from the batch before the thermal cycle, to show how a combiner unit without adhesive failure looks like. The analyzed parts in this test were parts number 1, 2, 7 and 9 from the fourteen parts batch. Part number 1 was selected because it had very low stress and it was the part that had the highest percentage of adhesive failure. Parts 2, 7 and 9 were chosen because the adhesive failed in the same areas, and the internal stress in these three parts was different in terms of intensity and distribution.

Figure 57 – Part number 1 before the thermal cycle

From Figure 58 to Figure 69, are shown the pictures of parts number 1,2,7 and 9. For each part, is displayed by the following order: a picture of the part with adhesive failure, the polariscope picture before and after the thermal cycle.

Figure 58 – Part number 1 after the thermal cycle

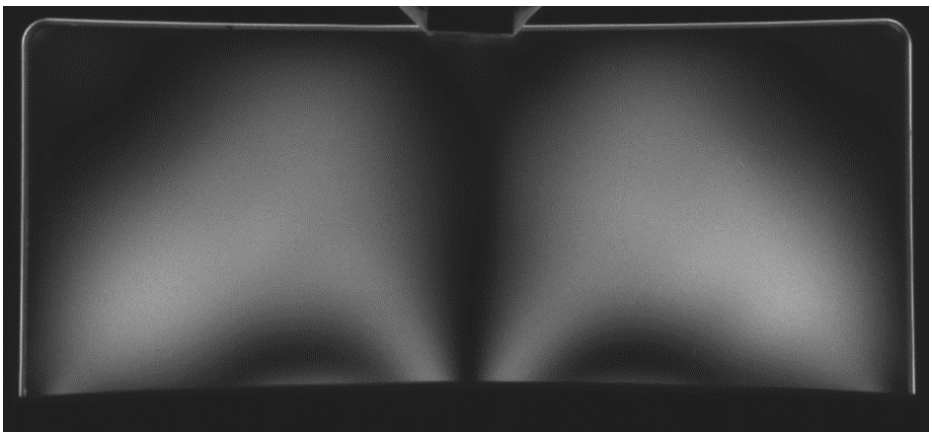

Figure 59 – Polariscope picture of part number 1 before the thermal cycle

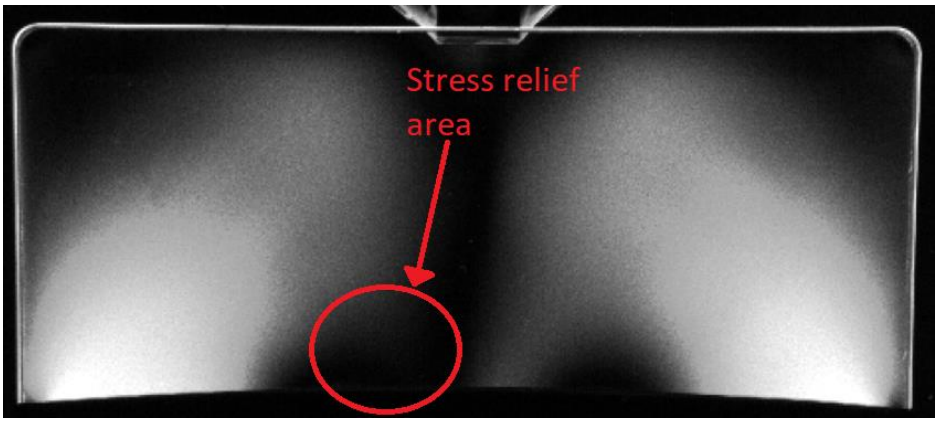

Figure 60 – Polariscope picture of part number 1 after the thermal cycle

Figure 61 – Part number 2 after the thermal cycle

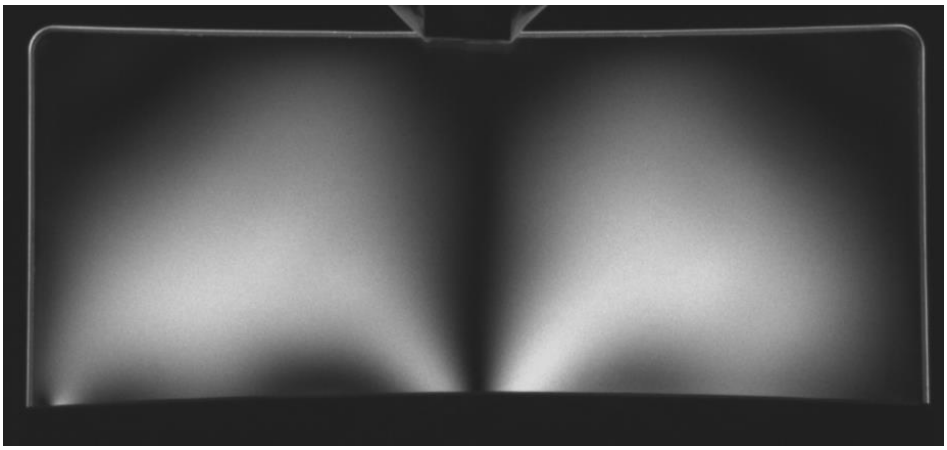

Figure 62 – Polariscope picture of part number 2 before the thermal cycle

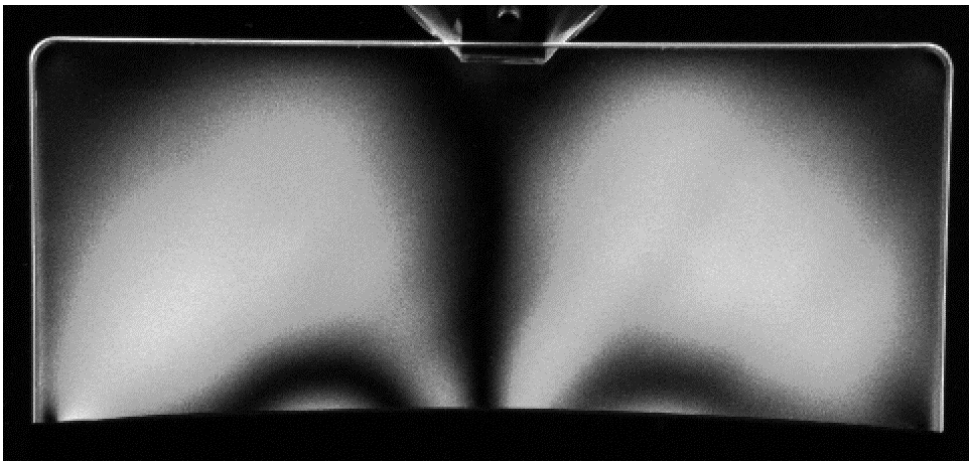

Figure 63 - Polariscope picture of part number 2 after the thermal cycle

Figure 64 – Part number 7 after the thermal cycle

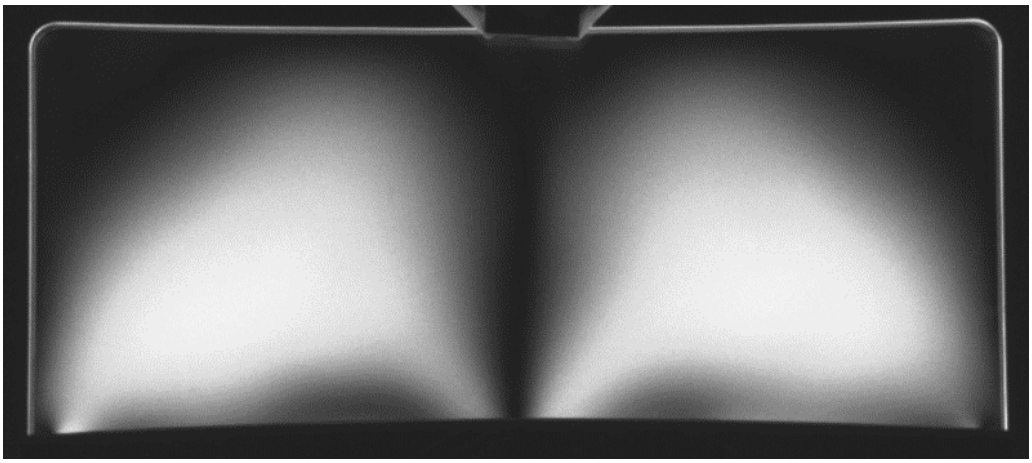

Figure 65 - Polariscope picture of part number 7 before the thermal cycle

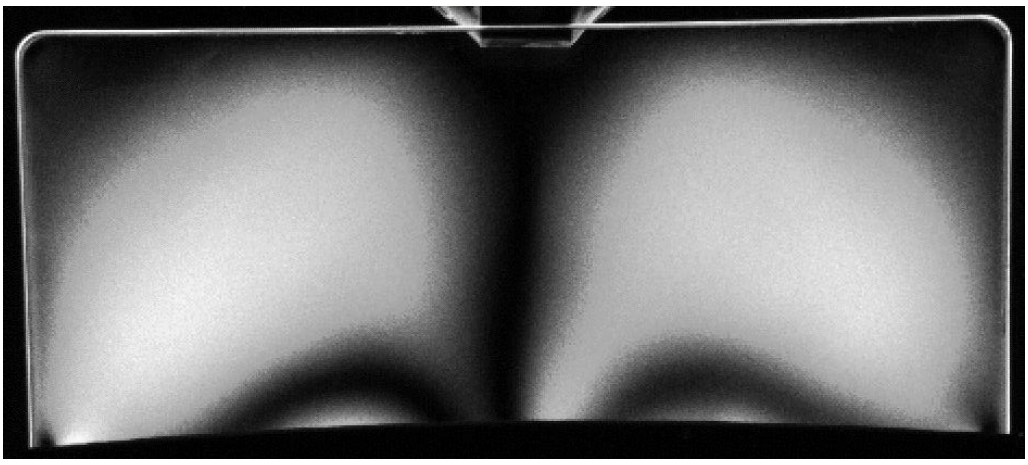

Figure 66 - Polariscope picture of part number 7 after the thermal cycle

Figure 67 – Part number 9 after the thermal cycle

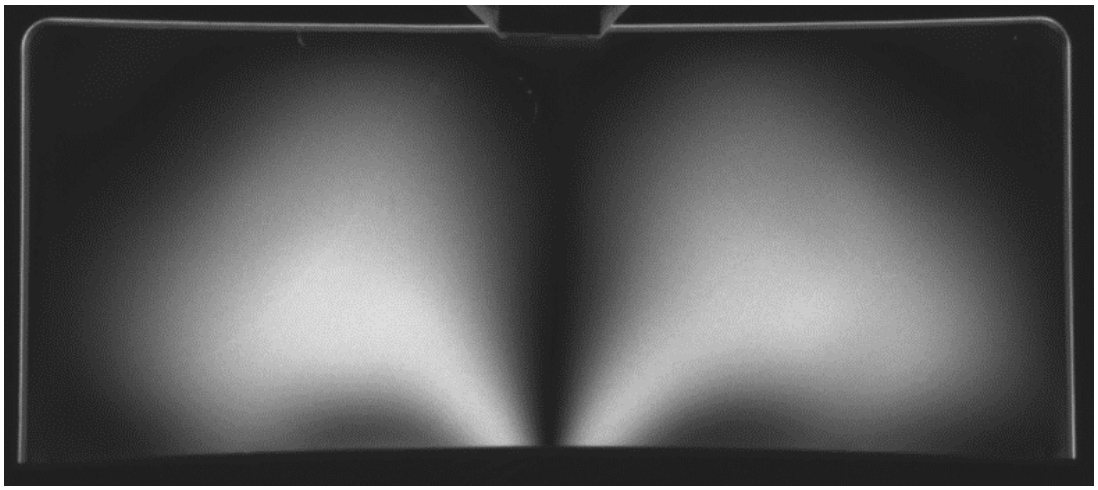

Figure 68 - Polariscope picture of part number 9 before the thermal cycle

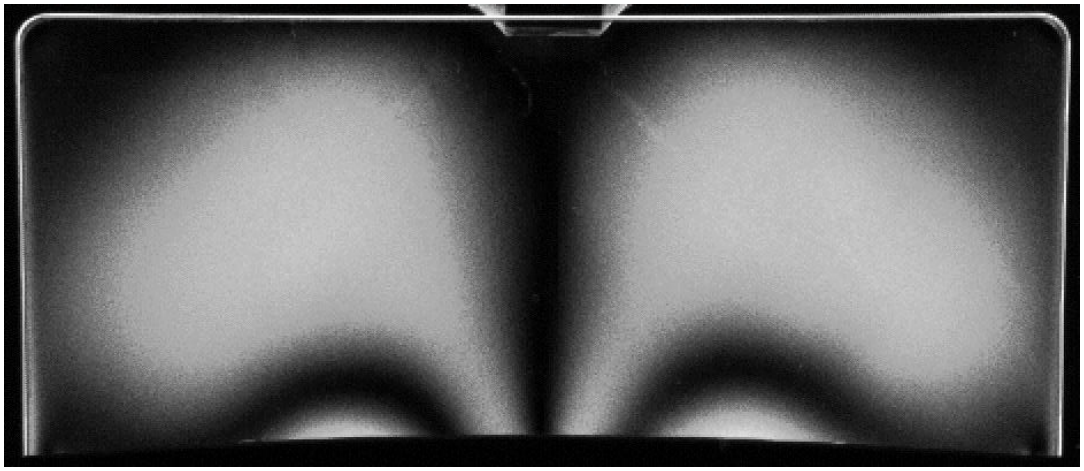

Figure 69 - Polariscope picture of part number9 after the thermal cycle

The first comparison was between the adhesive failure (after the thermal cycle) and the internal stress, (before the thermal cycle), to try to find a correlation between the internal stress in the combiner, and the areas where it was unglued from the support. Table 4 summarizes the analysis of the correlation between the adhesive failures with stress intensity of the four selected parts.

Table 4 – Summary of the adhesive failure with the stress intensity for parts 1,2,7,9

Part	Stress intensity	Approximate stress value	Adhesive failure level
1	Low	0.5 MPa	High
2	Medium	0.7 MPa	Low
7	High	0.9 MPa	Low
9	Medium	0.7 MPa	Low

Looking for part number 1 adhesive failure picture (Figure 58), is visible that a very high adhesive failure occurred. This part unglued all over the bonding surface, with special attention to the sides of this area. When looking to the polariscope picture before the thermal cycle (Figure 59), is visible that the intensity of the stress is very low when compared to the other parts. Analyzing the same information for parts 2,7 and 9, these three parts have very similar adhesive failure levels and patterns, like Figures 61,64 and 67 shows. As these three parts had similar adhesive failures, their polariscope picture before the thermal cycle (Figures 62, 65 and 66) were compared.

When comparing these three stress distributions, is visible that part number 2 has a low stress intensity, and it is very dispersed through the part (Figure 62). Part number 7 (Figure 65), has a higher intensity of stress when compared to part number 2, and the stress seems to be more concentrated in the part. Finally, analyzing part number 9 (Figure 68), is visible that the stress distribution is the most concentrated in the center of the part, despite the stress intensity, being similar to part number 2.

In the end, after analyzing all the parts, the main conclusion is that, after gluing there is an increasing of the internal stress and different pattern distributions, but stress remains low if compared with the glue that has an 18 MPa tensile strength. There is no possible correlation to make between the stress level and pattern, with the adhesive failure.

The second analysis was with the polariscope pictures after the thermal cycle (Figures 60, 63, 66 and 69). The purpose of this analysis was to see what was the effect of the adhesive failure with the stress distribution. The main conclusion, with this 14 parts batch, was that when the adhesive fails in the sides creates a reduction of stress in the center of the combiner. As an example, part number 1 (Figure 58), demonstrates a reduction of the stress intensity in the center (Figure 60), and it had severe adhesive failure on the sides. As for the other parts, this effect was not noticed in their polariscope pictures after the thermal cycle. In these parts, the delamination was not so severe.

5 Creation of a controlled conditions model

As described in chapter 3, to understand how a combiner behaves when stressed it is much easier to have a model with much less and preferably known variables.

To develop this idea, a test jig has been design. The concept was to support the combiner in four known points and apply a force in a known point. The combiner had to be movement and rotation free in order to have only the applied force causing displacements and stress in the part.

5.1 Jig Modelling

To model the jig, it was used CATIA V5 software (Figure 70). To make this study, the jig should be able to let the light pass through the jig, so the stressed part could be studied on the polariscope and in the 3D shape machine. At the same time, the supports and the force point must be strong enough so when the force is applied, the jig does not bend and the deformation is applied into the combiner.

Three groups of parts compose the jig. The first group, is composed just by the base structure. The second group of parts, is the force applicator, which has two parts, and their screws. Finally to maintain the combiner in his place there are two parts to align the combiner, called the guiding parts. In the end, the jig was painted black, to avoid reflecting light when used in the polariscope and in the 3D scanner.

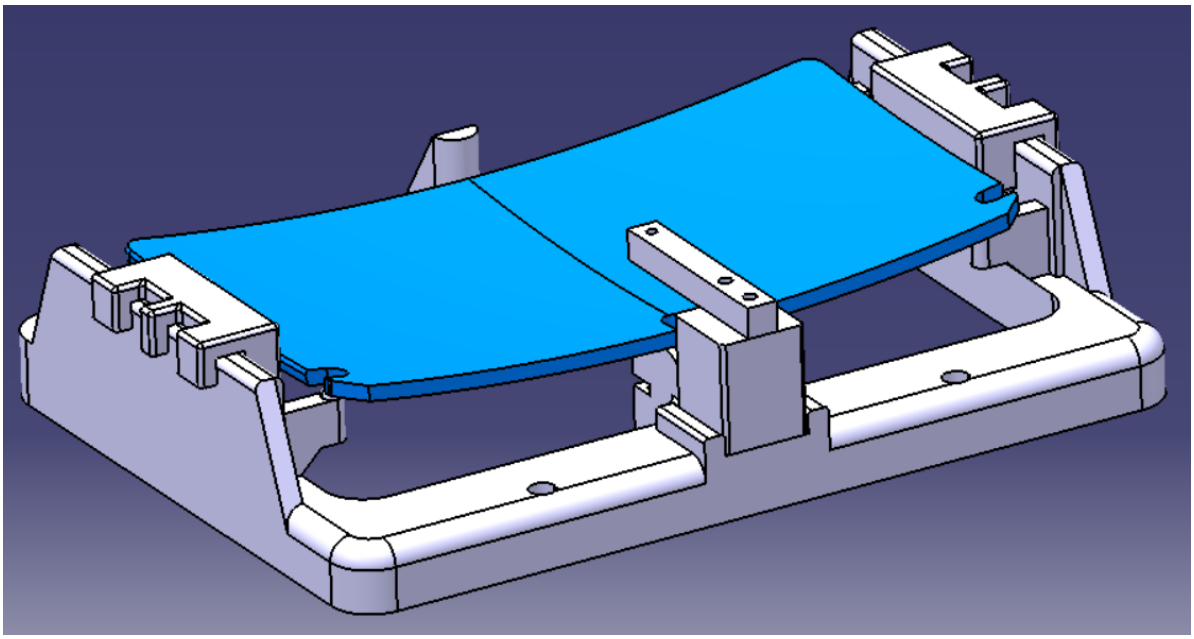

Figure 70 – CATIA V5 model of the Jig

5.1.1 Base structure

The Base structure (Figure 71) is the main part in the jig. This is the frame of the jig. This part has the function to support the combiner, and it is in this part where the Force applicator is mounted, and where the combiner guides are applied.

To apply the force, a screw will push the combiner to a certain point. To control that force, the concept was to apply a certain displacement and with a dynamometer, measure the force applied. To be able to control the displacement a stopper screw was fitted into the base structure.

The location of the stopper screw is on the same plane as the lower supports. On the upper part of the structure, there is a stopper to maintain the combiner fixed on the Y direction as figure 71 shows. That stopper is round, to reduce the contact with the combiner and allow free rotation.

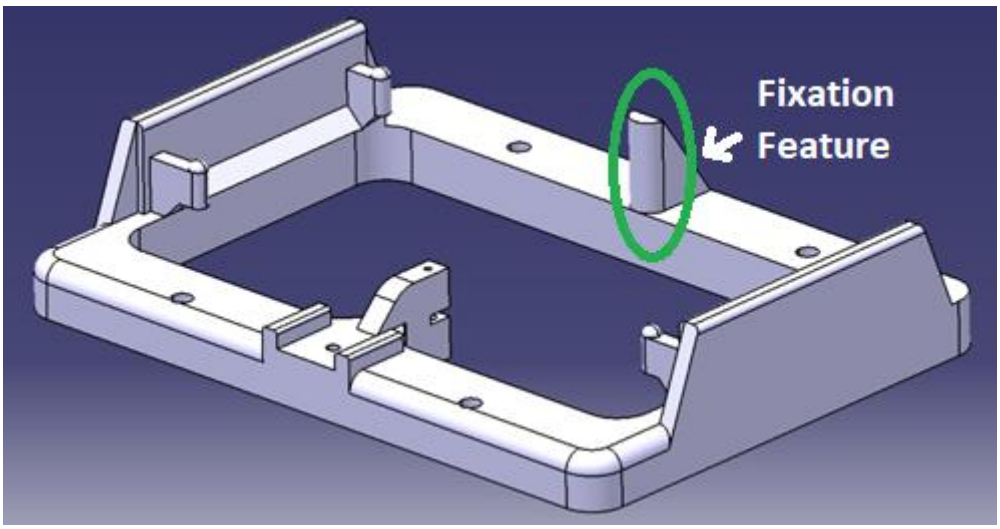

Figure 71 – CATIA V5 model of the base structure

As represented in Figure 71, the combiner supports are spherical, to virtually reduce the contact points with the combiner to a single point. The lower supports are in a more interior position compared to the upper supports (Figure 72), due to the fact that that those supports are very close to the guide cuts in the combiner, so the part is more secure. The upper supports, are close to the top of the combiner, and as there are no cuts in that area of the combiner, they are shorter, in order to raise the area of light coming from the polariscope.

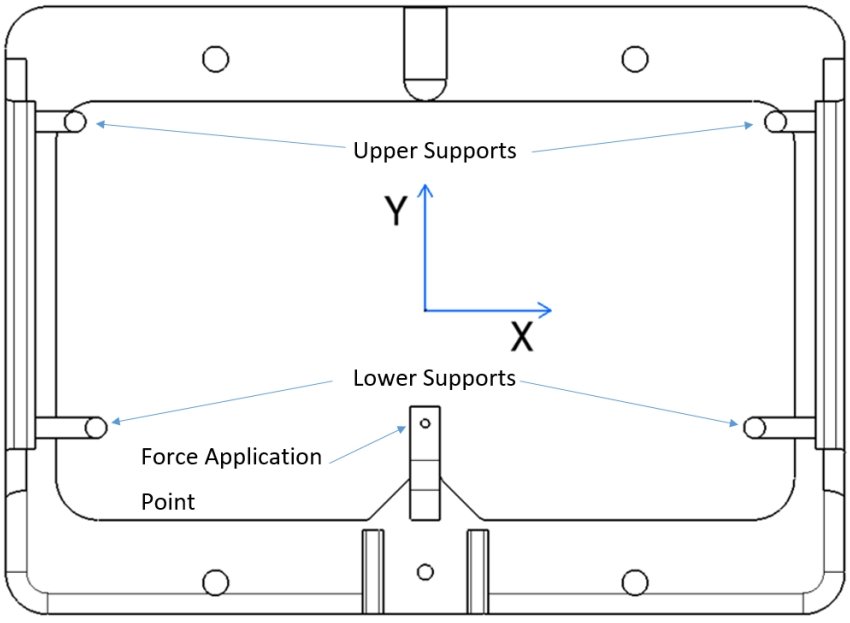

Figure 72 – Front view of the base support

The screw stopper, has a small cut to place a nut to fix the M2 screw that will be used as stopper. That feature is visible in Figure 73.

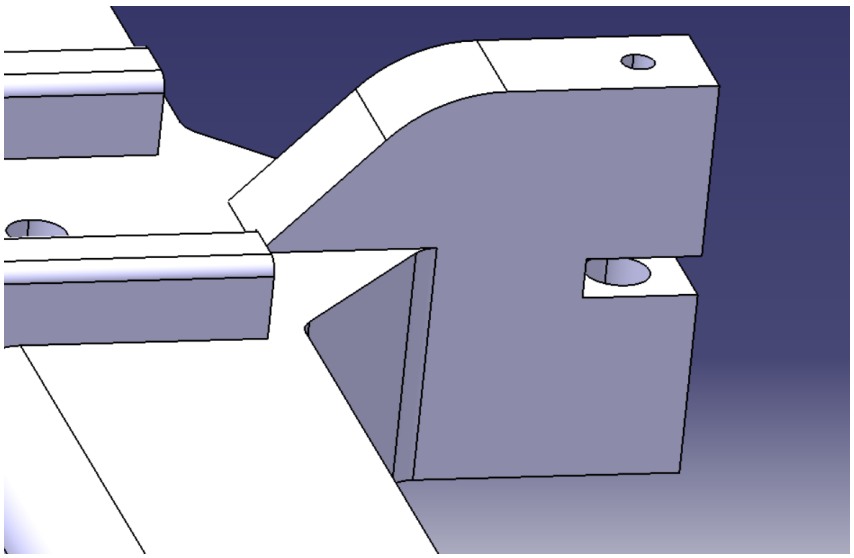

Figure 73 – Nut cut in the base structure in the CATIA V5 model

5.1.2 Force Applicator

The force applicator is composed by two parts: The tower support (Figure 75 and 76), and the screw support (Figure 74).

The screw support is the part where the screw that applies the force is mounted. This part cannot be very wide, to avoid covering the light in the polariscope. At the same time, that part is going to be subjected to a high force, which can cause bending in a part with that width. That could make the results unreliable. Therefore, it will be the only part made in aluminum unlike the rest of the part that will be 3D printed.

This part is a small block with a parallelepiped shape, with three holes. Two blind holes with Ø3, where the screws that attach this part to the tower will be, and a M3 hole, where the force applying screw will be. The location of this force applying screw is in the same axis as the lower supports and the stopping screw.

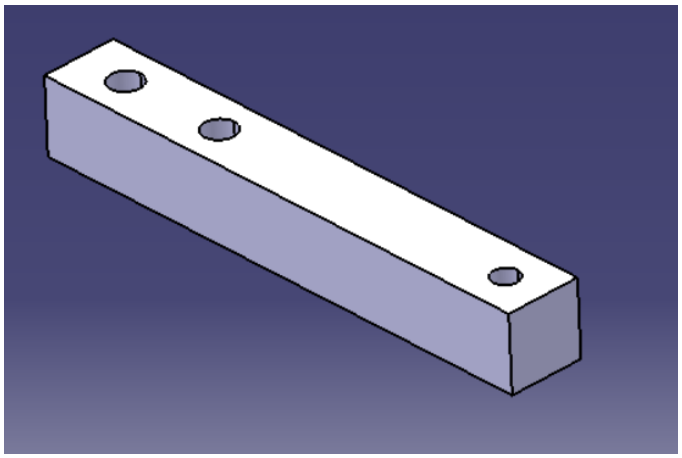

Figure 74 – Screw support in CATIA V5 model

The tower support has the purpose of maintaining the screw support in his position. It makes the connection between the base structure and the screw support. This part will not be in a place where is going to cover the light when the part is analyzed in the polariscope. This means that for rigidity reasons, it can be larger than the screw support, so it cope well with the force applied.

This part is a block with three drilled holes, two in the top to fix the screw support and another in the bottom to fix itself to the base structure.

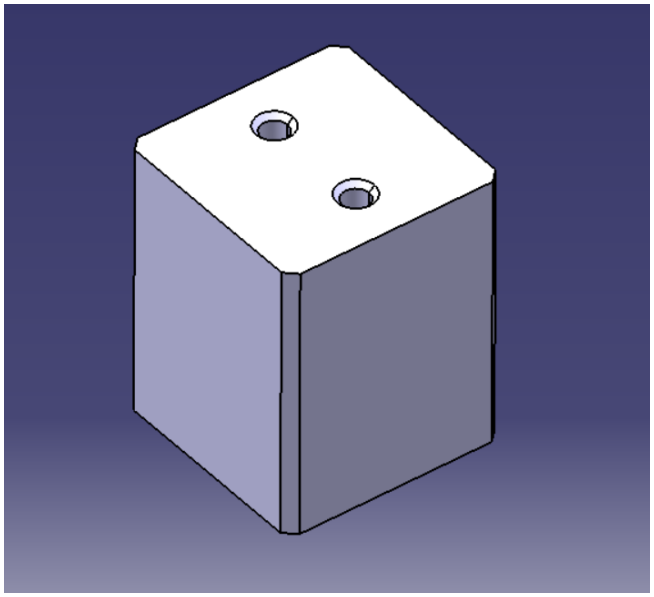

Figure 75 – Top of the tower support in the CATIA V5 model

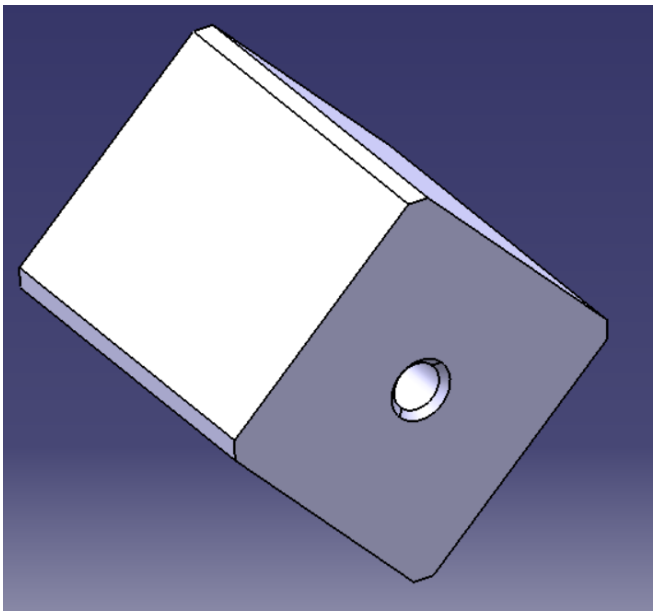

Figure 76 – Bottom part of the Tower support part in the CATIA V5 model

5.1.3 Combiner guiding parts

These two parts (Figure 77) were made to center the combiner in its desired position. These pieces are independent from the base structure, to allow a better positioning when aligning the combiner in the jig (Figure 78).

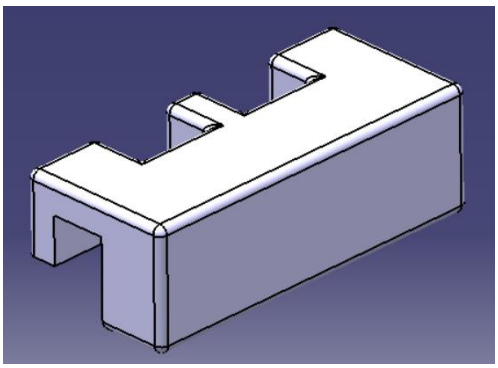

Figure 77 – Guiding in the CATIAV5 model

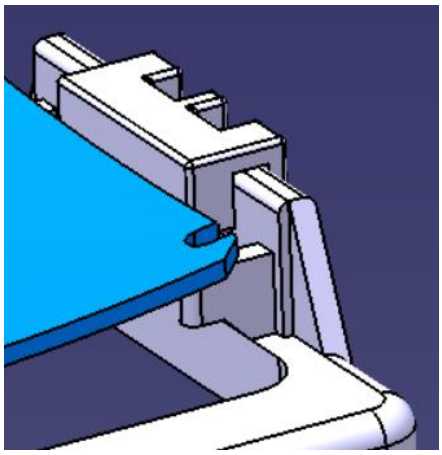

Figure 78 – Guiding applied in the base structure in the CATIA V5 model

5.2 Jig fabrication

This Jig was fully made in the Bosch car multimedia facilities. Most of the part was 3D printed in a desktop 3D printer. The rest of the part was made in the company's locksmith. It was important that the final product was cheap and at the same time made relatively quick, because there was a certain hurry in obtaining results for this study.

5.2.1 3D printed parts

To build this Jig, every part except the screw support was 3D printed. The 3D printer available in Bosch is a Objet30 Prime, represented in Figure 79.

Figure 79 – Objet30 Prime

This printer uses the Polyjet printing. What this means is that the printer has a base platform where a print head jets microscopic layers of a photopolymer liquid. Right after the liquid is deposited, a roller passes and creates a thin layer of material that is later cured with a UV light that comes right after the roller. (Singh 2011) Figure 80 demonstrates this process.

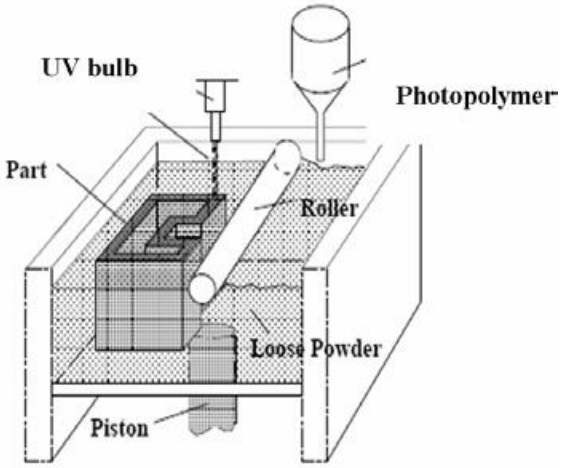

Figure 80 – Schematic of Polyjet printing process (Singh 2011)

This type of printing is not the fastest, but is by far the most precise. It has a precision more than 300 times better then FDM for example.

The material used was a photopolymer called VeroWhite. From the available in stock materials, this was the chosen one because is a durable, rigid and with an high dimensional accuracy material. (Lee, An e Chua 2017) As the base structure has some features that require high precision, and were complex, this material was the one that suited better the work in hand.

After the modelling ended, all parts were converted in STL files and then printed. The printing took about 12 hours (Figure 81).

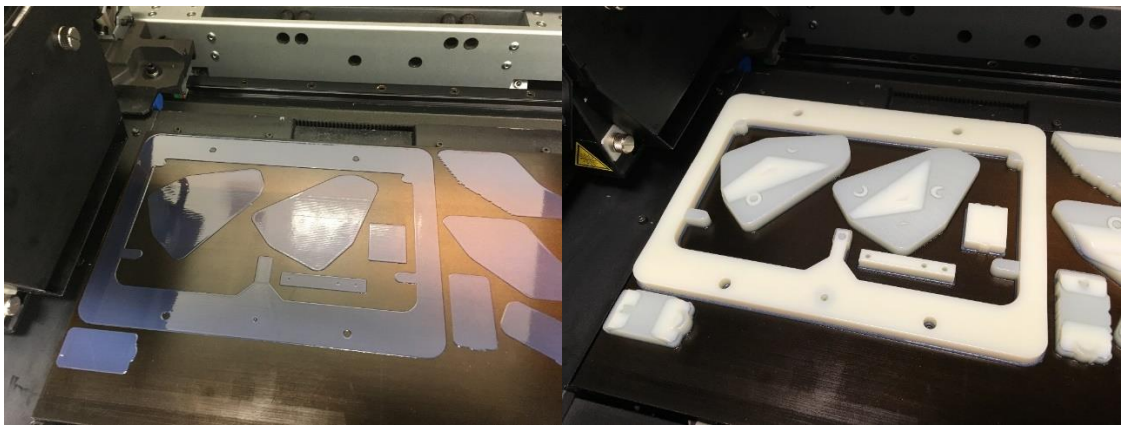

Figure 81 – First layers of material in the 3D printer (right) and the part 6 hours later the beginning of the print (left)

After the parts were printed (Figure 82), the parts were taken to the company locksmith to get the needed screws in place. The result is visible in Figure 83.

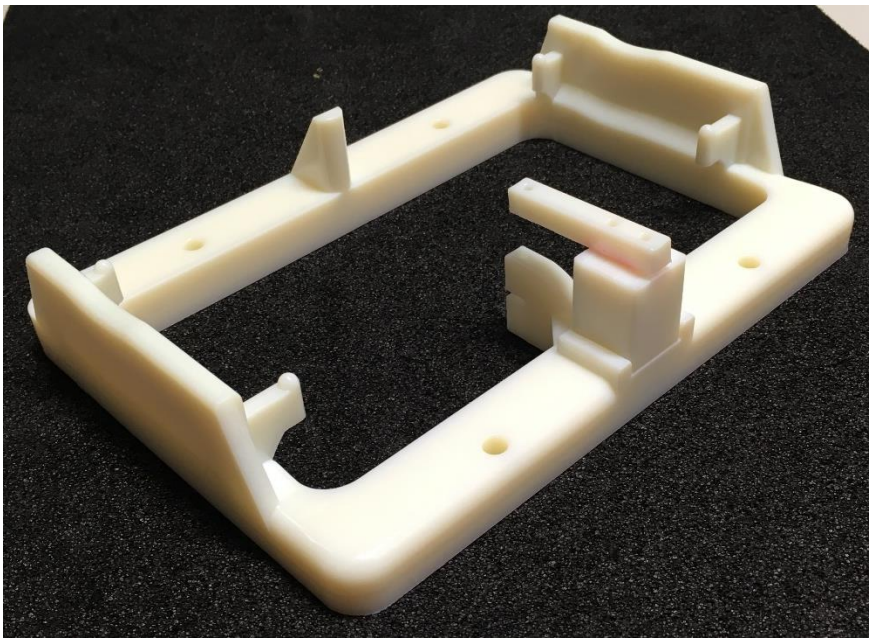

Figure 82 – Jig ready with every part 3D printed

5.2.2 Parts made in the locksmith and adding guiding

In the locksmith the screws were attached to the jig. Five screws were inserted: one M2 to work as stopper, three M3 to fix the screw support to the tower support and to apply the force and to fix the tower jig to the base structure, a M4 screw was used.

After the first tests, applying a force in a test combiner, a 3D printed screw support was used. As predicted it bended when a force was applied, so as it was described in section 5.1.2, it was replaced by an aluminum one. The result is shown in Figure 83. Figure 84 shows the final product after the jig has been painted.

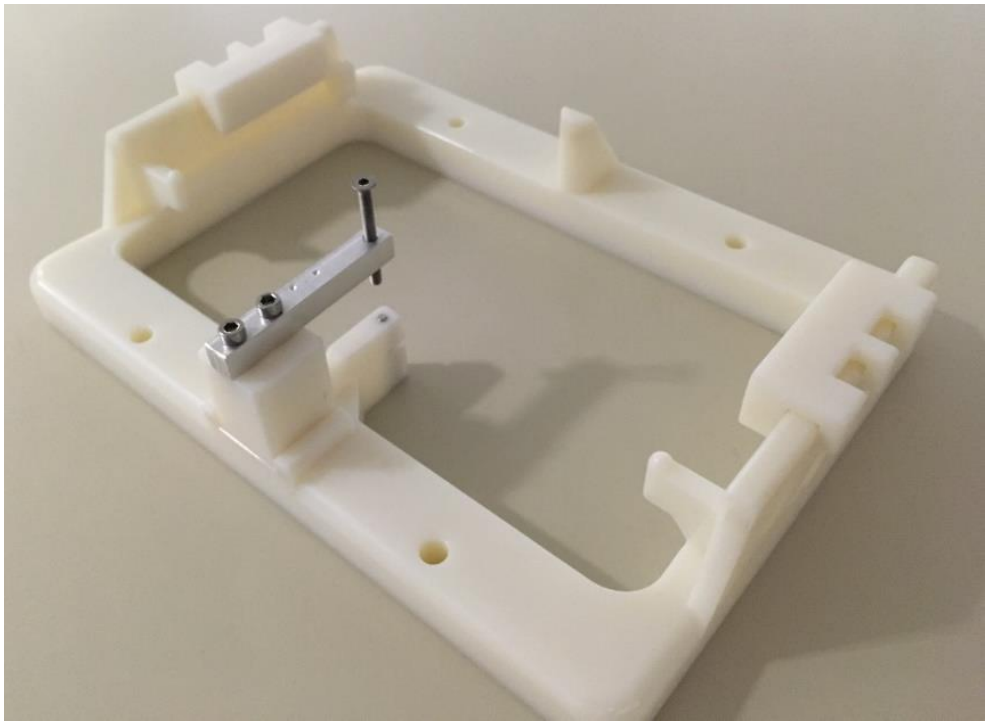

Figure 83 – The Jig with an aluminum screw support, guiding and the screws in place

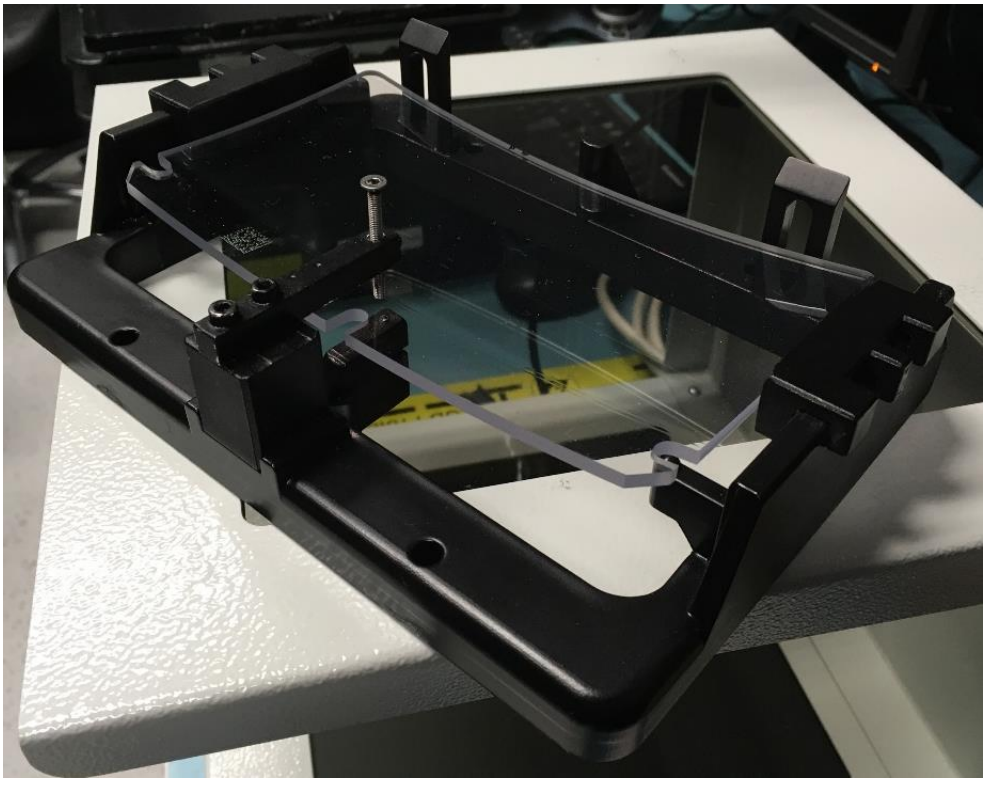

Figure 84 – Final product

6 Simulation and validation of controlled model

To understand better the combiner behavior, a simulation of this part was made using ABAQUS/CAE software. The purpose of this simulation was to analyze the effects of a force or displacement application in the part internal stress and on the shape of the part. To validate the simulation, a test with the model created in chapter 5 has been made.

6.1 Experimental force displacement determination with the controlled model

In this section, an experimental test was made, in order to validate the results obtained in the simulation made with ABAQUS/CAE.

The purpose of this test was to determine the force/displacement curve, in order to know what force was required to apply a certain displacement in the experimental model. This test also had the function of positioning the stopper screw in a specific point in order to know the force/displacement conditions when analyzing the combiner in the polariscope and in the 3D scanner.

6.1.1 Test

This test was made using a Zwick Roell Z010 machine (Figure 85). This machine can do tensile and compression tests.

Figure 85 – ZwickRoell Z010 machine

To know the correspondent force associated with a certain displacement, initially it was going to be used a dynamometer, and manually measure that point. To improve the precision in the results, a tensile and compression test machine was used (Figure 85). With this machine, the force / displacement curve was determined with the setup visible in Figures 86 and 87.

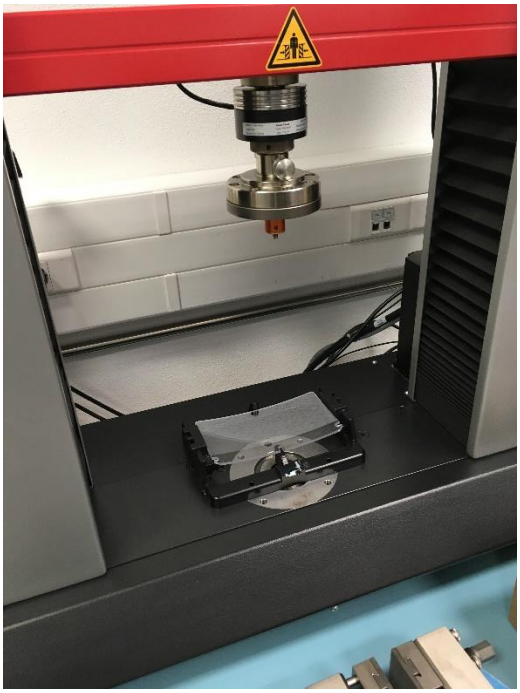

Figure 86 – The force displacement test setup 1

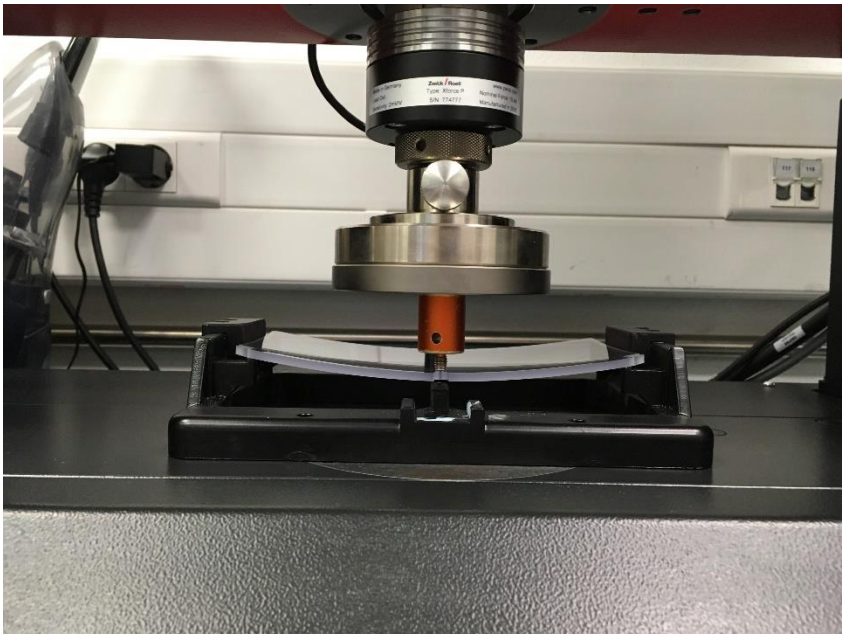

Figure 87 – The force displacement test setup 2

To measure the force and the displacement, a force was applied in the combiner with a speed of 1 mm/min, until the combiner hit the stopper screw. Five measurements were made. In Figure 88, is displayed the result from this measurement.

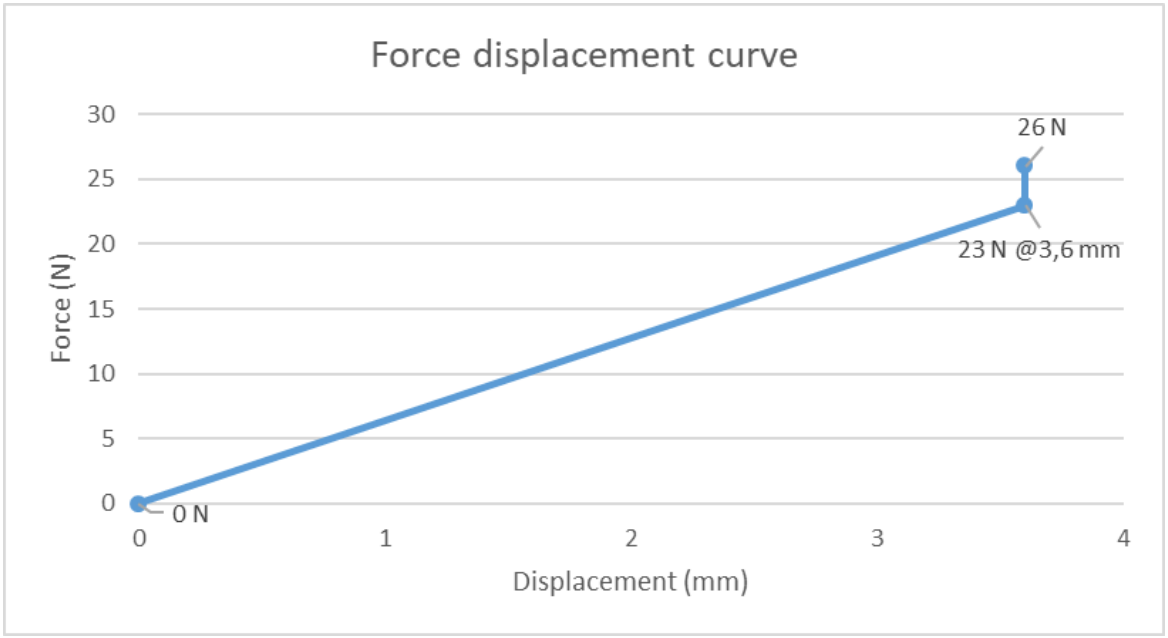

Figure 88 – Test results

In this measurement, it can be concluded that the combiner had an elastic behavior. When it hits the stopper screw, there is a sudden increase in the force and the force/displacement curve graph slope increases. The point to be used as reference is the point where the combiner hits the stopper screw, because it will be the conditions applied into the combiner when analyzed in the polariscope and in the 3D scanner machine. This force displacement point is 3.6mm for a 23 N force.

In these five measurements, there was a good repeatability between measurements, which indicates stability in the measurement process.

6.2 Geometry analysis of the combiner surface in the controlled conditions model

To analyze the combiner geometry, the same 3D scanner as described in section 4.2.1 was used. The used Matlab code was different from the one in section 4.2.1. This code was able to treat a bigger range of deformation, as the one applied in this test. The parameters that were compared with the ABAQUS CAE simulation were: the height deviation in Z direction, the absolute slope deviation, the slope deviation in X direction and the slope deviation in Y direction.

The result chart from the height deviation is in mm and the slopes charts are dimensionless.

In Figure 89, 90, 91 and 92, are respectively displayed the height deviation in Z, the absolute slopes, the slope deviation in X direction and the slope deviation in the Y direction.

The height deviation chart (Figure 89), gives the shape deviation of our combiner comparing with the nominal design. The slopes deviations charts represent the slope deviation when comparing with the nominal CAD design. The difference between them, is that in Figure 91 and 92, are represented the slope deviation in the X and Y direction respectively. In Figure 90, the absolute slope deviation is a vector sum from the slope deviations in X (Figure 91) and Y direction (Figure 92).

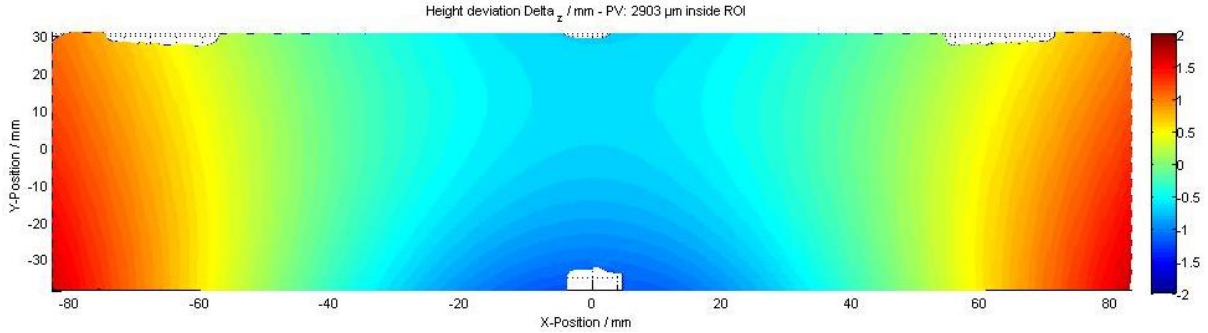

Figure 89 – 3D shape height deviations in Z of the combiner with a 3.6 mm displacement applied

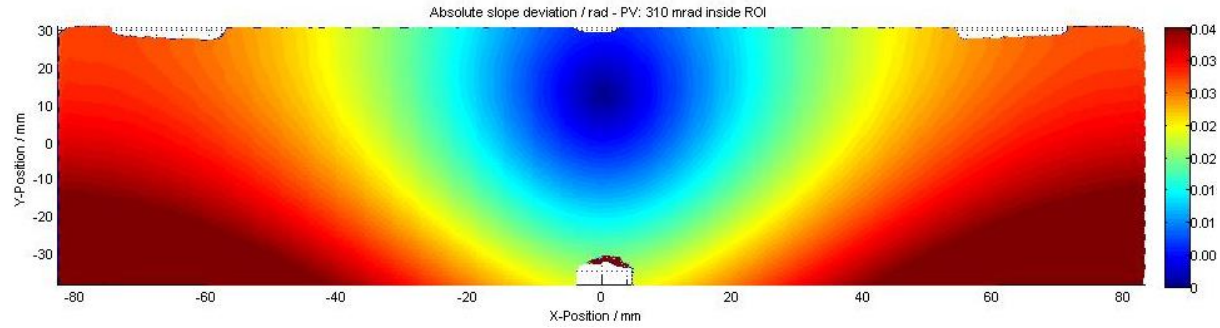

Figure 90 – 3D shape absolute slope deviation with a 3.6 mm displacement applied

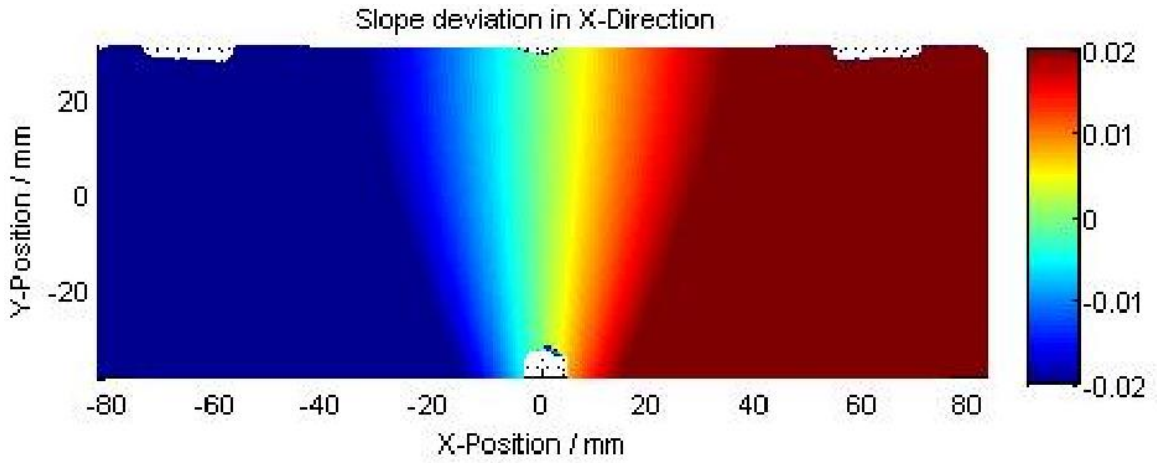

Figure 91 - Slope deviations in X direction measured in the 3D shape machine

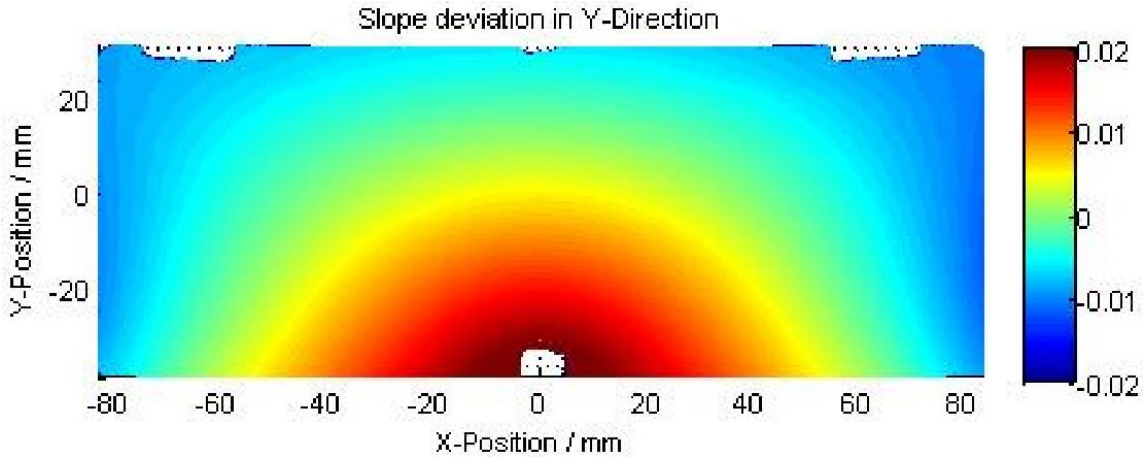

Figure 92 - Slope deviations in Y direction measured in the 3D shape machine

6.3 Combiner stress analysis in the controlled conditions model

To analyze the stress, the jig with the stressed combiner was inserted in the polariscope, as Figure 93 shows. In Figure 94, it is displayed a polariscope picture of the combiner unstressed in the jig.

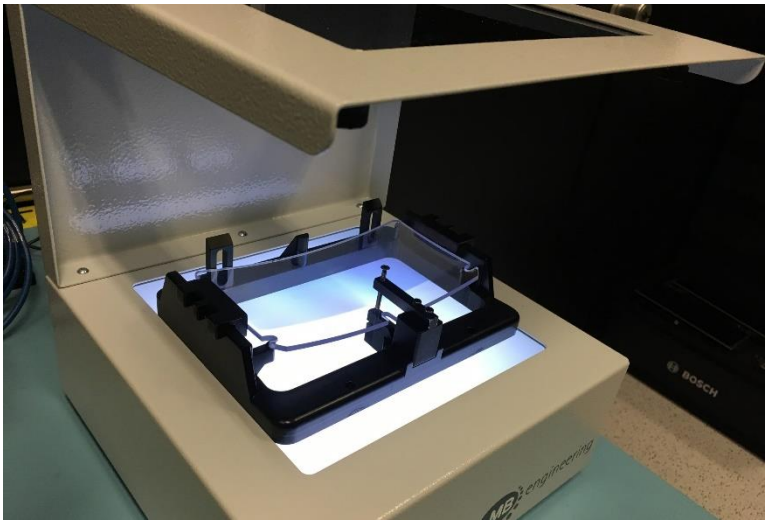

Figure 93 – Jig in the polariscope

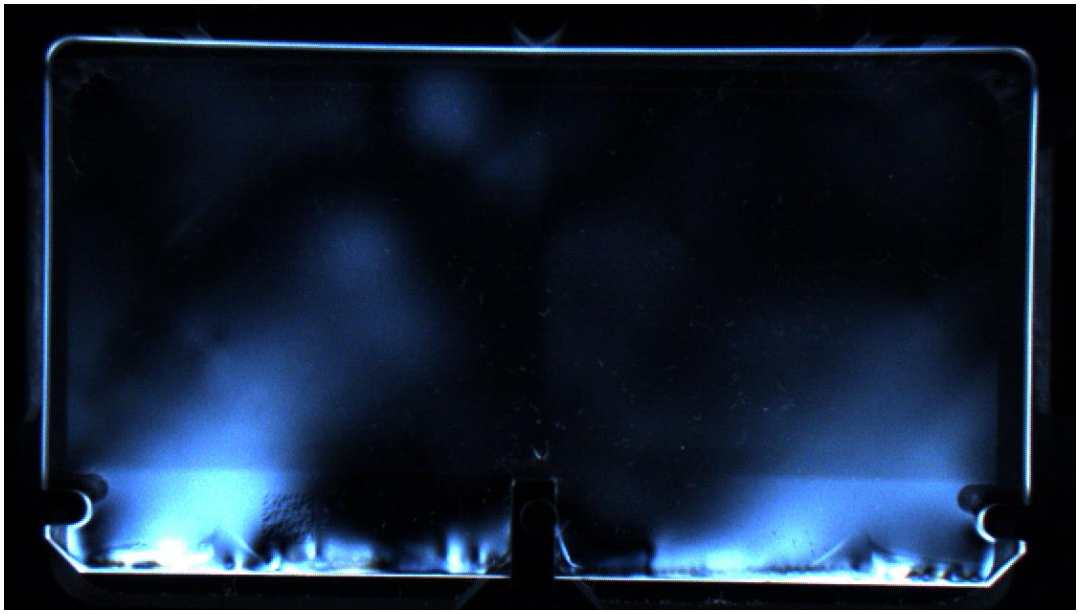

Figure 94 – Combiner unstressed in the jig

With a 23N force applied in the combiner, the picture seen in the polariscope is visible in Figure 95. It is visible that the stress intensity not only increased as the distribution stayed uniform through the combiner.

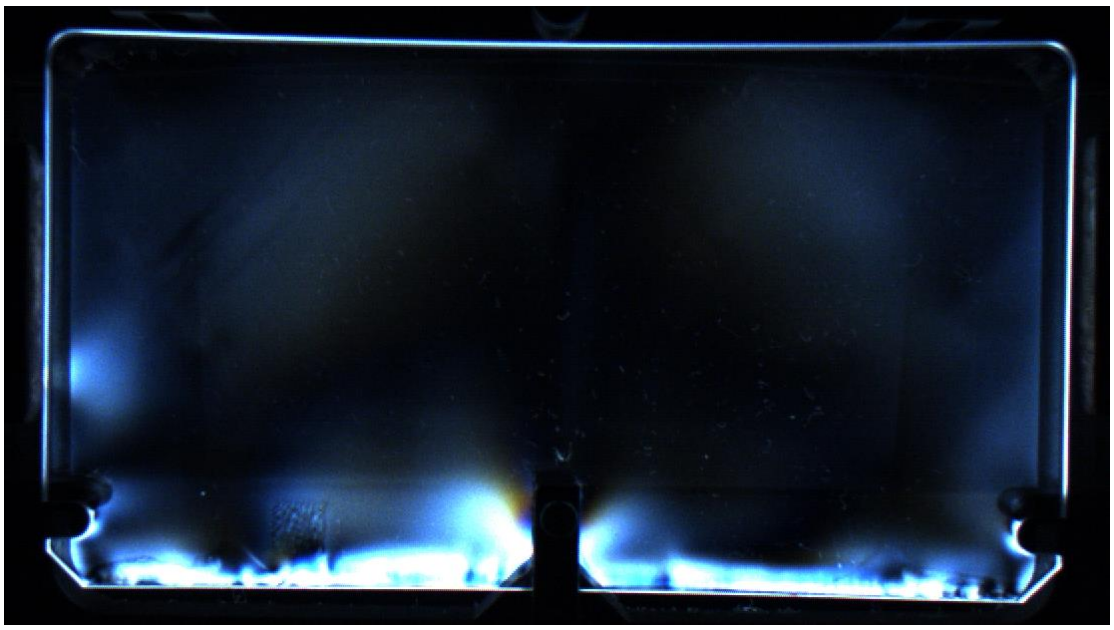

Figure 95 – Internal stress in the combiner seen with the polariscope

The highest stress point is the one where the force is applied. As this point is hidden behind the force applicator, the stress in that point cannot be studied. However, the most stressed area is the area around the point (point 1 from Figure 96). In fact, by looking to the color in that area, is visible a blue near violet and yellow. That means that the light retardation is around 1150 nm. That corresponds to a stress of:

Point 1

$\delta \approx 1150$ nm (blue after yellow)

t = 3.3 mm

$C_B \approx 84$

$$\sigma = \frac{1150}{3.3 * 84} = 4.14\ MPa \qquad 6.1$$

To have more results to analyze, in Figure 96 are marked other points where the stress was calculated.

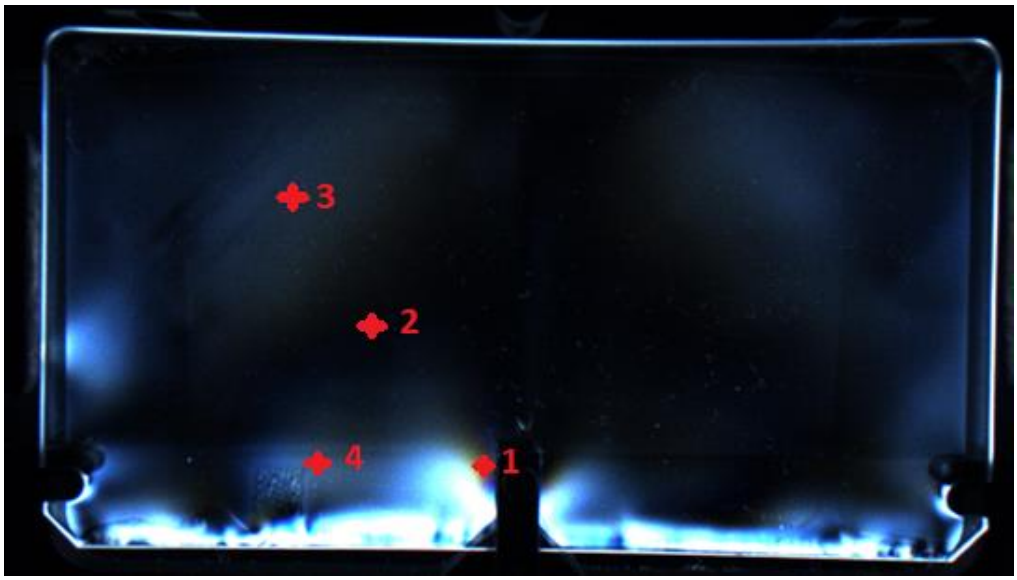

Figure 96 – Points where the stress was calculated

Point 2

δ ≈ 0 nm (dark)

t = 3.3 mm

$C_B \approx 84$

$$\sigma = \frac{0}{3.3 * 84} = 0\ MPa \tag{6.2}$$

Point 3

δ ≈ 100 nm (light grey)

t = 3.3 mm

$C_B \approx 84$

$$\sigma = \frac{100}{3.3 * 84} = 0.36\ MPa \tag{6.3}$$

Point 4

δ ≈ 250 nm (clear grey)

t = 3.3 mm

$C_B \approx 84$

$$\sigma = \frac{250}{3.3 * 84} = 0.9\ MPa \tag{6.4}$$

The internal stress pattern show, that there is an increase pointed to the force application point. Nevertheless, it is important to check that there is a central area where there is no stress (as the part is completely dark). These dark areas will be discussed later in section 6.5.3.

6.4 ABAQUS CAE simulation

To get a better comprehension of the combiner behavior, an ABAQUS CAE model has been created.

Figure 97 shows the CATIA V5 part that was used in the model. However, to simplify the simulation it was used a shell element part created from the middle surface (Figure 98) of the original CATIA V5 part. Later the thickness of the part was chosen in the ABAQUS simulation.

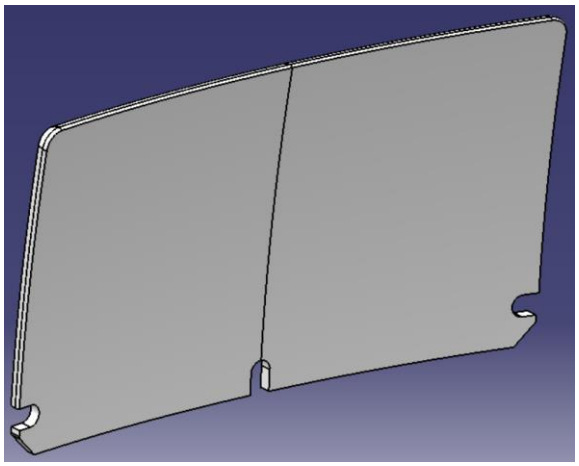

Figure 97 – Original CATIA V5 design of the combiner

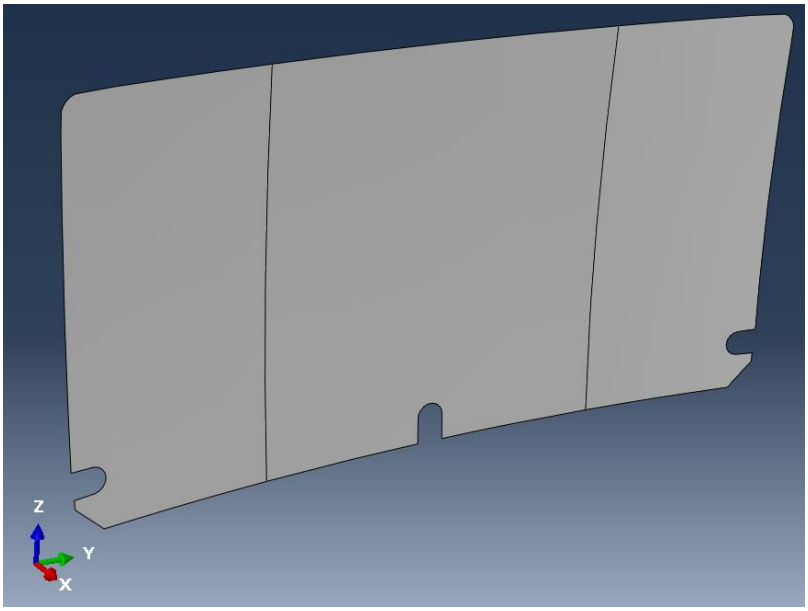

Figure 98 – Combiner middle surface

The used properties for the polycarbonate in this test were a 2400 MPa Young's modulus and a Poisson's ration of 0.42.

The used section, was a Shell type, homogeneous with a thickness of 3.3 mm as measured in the lab. As visible in Figure 99, partitions were made. These partitions had the purpose of making the mesh smoother, and to create the points where the supports and the applied force were going to be located. The Boundary conditions used were: lock in X direction the movement in the four supporting points and do lock in Y and Z the movement in the force/ displacement application point.

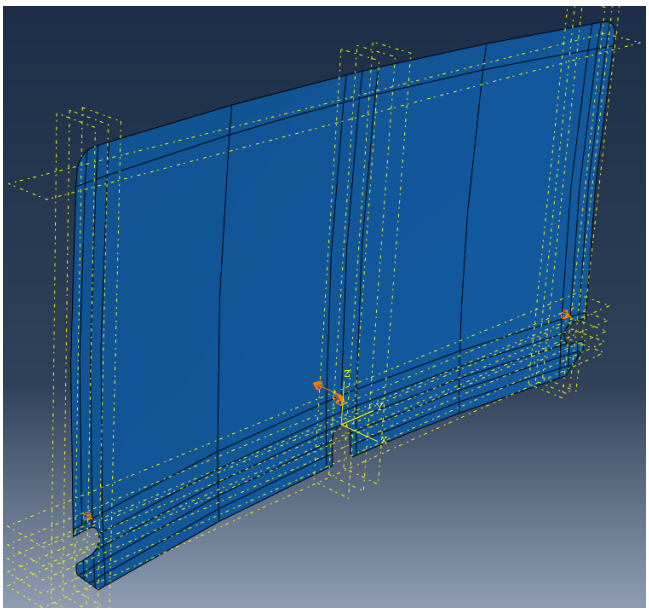

Figure 99 – Part with Boundary Conditions applied and partitions made

The mesh used, had an approximate global size of 3mm, a maximum deviation control factor of 0.4 and a minimum size control by fraction of global size of 0.4. To smooth the mesh, some areas near the part cuts, had to be seeded manually. Figure 100, shows the used mesh.

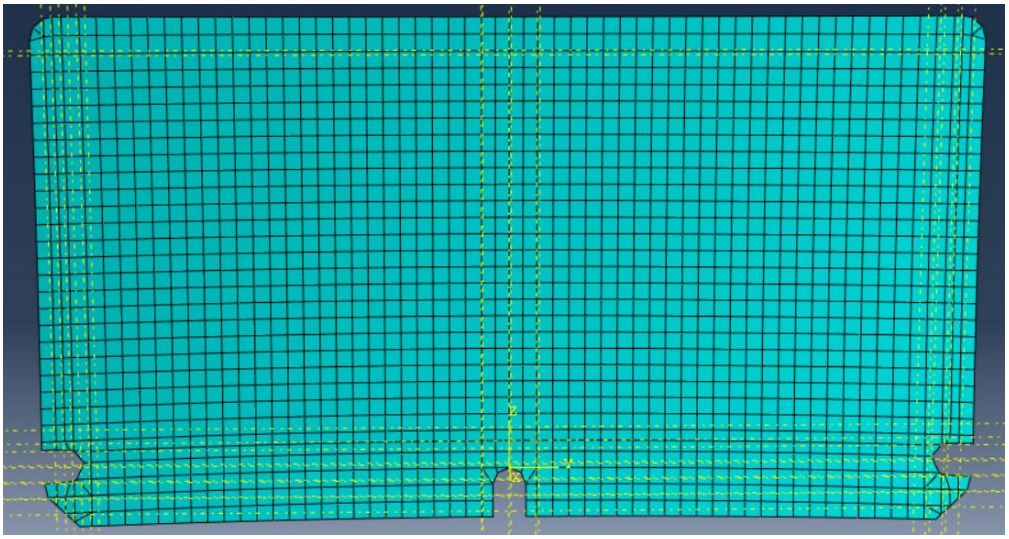

Figure 100 – Mesh used in the ABAQUS CAE simulation

6.5 ABAQUS CAE simulation validation

To validate the simulation, the results given by the software were compared with the experimental results. So in this section, the displacement associated with the applied force was compared with the Force / displacement test. The 3D Shape results (Z displacements, the X and Y slopes) were used as comparison with the same results in the simulation. For last, the stress distribution in the simulation was compared with the Polariscope picture of the stressed part.

6.5.1 ABAQUS CAE Force/displacement validation

As described in section 6.1.1, the force displacement test, resulting from the experimental setup, has the results shown in Table 5.

Table 5 - Force / displacement results

Applied Force	23N
Displacement	3,6 mm

To compare this results, in Figure 101 and 102, is shown the Reaction Force when a 3,6 mm displacement is applied and the displacement when a 23N force is applied in the simulation model.

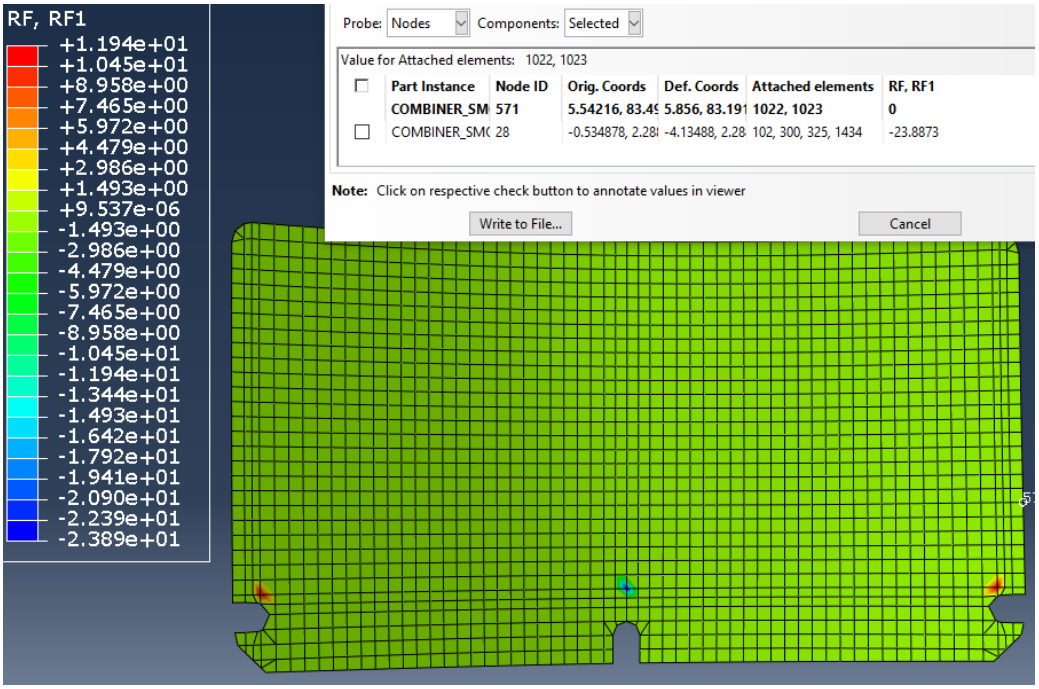

Figure 101 – Part reaction force distribution in ABAQUS CAE with a 3.6mm displacement is applied

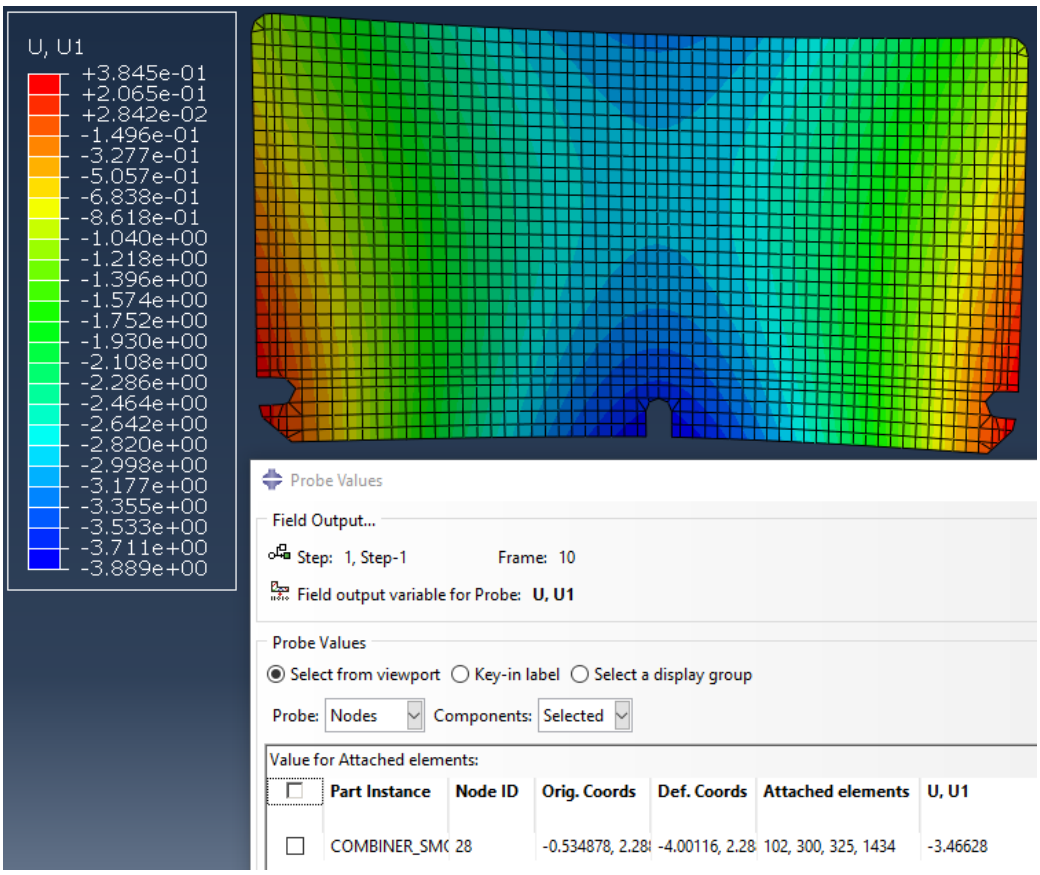

Figure 102 – Spatial displacement (U) in X direction

The results showed a difference of 0.13 mm between the real model and the simulation (Table 6). This difference is related to the combiner thickness approximation in the simulation and possibly with a small difference of the Young modulus in the combiner with the spec sheet value. In table 6, there is a summary of these results. Despite this approximations (that reduced the model complexity), the difference between both results was close to 4%.

Table 6 - Force / displacement validation results

	FORCE	**DISPLACEMENT**
Real Model	23 N	3,6 mm
SIMULATION		
With 23N applied	23N	3,47 mm
With 3,6mm displacement imposed	23,89 N	3,6 mm

6.5.2 ABAQUS CAE simulation geometry validation

In this section, the 3D shape results are validated. The compared information were the Z surface displacements and the surface slopes (the absolute ones and in X and Y direction).

Before the comparison between the real model and the simulation, it is important to notice that the 3D scanner contains a mask that restrains the collected data to a certain area. In order to do a correct comparison the read values in the simulation, must be same that are analyzed in the 3D scanner data.

The first comparison is between the Height deviation in Z. In Figure 103 is visible the height deviation in Z in the simulation.

In a first analysis, the curve obtained in the experimental model in Figure 89, the curve obtained in this simulation (Figure 103) has the same shape.

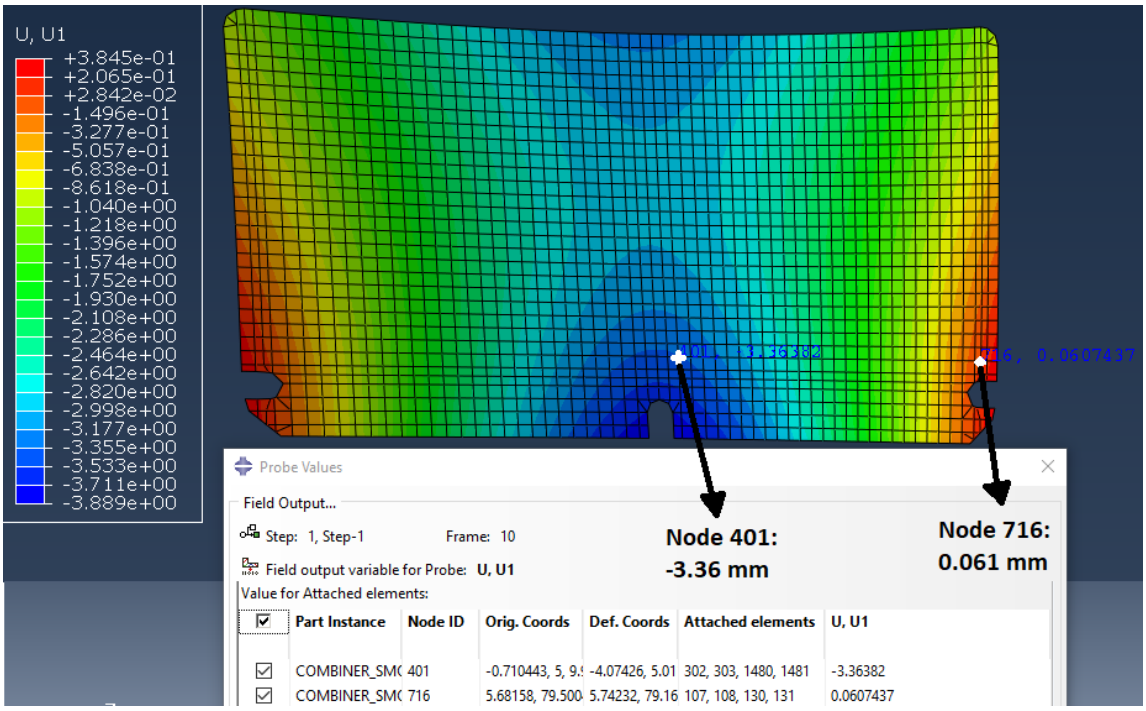

Figure 103 – Height deviation profile in the ABAQUS CAE simulation

The selected points in Figure 103, are the points that correspond to the maximum and minimum deviation that is read by the scanner. In section 6.2, the results of the experimental model are available. In table 7 is compared the simulation and the experimental model values.

Table 7 – comparison between real model and ABAQUS CAE peak-to-peak values

	Minimum deviation	Maximum deviation	Peak-to-peak deviation
3D scanner	-	-	2.903 mm
Simulation	-3.36 mm	0.06 mm	3.42 mm

In these values, the difference is from 0.517 mm, which is a bit higher than the Force / displacement values. Despite the error that is induced with the simulation approximation, the biggest error is inserted by selecting the points that will be compared with the experimental model. In this comparison is also important to notice that the chart curvatures are very similar, and the areas of minimum and maximum deviations are similar to the ones visible in the 3D scanner data.

For the slopes, the comparison is more subjective, only the slope curves will be compared. A more objective comparison (with Figures 90 to 92) could not be made because the slope data in X and Y direction is out of scale in certain areas. However, there are areas where there is no slope deviation and those areas are visible. This analysis will be important the stress validation section.

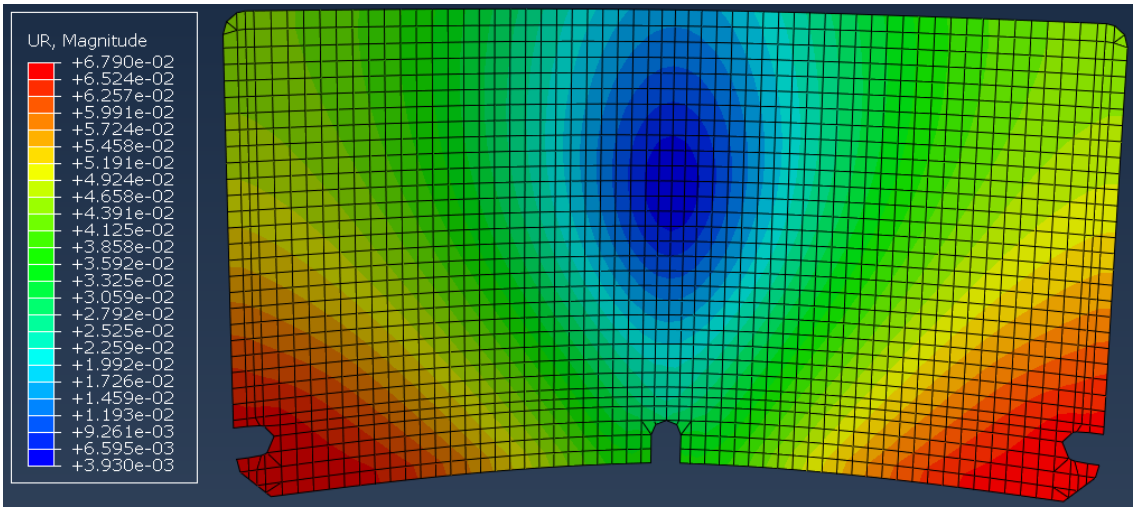

Figure 104 – Absolute slope in ABAQUS CAE simulation

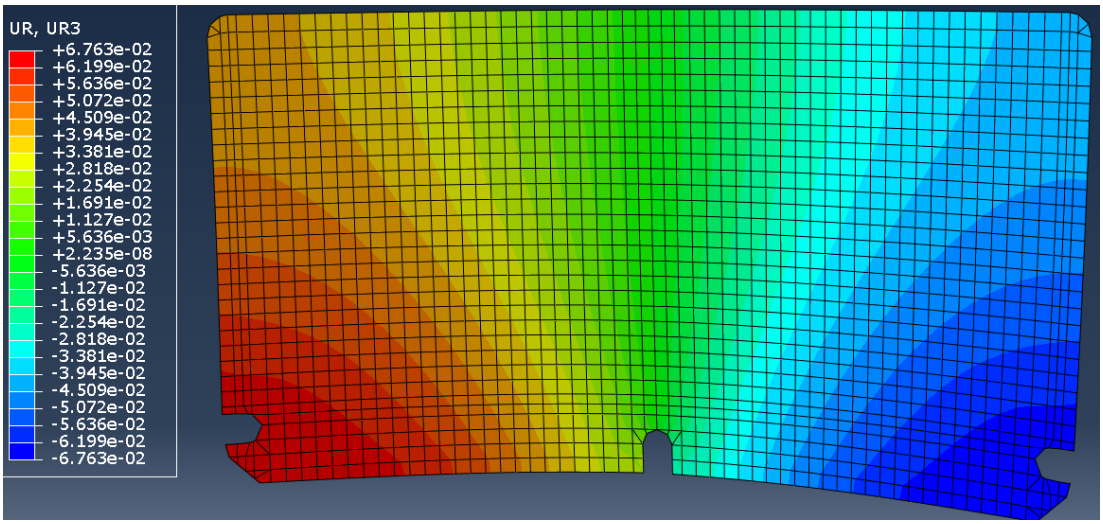

Figure 105 - Slopes in X direction in ABAQUS CAE simulation

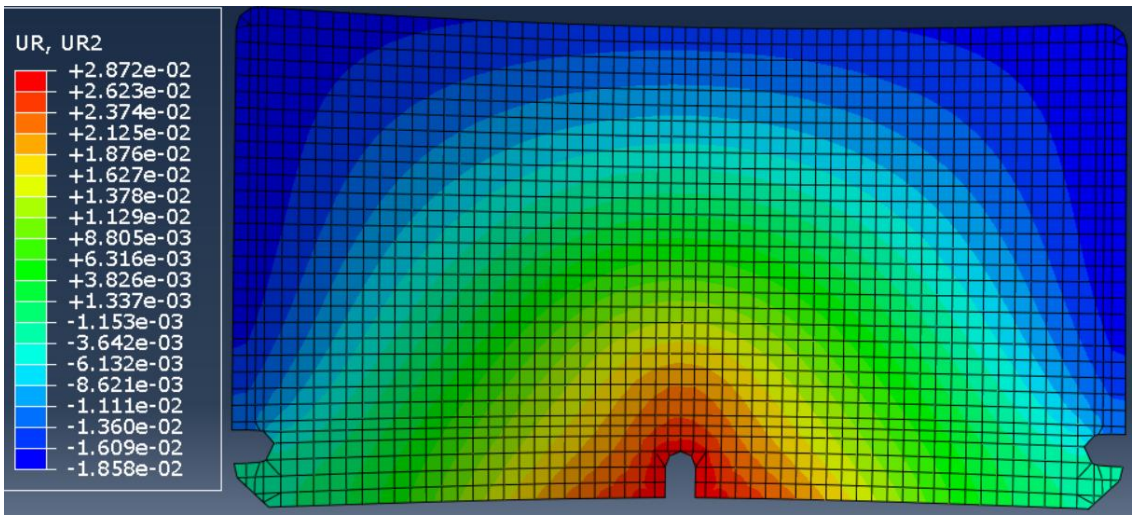

Figure 106 - Slopes in Y direction in ABAQUS CAE

When compared to the Figures 90 to 92 in section 6.2, with the simulation ones (Figure 104 to 106) the slope curves are similar, which indicates that in a geometrical perspective, the simulation is working well.

6.5.3 Stress validation

The ABAQUS CAE internal stress distribution is visible in Figure 107. This stress distribution is calculated using the Von Misses criteria.

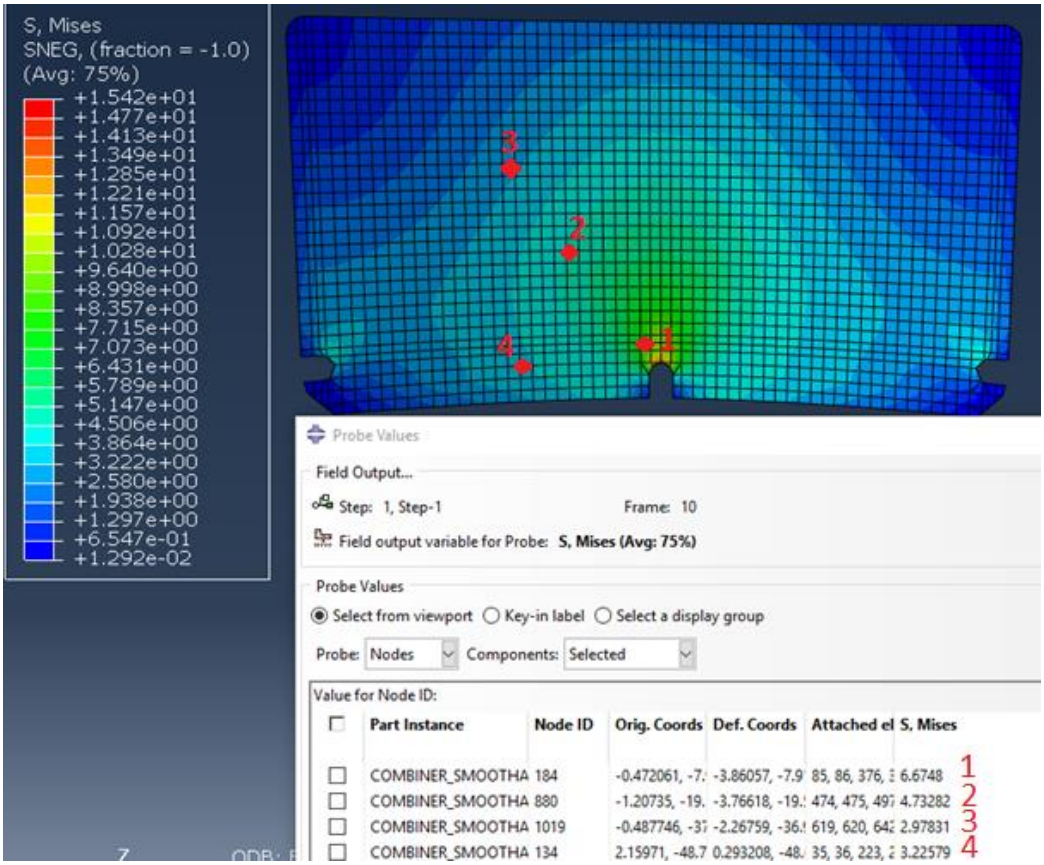

Figure 107 – Stress distributions in ABAQUS CAE model when a 23N force is applied

The maximum stress is from 15.42 MPa. However, that value can not be used for comparison because in the experimental model the maximum stress point is hidden behind the force applicator. Therefore, the max stress point measured in section 6.3, is a bit to the side from that point. To compare correctly, the node analyzed in the simulation is 3mm to the left of the maximum stress point, where the stress is 6.67 MPa. Table 8 shows the comparison between the results.

Table 8 – Comparison between the real stress values and the ABAQUS CAE simulation

Stress in the experimental model	Max stress in the simulation	Difference
4.14 MPa (MAX stress)	6.67 MPa	1.6x bigger in the simulation
0 MPa	4.73 MPa	
0.36 MPa	2.98 MPa	
0.9 MPa	3.23 MPa	

Unlike the geometric validation, the comparison between the stress in section 6.3 (in the real model), and in the ABAQUS CAE simulation, there is a higher difference between results.

The first analysis to make is to compare the gap between maximum stress values. Despite the approximations made, the difference in these points is not that high. The polariscope is not very precise to measure the stress intensity, as this setup requires a very subjective color analysis.

For the other points with lower stress, the difference is much higher. This is related to the difficulty to measure low stress in the part (stress lower that 1 MPa).

As for the stress distribution, the pattern of the stress has some similarities, being a curve that starts in one lower support and goes until the other lower support, around the point where the force is applied. However, unlike the real model the stress increases since the top corner where the stress is very low, constantly until the point where the force is applied. Figure 108, shows the areas in the combiner stressed in the polariscope where there is no stress.

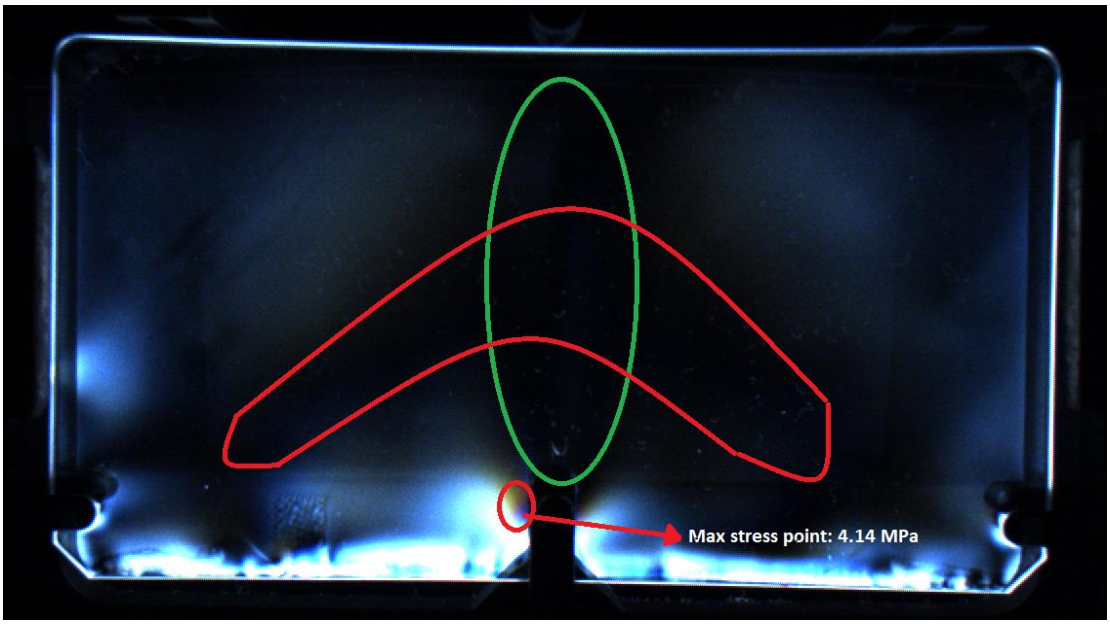

Figure 108 – Picture of the combiner stressed in the jig in the polariscope with the unstressed areas represented

In a deeper analysis, these areas with no stress in the polariscope are coincident with the areas with no slope deviation, as Figure 109 shows.

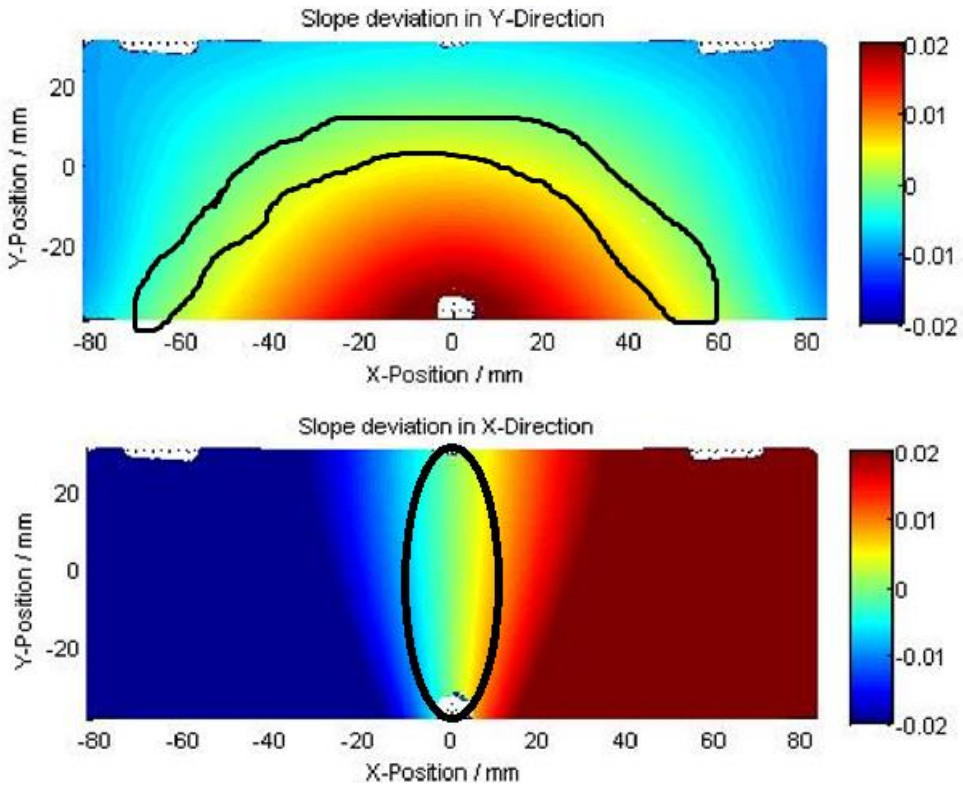

Figure 109 – Areas of the combiner where there is no slope deviation (in X and Y direction)

This evidences that might be a correlation between the slope deviation and the stress distribution, nevertheless there is still a big difference in the stress values.

7 Conclusion and Future work

7.1 Final conclusions

The main goal in this thesis was to understand the behavior of the combiner when glued to its support. It was also proposed to create a correlation between the internal stress in the combiner and the adhesive failure that occurred when the combiner unit was submitted to higher temperature and humidity conditions.

The first analysis was to verify the combiner support geometric stability when submitted to higher temperature and humidity conditions. Therefore, the first batch of parts was submitted to a thermal cycle. The results showed that the parts changed their dimensions, and some points that were out of specification, stayed more proximate of the part nominal dimensions. In the second study, a second batch of parts was submerged in water. In this test, the part did not change its dimensions. However, as the parts water absorption was not studied, it was not possible to establish a correlation between the water absorption and the part dimensions.

The second analysis was about the combiner geometry and internal stress, before and after the combiner unit gluing process. The geometry analysis results shows that the studied combiners before the gluing process were fulfilling the specifications and had a peak-to-peak deviations between 23.57 and 44.93 μm. After the gluing process the deviations of the combiners, increased 6 times compared to the initial deviations, to a range between 208.76 and 221.40 μm. As the combiner supports peak-to-peak deviations (measured in section 4.1) were between 150 μm and 344 μm, this analysis indicates that the combiner supports were inducing deformations into the combiner.

To study the combiner internal stress, first two unstressed combiners were analyzed. Both parts showed that the combiner had residual stress, especially in the lower part of the combiner. These residual stresses are due the injection and the milling process that are part of the combiner fabrication process. After this study, a batch of 14 combiners was glued and the parts were analyzed in the polariscope. The results showed that the combiners suffered an increase in the stress intensity, and the stress distribution stayed more uniform in all the parts. Using photoelasticity, the internal stress in one part of the batch was analyzed, and the measurements shown that the parts internal stress was below 1 MPa.

With these studies made, the same batch of 14 parts was submitted to a thermal cycle for 48h at 85ºC, in order to force the adhesive to fail. After the test, all the parts suffered from adhesive failure, between 10 to 60% of the bonding area. After this test, an analysis was made where the parts internal stress before the thermal cycle was compared with the adhesive failure, in order to create a correlation between them. The analysis showed that it was not possible to create such correlation. Also, the internal stress in the part after the thermal cycle was analyzed. This analysis showed that the parts that suffered from adhesive failure in the sides of the bonding area, had a stress release in the center of the combiner.

To understand better the combiner stress and deformation behavior when submitted to a force, a simplified experimental model was made. This experimental model has the capacity to apply a known force in the combiner while supporting it in known points. To implement this model, a jig was designed and developed. After the model creation, the stressed combiner was analyzed in the 3D scanner and in the polariscope. The results obtained from this model were used as validation of a simulation of this experimental model.

A simulation of the experimental model has been made and the results were compared with the experimental model ones. This showed that the simulation could be a valid tool predict the stress and the deformations in a combiner.

7.2 Future work

As future work, the influence of the humidity absorption of the combiner support in its dimensions should be studied.

To measure stress, the used setup should be developed to increase the measurement precision. During this work, a study was made to characterize the color using RGB image-decomposing using the technic studied in a Palermo University study. (Ajovalasit, Petrucci e Scafidi 2014) Due the lack of time, it was not possible to implement this system. Also, it could be studied another method to measure internal stress in the combiner like interferometry.

To increase the precision of the experimental model results, a mechanical characterization of the combiner material should be made.

As the simulation results were validated by the experimental model, the precision of the simulation made could be increased, by using the real part thickness and not an approximation.

Also, the simulation should have introduced the combiner support, the adhesive and consider the residual stress the combiner has before being glued.

8 Bibliography

Ajovalasit, A., Giovani Petrucci, e Michele Scafidi. "Review of RGB photoelasticity." *Optics and Lasers in Engineering*, 2014: 58-73.

Annie, Pauzié. "Head Up Display in Automotive: A New Reality for the Driver." Em *Design, User Experience, and Usability Part 3*, de Aaron Marcus, 505-516. Springer, 2015.

B. Mouhmid, A. Imad, N. Benseddiq, S. Benmedakhène, e A. Maazouz. "A study of the mechanical behaviour of a glass fibre reinforced polyamide 6,6: Experimental investigation." 2006.

B. Murphy, Douglas, Kenneth R. Spring, e Michael W. Davidson. *MicroscopyU.* 2018. https://www.microscopyu.com/techniques/polarized-light/introduction-to-polarized-light (acedido em 12 de 2018).

BLANCHE, PIERRE-ALEXANDRE. *College of Optical Sciences.* University of Arizona. 2018. https://wp.optics.arizona.edu/pablanche/research-interest/volume-phase-grating/ (acedido em 12 de 2018).

Bosch, Robert. *Bosch Brand.* 2018. http://www.brand.bosch.com/ (acedido em 9 de 1 de 2019).

—. *Bosch Figures.* 2018. https://www.bosch.com/our-company/our-figures/ (acedido em 9 de January de 2019).

—. *Bosch History.* 2018. https://www.bosch.com/our-company/our-history/ (acedido em 9 de 1 de 2019).

—. *Bosch Portugal.* 2018. https://www.bosch.pt/a-nossa-empresa/bosch-em-portugal/braga/ (acedido em 9 de 1 de 2019).

Daddario, Matthew. *medium.* 24 de July de 2017. https://medium.com/helm-experience-design/push-to-start-a-brief-history-of-car-dashboards-6fdf7989e144 (acedido em 12 de 2018).

dictionaries, Oxford. *Oxford dicionaries.* 2018. https://en.oxforddictionaries.com/definition/head-up_display (acedido em 11 de 2018).

F. J. G. Silva, R. P. Martinho, R. J. D. Alexandre, e A. P. M. Baptista. "Increasing the wear resistance of molds for injection of glass fiber reinforced plastics." Em *18th International Conference on Wear of Materials*, de K. C. Ludema e S. J. Shaffer, 2494-2499. 2011.

federation, British plastics. *bpf.* 2018. http://www.bpf.co.uk/plastipedia/polymers/polycarbonate.aspx (acedido em 11 de 2018).

Feingold, Joel. *Strainoptics, Inc.* 08 de October de 2002. https://www.strainoptics.com/training/ (acedido em 12 de 2018).

Flora, David. *autonomes fahren.* 11 de June de 2014. https://www.autonomes-fahren.de/head-up-display-von-bosch/ (acedido em 11 de 2018).

Harder, Don. *flickr.* 24 de June de 2012. https://www.flickr.com/photos/dharder9475/7452015944/in/photostream/ (acedido em 12 de 2018).

Howard, Bill. *Extreme Tech.* 2 de January de 2012. https://www.extremetech.com/extreme/111269-10-best-tech-cars-for-2012/3 (acedido em 11 de 2018).

Lee, Jian-Yuan, Jia An, e Chee Kai Chua. "Fundamentals and applications of 3D printing for novel materials." *Applied materials Today*, 2017: 120-133.

Lee, Joong Hee, Sunghwan Park, Wonjoon Kim, Waqas Hassan Tanveer, Misuk Kim, e Myung Hwan Yun. "The Investigation of Study Trends for Heads-Up Displays (HUD) in Visualized Form undern the Perspectives of Human Factors." *The HCI Society of Korea*, 2016: 373-380.

Magnus, Dr. M. "Michel-Lévy Color Chart - Identification of minerals in polarized light." *www.zeiss.com.* February de 2011. https://applications.zeiss.com/C125792900358A3F/0/E037A9841E664961C1257906004802D6/$FILE/70_2_0110_e_michel_levy.pdf (acedido em 11 de 2018).

Nica, Gabriel. *Auto Evolution.* 10 de 10 de 2013. https://www.autoevolution.com/news/2014-mini-cooper-gets-new-driver-assist-systems-photo-gallery-68702.html# (acedido em 10 de 1 de 2019).

Panait, Mircea. *Auto evolution.* 22 de June de 2018. https://www.autoevolution.com/news/ford-claims-2019-focus-has-fighter-jet-technology-126565.html#agal_0 (acedido em 11 de 2018).

Porsche. *www.porsche.pt.* 2018. https://www.porsche.com/portugal/models/panamera/panamera-e-hybrid-models/ (acedido em 12 de 2018).

Post, Daniel. "Photoelasticity." Em *Manual on Experimental Stress Analysis (Fifth Edition)*, de James F. Doyle e James W. Phillips. Society for Experimental Mechanics, 1989.

S. Rudzinski, L. Häussler, Ch. Harnisch, E. Mäder, e G. Heinrich. "Glass fibre reinforced polyamide composites: Thermal behavior of sizings." *Composites Part A: Applied Science and Manufacturing*, 2010: 157-164.

Scollar, Irwin. *Radial Distortion Correction.* 27 de March de 2011. http://www.uni-koeln.de/~al001/radcor_files/hs100.htm (acedido em 12 de 2018).

Silva, Lucas Filipe Martins da, António G. de Magalhães, e Marcelo F. S. F. de Moura. *Juntas adesivas estruturais.* Publindústria, 2007.

Singh, Rupinder. "Process capability study of polyjet printing for plastic components." *Journal of Mechanical Science and Technology 25*, 2011: 1011-1015.

Yeager, Mark. "Photoelastic Stress Analysis of Polycarbonate Medical Parts." *Bayer Material Science LLC*, 2010.

Appendix A: Other activities

Throughout the internship, several activities, due to the full integration in the CM-CI2/ECM8 team, were performed. These tasks were related with the Ford project needs.

1. Tests and data collection

During the development and continuous improvement made in the FORD CHUD, there was always a need to test new batches of parts and modifications in the unit. In order to fulfil this need, many tests in the actual production line were made to verify if the modifications, were in fact being beneficial.

2. Trip to the Combiner Support supplier

During this internship, there was the possibility to join the team in a trip to the Combiner Support supplier, to verify if the measurements made by the Supplier using the CMM machine were being made the same way as they were being made by Bosch. This trip gave the possibility to understand the production process of the Combiner Support.

3. Studies to reduce the transmission of deformation of the Combiner Support to the Combiner

In the beginning of this internship, in parallel with the work developed for this thesis there was made a small effort to think in alternatives in the bonding between the combiner and the combiner support, in order to reduce the transmission of deformations between both parts.

After a studying the adhesive properties, a suggestion of gluing both parts without any contact between both parts has been made. The idea was to remove the lateral pads and the spheres, and design a jig that would define the position between both parts. The contraction of the glue when cured, was smaller than the deformation that was being transmitted by the combiner support, so in theory this could reduce the stress and deformation in the combiner.

4. Combiner surface roughness measurement

Making the experimentation of sand blasting the combiner gluing area, was needed to measure the roughness of the combiner after being sand blasted. To do this, using a hommelwerke LV-50 surface roughness-measuring instrument.

Using a diamond tip with 5 microns radios, called tk300 this tip could measure roughness from a range between minus and plus 300 microns. In Figure 111 is the setup used for this measurement is shown. With this test, it was measured not only the roughness as the surface profile. The roughness values are not displayed due confidentiality reasons.

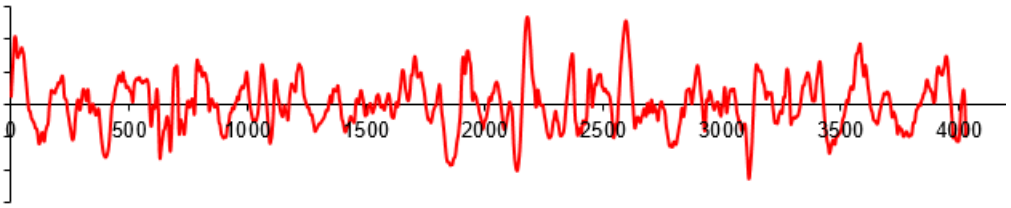

Figure 110 – Surface profile

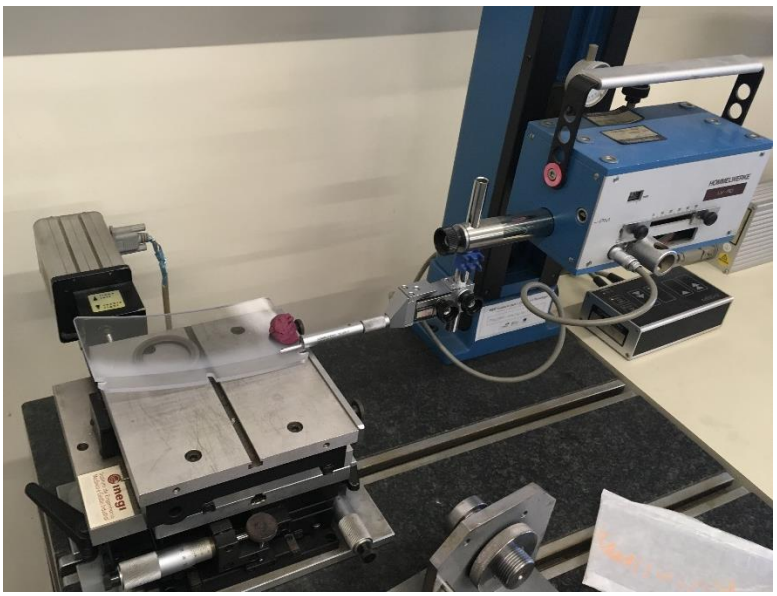

Figure 111 – Hommelwerke LV-50 surface roughness measuring setup